OTDM Networking for Short Range High-Capacity Highly Dynamic Networks

Medhin, Ashenafi Kiros

Publication date:
2015

Document Version
Publisher's PDF, also known as Version of record

OTDM Networking for Short Range High-Capacity Highly Dynamic Networks

Ph.D. Thesis
Ashenafi Kiros Medhin

November 14th, 2015

DTU Fotonik
Department of Photonics Engineering

DTU Fotonik
Department of Photonics Engineering
Technical University of Denmark
Ørsteds Plads 343
DK-2800 Kgs. Lyngby
Denmark

Preface

The work presented in this thesis was carried out as a part of my PhD project in the period of November 1st, 2012 to November 14th, 2015. The work took place at DTU Fotonik (Technical University of Denmark, Department of Photonics Engineering) with an external visit to the International Business Machines (IBM) labs in Yorktown Heights, NY, USA.

The PhD project was mostly financed by the European Research Council ERC-StG project Serial Optical Communications for Advanced Terabit Ethernet Systems (SOCRATES) and supervised by:

- Leif Katsuo Oxenløwe (main supervisor), Professor, DTU Fotonik, Technical University of Denmark, Kgs. Lyngby, Denmark
- Michael Galili (co-supervisor), Associate Professor, DTU Fotonik, Technical University of Denmark, Kgs. Lyngby, Denmark

Abstract

This PhD thesis aims at investigating the possibility of designing energy-efficient high-capacity (up to Tbit/s) optical network scenarios, leveraging on the effect of collective switching of many bits simultaneously, as is inherent in high bit rate serial optical data signals. The focus is on short range highly dynamic networks, catering to data center needs. The investigation concerns optical network scenarios, and experimental implementations of high bit rate serial data packet generation and reception, scalable optical packet labeling, simple optical label extraction and stable ultra-fast optical packet switching, with the constraint that there must be potential energy savings, which is also evaluated. A survey of the current trends in data centers is given and state-of-the-art research approaches are mentioned. *Optical time-division multiplexing* is proposed and demonstrated to generate Tbit/s data packets, and time lens based serial-to-parallel converter is employed to demultiplex each high-capacity packet into lower bit rate tributaries. A novel optical label scheme is suggested and experimentally demonstrated, where the label information is inserted in-band in the broad signal spectrum and its scalability is demonstrated by generating up to 65.536 distinct optical labels for 1.28 Tbit/s data packets. The optical label information is extracted and decoded using a simple opto-electronic based label detection module. In particular, four stable switching control signals are decoded from 640 Gbit/s variable length data packets. Finally, three optical switching scenarios of high-capacity data packets, including a record-high 1×2 optical packet switching of 1.28 Tbit/s serial packets, are experimentally demonstrated using electro-optic based $LiNbO_3$ switches.

Resumé

Denne Ph.d. afhandling adresserer muligheden for at designe energieffektive høj kapacitets (op til Tbit/s) optiske netværks scenarier, der kan udføre samlet switching af mange bits simultant som er typisk for høj bit rate optiske signaler. Fokus er på særdeles dynamisk kort-distance netværk som kendetegner data centre. De optiske netværks scenarier udforsker eksperimentelt høj kapacitets pakke dannelse og modtagelse, skalerbare optisk pakke labels, simpel label ekstraktion, stabil og ultrahurtig optisk pakke switching samt evaluering af de mulige potentielle nødvendige energibesparelser. Et overblik af de nuværende trends i datacentre bliver præsenteret og state-of-the-art forsknings løsningsforslag bliver resumeret. Det bliver beskrevet og demonstreret hvorledes en optisk tids-deling multiplexing sender benyttes til at danne Tbit/s datapakker. En seriel til parallel konverter tidslinse, er benyttet til at demultiplekse hver enkelt høj kapacitets pakke ned til de lave bitrate signaler som indgår i signalet. Optisk label information er inkluderet i det brede spektrum af signalet ved at benytte en ny optisk båndstopfilter label teknik. Denne tekniks skalerbarhed er eftervist ved at generere op til 65.536 forskellige optiske labels til 1.28 Tbit/s datapakker. Informationen i disse optiske labels er ekstraheret og aflæst ved at benytte et simpelt optisk-elektronisk baseret label detekterings modul. Særligt bør fremhæves hvorledes fire stabile switch kontrol signaler er blevet aflæst i 640 Gbit/s data pakker med variabel længde. Til sidst er tre optiske switching scenarier med høj kapacitets data pakker, herunder rekord høj 1×2 optiske pakke switching af 1.28 Tbit/s serielle pakker, blevet eksperimentelt demonstreret ved at benytte elektrisk-optisk baserede $LiNbO_3$ switches.

Ph.D. Publications

The following publications have resulted from this Ph.D. project.

Articles in international peer-reviewed journals: (4)

J1 M. Galili, H. Hu, H. C. H.Mulvad, **A. K. Medhin**, A. Clausen, and L. K. Oxenløwe, "Optical Systems for Ultra-High-Speed TDM Networking," *Photonics*, **1**, 83-94 (2014).

J2 **A. K. Medhin**, M. Galili, and L. K. Oxenløwe, "Scalable In-Band Optical Notch-Filter Labeling for Ultra-High Bit Rate Optical Packet Switching," *Journal of Lightwave Technology*, **32**, 4871-4878 (2014).

J3 J. H Song, F. E. Doany, **A. K Medhin**, N. Dupuis, B. G. Lee, and F. R. Libsch, "Polarization-independent nonuniform grating couplers on silicon-on-insulator," *Optical Letters*, **40**, 3941-3944 (2015).

J4 V. Kamchevska, **A. K. Medhin**, F. Da Ros, F. Ye, R. Asif, A. M. Fagertun, S. Ruepp, M. Berger, L. Dittmann, T. Morioka, L. K. Oxenløwe, and M. Galili, "Multidimensional Switching: A Step Towards Flat, Scalable, Energy Efficient, All-Optical Data Center Networks," *Journal of Lightwave Technology*, (submitted as invited) 2015.

Contributions to international peer-reviewed conferences: (9)

C1 **A. K. Medhin**, M. Galili, and L. K. Oxenløwe, "Novel Optical Labeling Scheme for Ultra-High Bit Rate Data Packets," in *Opto Electronics and Communications Conference*, OECC (2013), Paper-TuPT-3.

C2 **A. K. Medhin**, M. Galili, and L. K. Oxenløwe, "640 Gbit/s Optical Packet Switching using a Novel In-Band Optical Notch-Filter Labeling Scheme," in *Optical Fiber Communication Conference*, OFC (2014), Paper Th1D.4.

C3 H. Hu, F. Ye, **A. K. Medhin**, P. Guan, H. Takara, Y. Miyamoto, H. C. H. Mulvad, M. Galili, T. Morioka, and L. K. Oxenløwe, "Single Source 5-dimensional (Space-, Wavelength-, Time-, Polarization-, Quadrature-) 43 Tbit/s Data Transmission of 6 SDM×6 WDM ×1.2 Tbit/s Nyquist-OTDM-PDM-QPSK," in *Conference on Lasers and Electro-Optics*, CLEO (2014), Paper- JTh5B (Post deadline).

C4 H. Hu, **A. K. Medhin**, F. Ye, Y. Ding, R. Asif, P. Guan, H. Takara, Y. Miyamoto, H. C. H. Mulvad, M. Galili, T. Morioka, and L. K. Oxenløwe, "1.28 Tbaud Nyquist-OTDM Transmission over a 7-Core Fiber Using an On-Chip SDM Coupler," in *Opto Electronics and Communications Conference*, OECC (2014), paper THPDP2-2 (Post deadline).

C5 **A. K. Medhin**, V. Kamchevska, M. Galili, and L. K. Oxenløwe, "1x4 Optical Packet Switching of Variable Length 640 Gbit/s Data Packets using an In-Band Optical Notch-Filter Labeling Scheme," in *European Conference on Optical Communications*, ECOC (2014), paper P.4.11.

C6 **A. K. Medhin**, V. Kamchevska, H. Hu, M. Galili, and L. K. Oxenløwe, "Experimental Demonstration of Optical Switching of Tbit/s Data Packets for High Capacity Short-Range Networks", in *Conference on Lasers and Electro-Optics*, CLEO (2015), paper SW3M.5 (upgraded to invited).

C7 V. Kamchevska, **A. K. Medhin**, F. Da Ros, F. Ye, R. Asif, A. M. Fagertun, S. Ruepp, M. Berger, L. Dittmann, T. Morioka, L. K. Oxenløwe, and M. Galili, "Experimental Demonstration of Multidimensional Switching Nodes for All-Optical Data Centre Network," in *European Conference on Optical Communications*, ECOC (2015), papaer Tu.1.2.2.

C8 A. T. Clausen, H. Hu, F. Ye, **A. K. Medhin**, Y. Ding, R. Asif, M. Galili, T. Morioka, and L. K. Oxenløwe, "Increase in Data Capacity Utilising Dimensions of Wavelength, Space, Time, Polarisation and Multilevel Modulation Using a Single Laser," in *International Conference on Transparent Optical Networks*, ICTON (2015), paper Th.A1.1 (invited).

C9 **A. K Medhin**, F. E. Doany, J. H Song, N. Dupuis, B. G. Lee, F. R. Libsch, and C. Schow, "Demonstration of a Polarization Insensitive Non-Uniform Grating Coupler," accepted in *Asia Communications and Photonics Conference*, ACP (2015), paper ASu1B.4.

Contents

Chapter 1

Introduction

Optical communication has been playing a key role in revolutionizing telecommunications and data communications industries to satisfy the continuously growing bandwidth demand. The unprecedented growth of current bandwidth demand is mainly driven by emerging services such as ultra-high and high definition videos on demand, and cloud computing just to mention few. Figure 1.1 shows the continuing, relentless global IP traffic growth that is forecasted by Cisco [1] to increase nearly three times from 2014 to 2019, corresponding to a compound annual growth rate (CAGR) of 23%. Albeit to its indisputable contributions, further research in the optical communication systems is paramount in order to cope with this large data traffic demand for bandwidth.

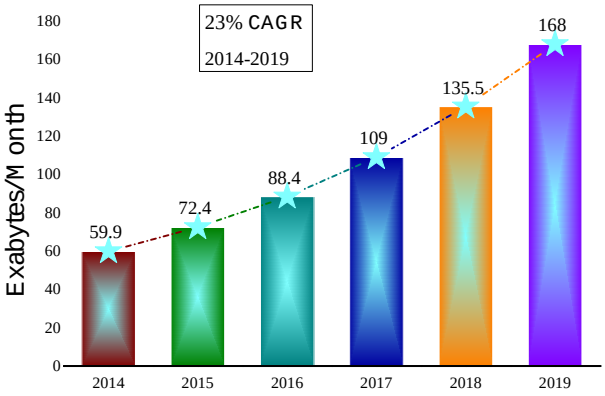

Figure 1.1: Cisco visual networking index forecasts 168 exabytes per month of IP traffic by 2019 [1].

Optical fiber, known as a low loss transmission medium, provides enormous bandwidth, beyond 10 THz [2], that is being used for high-capacity data transmission. A lot of research and innovation have been conducted to efficiently harvest the huge fiber capacity mainly using wavelength-division multiplexing (WDM) [3, 4], orthogonal frequency-division multiplexing (OFDM) [5], space-division multiplexing (SDM) [6] or multi-dimensional multiplexing techniques [C4] as well as by introducing advanced data modulation [C3]. In par with those techniques, optical time-division multiplexing (OTDM) has been pursued to increase the capacity of an individual data channel serially similar to an electrical time-division multiplexing (ETDM) but at very high bit rate.

Serial optical communication can be very attractive for optical networks because it can add flexibility to the high-capacity serial data on the optical domain [7]. The current optical networks, which are mostly deployed using high capacity WDM technologies complemented by lower bit rate ETDM, can only acquire flexibility with the help of optical-to-electrical-to-optical (OEO) conversions at each switching node. OEO may not only consume considerable electrical power but processing speed of the OEO interface may also be a major concern as the data rate, for instance Ethernet data rate [8], is scaling at high pace to live up with the exponential growth of IP traffic [1]. Moreover, the slow processing speed can introduce unwanted delay to latency critical application. These limitations may have severe consequences in high-capacity short-range network like datacenter (DC) and high-performance computing (HPC).

High-capacity serial optical data packets, using OTDM functionality, may be beneficial for highly dynamic short range networks, for example intra- and inter-DC. Because OTDM, like ETDM, has the potential to add flexibility to high-capacity data packets on the optical domain that can reduce if not eliminate the power-hungry OEO conversions even though the enabling technologies are at their infancy stage. In this PhD thesis, serial optical communication has been investigated to design network scenarios for high-capacity short-range networks including high-capacity data packet generation, scalable optical packet labeling, simple optical label extraction and very fast optical packet switching (OPS).

1.1 Description and scope of the thesis

This PhD work is part of a five year European Research Counsel (ERC)-project called Serial Optical Communications for Advanced Terabit Ether-

net Systems (SOCRATES) which started in September 2009. The explosive growth of telecommunication bandwidth demand [1] and power consumption of the Internet are the two main motivations behind SOCRATES. The primary focus of SOCRATES is to develop a new technology, based on serial optical communications, that can accommodate for the ever growing bandwidth demand and reduced power consumption. In modern telecommunication, cost-per-bit may not be the key issue due to the enormous bandwidth of optical fiber, but power-per-bit can be. SOCRATES has aimed at developing all-optical power-efficient serial communication scenario as serial communication uses fewer components by relying on ultra-short pulses and very high bit rates. Scaling the serial data rate have traditionally lead to reduced complexity and lower power consumption. Hence, SOCRATES has targeted to reach the ultimate serial bit rate, which can be perfectly matched with the future standards of the Ethernet alliance road-map shown in Figure 1.2 [8], and develop network scenarios to fully take advantage of the serial nature of the data, whilst maintaining a focus on limiting the power consumption.

As part of SOCRATES, this PhD work has focused on designing optical network scenarios for Tbit/s serial data packets in compliance with future Ethernet road-map (see Figure 1.2) that can help to build a 1 Tbit/s optical Ethernet scenario. Moreover, this PhD project has addressed ultra-fast switching scenarios including a variety of functionalities, enabling complex networks based on high bit-rate serial optical data signals.

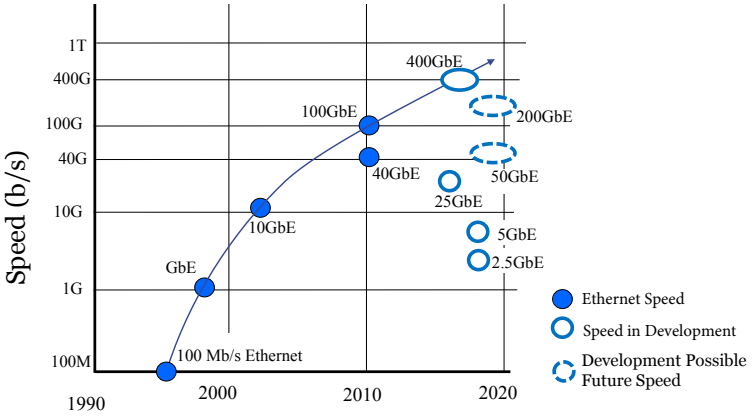

Figure 1.2: Past, present and future standards of the Ethernet (source: road-map subcommittee and the Ethernet alliance 2019 [8]).

1.2 Contribution of the PhD thesis

The following list briefly describes the main results and contributions of this PhD:

- **Scalable in-band notch-filter labeling Technique**. A novel optical labeling scheme is proposed for high-capacity (640 Gbit/s or above) serial data packets. The optical label is encoded by carving out of the broad data spectrum. A maximum of eight and sixteen spectral notches (holes) are applied to optically labeled 640 Gbit/s and 1.28 Tbit/s serial data packets, respectively. This makes the optical labeling very scalable as up to 2^{16}= 65.536 unique labels can be generated.

- **Packet length independent label detection scheme**. A simple opto-electronic based module has been built to generate stable and clean electrical control signal using optical label information of each 640 Gbit/s and 1.28 Tbit/s serial packets. Stable electrical control signals are generated from 640 Gbit/s variable length data packets, thus verifying both the optical labeling and label detection modules are packet-length independent.

- **Optical networking scenarios for high-capacity serial data packets**. Each high-capacity data packet is routed using very fast $LiNbO_3$ optical switch after the electrical control signal is extracted from the data packet. A record-high 1×2 OPS of 1.28 Tbit/s serial data packet is experimental proposed and demonstrated for short range networks like DCs.

1.3 Structure of the thesis

The PhD thesis is organized in four main chapters: Chapter 3, Chapter 4, Chapter 5 and Chapter 6 complementing each other to realize optical switching scenarios for high-capacity serial data packets.

Chapter 2 deals with short range high-capacity networks in general and DCs in particular. After a brief introduction about DCs, it focuses on the state-of-the art of current DCs including evolution, organization and traffic characteristics. Then, the chapter discusses the biggest challenges in DCs today such as scalability and power consumption, mainly driven by the rapid growth of bandwidth demand inside DCs. At the end of the

chapter, optical technologies are reviewed focusing on the state-of-the-art research approaches to overcome the current DC challenges by proving huge bandwidth and reducing power-hungry operations like OEO conversions.

Chapter 3 introduces a high-capacity optical network scenario using standard OTDM transceiver blocks and links the four main chapters together. The chapter starts with the evolution of serial optical communication through time and reviews the major milestones achieved in terms of capacity and spectral efficiency. A short range optical network scenario is proposed for high-capacity serial data packets including a brief description on how the main functional blocks are implemented through out the thesis. 640 Gbit/s and 1.28 Tbit/s serial data packet generations from 10 Gbit/s tributaries are described using a standard OTDM transmitter setup after the main building blocks of the scheme are illustrated. Finally, working principles of two commonly used OTDM demultiplexers: a pulse-by-pulse switch and a time lens based serial-to-parallel conversion are briefly discussed and followed by successfully experimental demonstration of high-capacity data packet receptions.

Chapter 4 presents an optical labeling of high-capacity data packets scheme using a newly proposed in-band notch-filtering techniques. The chapter starts with a thorough investigation of different optical labeling schemes that has been demonstrated in the lab. After the optical labeling scheme is proposed using a simplified network scenario, it is characterized in terms of transfer function, bandwidth and suppression ratio of the filter that encodes the label information, and spectral position when employing it to label high-capacity serial packets. Since it is in-band labeling, its impact on data quality is investigated in simulation evaluating the eye-opening penalty (EOP). Finally, the proposed optical labeling is experimentally verified using 640 Gbit/s and 1.28 Tbit/s data packets and its impact on the data quality is characterized using bit-error ratio (BER) measurements. Scalability of the labeling technique is verified by employing eight and sixteen optical notch-filters (ONFs) within the spectra of the 640 Gbit/s and 1.28 Tbit/s data packets leading to 256 and 65.536 unique optical labels, respectively.

Chapter 5 deals with extraction of the optical label of the high-capacity data packet and generation of stable electrical signals that can control an optical switch fabric. The label extraction is characterized in simulation using simple opto-electronic module and confirmed by detailed experimental demonstrations for 640 Gbit/s and 1.28 Tbit/s data packets. Quality of the detected optical label is studied in simulation for different parameters

of the in-band labeling and label detection modules. Packet length independence of both modules is experimentally demonstrated using 640 Gbit/s variable length data packets. Finally, the chapter discusses scalability of the label detection module to extract many in-band optical labels from a given high-capacity data packet.

Chapter 6 concerns OPS of high-capacity serial data packets using elctro-optical based $LiNbO_3$ switches. After a brief introduction on the working principle, architecture and power consumption of the optical switch are presented, three different OPS scenarios are experimentally demonstrated using the proposed optical labeling and label detection schemes. The first experimental demonstration deals with 1×2 OPS of 640 Gbit/s serial data packets whereas the second scenario discusses 1×4 OPS of variable length 640 Gbit/s serial data packets. At the end of the chapter, a record-high 1×2 OPS of 1.28 Tbit/s data packets is demonstrated.

Finally, Chapter 7 summarises the main results presented in this thesis and provides a brief outlook on possible future developments..

Chapter 2

Short range high-capacity networks

2.1 Introduction

Traditionally, optical networks are categorized as long haul, metropolitan and access networks based on their technical and operational requirements such as capacity and distance of coverage [9]. Optical networks that interconnect continents and countries, covering thousands of km with the help of optical amplifiers, are considered as long haul networks. Metropolitan (regional) networks are mostly used to interconnect regions and cities whereas access networks are the "last mile" optical networks providing access to the end users. Long haul networks carry high-capacity data traffic aggregated from metropolitan networks, whilst access networks carry low bit rate data traffic within short distances. Fiber optical technologies are the "de facto standard" solutions to deal with the aggregated data traffic at the long haul and metropolitan networks because of their enormous bandwidth. In the last decade, broadband access networks based on optical technologies such as fiber-to-the-home have been deployed at a tremendous speed that enabled the booming of various Internet based applications ranging from the traditional online search engines to new web applications such as interactive maps, social networks, cloud services, mobile applications, software packages and high definition video streaming [10].

Almost all of the aforementioned applications are running in short range networks called datacenters (DCs) that are transparent to the end user [10]. A DC is a public or privately owned-facility that is used to house a physical and virtual network-based infrastructures such as computer systems and

associated telecommunications and storage systems. It is a pool of computational, storage and network resources interconnected using a communication network called datacenter network (DCN). As a standard requirement, any DC requires extensive back-up (redundant) of power supplies, networking devices and connections, cooling systems, and security devices. Hence, large DCs are industrial scale operations that consume as much electrical power as a small town [11].

Current DCs are constructed using tens of thousands of servers [10] to form the backbone of a wide variety of bandwidth-hungry services offered via the Internet today. Due to the emergence of these bandwidth-hungry Internet technologies, global DC IP traffic has continued to rise by 23% compound annual growth rate (CAGR) from 2013 to 2018 as shown in Figure 2.1. It is forecasted to reach 8.6 zettabytes per year by the end of 2018 compared to the current 4.7 zettabytes per year [12]. This will definitely make the DC traffic one of the fastest growing sectors of the global Internet industry [12].

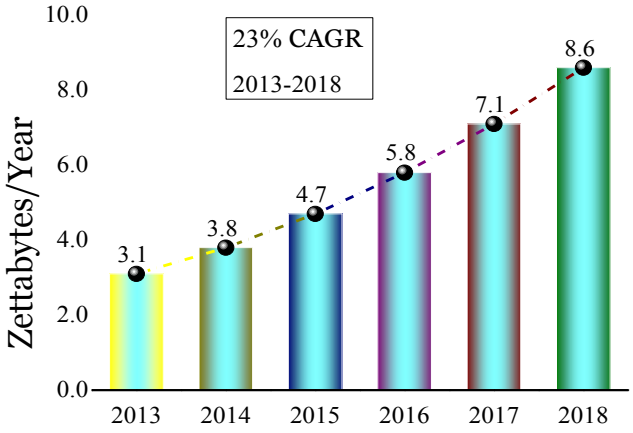

Figure 2.1: Global DC IP Traffic growth [12].

This chapter summarizes the state-of-the-art of current DC. In particular, Section 2.2 covers the evolution of DC up to date, commonly used hierarchical architecture and current traffic characteristics within the DC. Due to the tremendous growth of bandwidth-hungry applications and services, the traffic characteristic with the DC is mostly server-to-server. The need for more bandwidth and shift in traffic flow are creating many challenges to the current DCN organization. The main challenges, as detailed

in Section 2.3, are scalability and power consumption. Hence, a lot of research works have been reported to overcome these challenges, for instance, by employing different types of optical switches in the DC architecture as discussed in Section 2.4.

2.2 Datacenters today

This section concerns the evolution of current DC over time, typical DC organization and traffic flow in the DC.

Evolution

Over the last few decades, DCs have gone through a tremendous transformation [11, 13]. During the pre-DC era, desktop personal computers were used to provide computing, storage and the networking that interconnected them. However, high performance computing devices such as servers and mainframe computers were installed to handle the growing storage demand, the need for higher processing capabilities and the necessity for collaboration between enterprises. As time went on, the high performance computing devices could not cope with the continually growing load and the widespread collaborative needs of the clients. Hence, the DCs were migrated into more centralized structure that facilitated easy management, operation and maintenance. The architecture of these modern DCs were originally designed by physically isolating servers (i.e, computing devices), storage devices and the networking technologies used to interconnect them.

In the last decade, DCs have seen a fundamental paradigm shift due to the introduction of new and quickly emerging technologies and services: virtualization, cloud computing and elasticity. These technologies enabled DCs to evolve into complex ownership scenario unlike traditional DCs that have been fully owned and operated by a single enterprise. The main attributes of virtualization are consolidation and cost savings within a DC and high level aggregation across DCs. These attributes allow to realize the possibility of "DC out-sourcing", for example Amazon web services [11], where many enterprises are able to operate a large DC without ownership of the physical infrastructure. Cloud computing, a service whose foundation is built by virtualization, is the delivery of on-demand computing resources for short periods, for instance, based on pay-for-use while underlying management of these computing resources is done without the knowledge of the end-user. The quick growth of these services are causing shift in the

networking traffic pattern that can be a big challenge to the current DC network architecture.

Organization

In principle, a fully meshed DCN is the most suitable architecture as every server is interconnected with every other server and this provides a full bisection bandwidth, easy network management and better computing resource utilization. However, such a DCN is unpractical as it is very expensive and extremely complex to implement. Hence, most DC architectures today are constructed using a massively parallel computing infrastructure, consisting of clusters with thousands of powerful serves interconnected together in three- or four-tier hierarchical networking structure [10]. Typical block diagram of current DC architecture, adapted from [9], is depicted in Figure 2.2 using a three-tier structure. The main objective of the content switches and load balance devices is to handle the request from the DC clients that is arrived through the Internet. Each individual racks consists of hundreds of servers that are connected to top-of-rack (TOR) switches, typically Ethernet commodity switches. Each TOR switch is then connected to aggregate switches, commonly using optical transceivers.

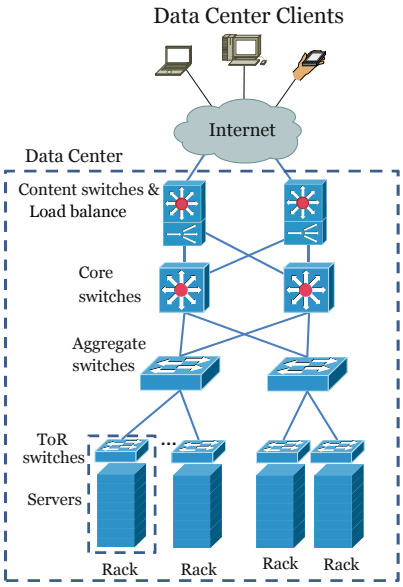

Figure 2.2: Architecture of current data centers [9].

When the scale of the two-tier architecture is not enough, for example due to limited number of ports [14], a third level is required, as in the case of the architecture shown in Figure 2.2, to interconnect the aggregate switches using core switches. The hierarchical architecture can be easily upgraded by adding new hardware with higher capacity when a given system, for example a TOR switch, cannot support the bandwidth demand. But, the up-front investment of scaling-up network fabrics can be very expensive especially at the higher tier levels where the high-capacity (aggregated) traffic needs to be handled with higher availability and reliability.

In addition to cost, other main drawbacks of the architecture are its inability to scale beyond the current capacity limit, high power consumption of the electrical switches, and large end-to-end latency. The main sources of the power consumption are the redundant optical-to-electrical-to-optical (OEO) conversions performed at each switch of each tier and the electronic switch fabric including the associated buffering. Therefore, future DCN architectures should be built based on scalable, innovative and agile designs in order to handle the rapidly growing traffic demand using better resource utilization including reduced power consumption.

Traffic characteristics

Based on their destinations, data traffic flow in the DC can be categorized in three broad groups [12] namely: data traffic that remains within the DC itself, traffic that flows from DC to DC and data traffic that flows from the DC to end users over the Internet. Figure 2.3 shows the three traffic categories in 2013 and by 2018 based on the Cisco Global Cloud Index forecast [12]. In 2013, more than three-quarter of the data traffic flow was within the DC and such flow will still remain as the dominant category by 2018 albeit its slight decline in percentage. Traffic flow within the DC is driven by many factors such as database and storage replication (redundancy), data backup and read/write operations between application servers and storage devices. Due to the emergence of cloud services and content distribution networks, the data traffic between DCs is scaling at faster rate compared to the other categories, whilst the data traffic from DC to end users is forecasted to flow at almost steady rate as it will grow only by 0.3% from 2013 to 2018.

The hierarchical three-tier DC as shown in Figure 2.2 is designed around the traffic of client-server based applications where the data traffic flows in North/South pattern. This means, the data traffic flows from the servers up to the TOR, aggregate and core switches and finally reaches the Internet. While the majority of the traffic in university campus DCs may flow

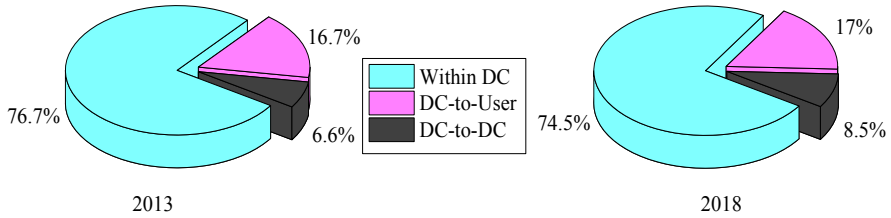

Figure 2.3: Global DC traffic by destination. Most traffic flows within the DC. Source: Cisco Global Cloud Index, 2013–2018 [12].

in North/South pattern, private DCs, which are dominated by the virtualization and cloud services, generate traffic flow between server-to-server or virtual machine-to-virtual machine [15] as shown in Figure 2.3. Hence, handling such traffic pattern using the current hierarchical architecture is becoming a challenging task for the DC.

2.3 Challenges in datacenters

As DCs today see a noticeable growth and evolution to deal with the non-stop transformation towards digital business, the giant companies such as Google, Amazon, Facebook and Microsoft are keep scaling the number of servers in their warehouses. However, increasing the computing and storage hardware infrastructure is becoming a challenging task as, for instance, connecting all these servers using the current architecture raises two big issues: power consumption and scalability due to the limited port density of the best available network equipment.

Scalability

As previously mentioned, the hierarchical approach is not suitable for the current traffic flow, thus the need for scalable architecture is paramount. Large-scale DCs can be built using clusters of hundreds of servers with TOR switches on top that are aggregated on group of large, high-radix cluster switches [16], for example a merchant switch silicon [17]. In spite of the main objective of the "cluster" approach being to solve some limitation of the traditional networks such as over-subscription, its scalability is limited by the port density of the switches. Port density limitations can be solved by increasing the number of cluster switches, however, they need the biggest networking devices that can add enormous complexity to the network on

top of the associated capital and operational cost. Moreover, the impact of network failure in these large DCs can be paramount as all large switches have proprietary internal architectures that need extensive platform-specific knowledge to properly operate and troubleshoot them. As a final remark, the current electrical switches including those expensive high-radix cluster switches from a limited set of vendors [16] are not scalable enough to cope with growing bandwidth demand.

Power consumption

Power consumption is quickly becoming the main concern of the current deign and deployment of DCNs, as DCs are consuming a tremendous amount of electricity. For example, the electrical energy consumption of all USA stationed DCs in 2013 was 91 billion kilowatt-hours, according to the natural resources defense council report [18], and it is forecasted to increase up to 139 billion kilowatt-hours, i.e., 53% increase by 2020. This high power consumption of the DC has a big impact on the environment. 14% [1] of the total ICT greenhouse gases emission in 2007 was accounted by DCs and it is expected to reach 18% by 2020 [19].

This energy consumption is the result of the many power hungry functionalities including cooling and IT related processing. Figure 2.4(a) shows distribution of the power consumption inside a DC [20]. 40% of the total IT power is consumed by servers while 37% and 23% of the IT power is consumed by storage and associated networking devices, respectively. Increasing the number of servers, storage devices or networking equipments will not only increase the total IT power in the DC but it will also scale the power needed for cooling and other associated devices. Therefore, power-efficient networking devices have the potential to significantly reduce the overall power consumption of the DC. For example, 1 W reduction in IT power corresponds, as reported in [21], approximatively to 2.8 W saving in total power consumption. Hence, reducing the power consumption of networking devices can have a major impact on the total power consumption of the DC.

As switches are the most power hungry networking devices, their power consumption distribution [11] is depicted in Figure 2.4(b). While more than half of the switch power is consumed by chassis, 47% of the power is consumed by line-cards and port transceivers. Power consumption at the port transceivers includes the mandatory OEO conversions. Minimizing the

[1] This accounts for 2% of the global greenhouse gases emission [19].

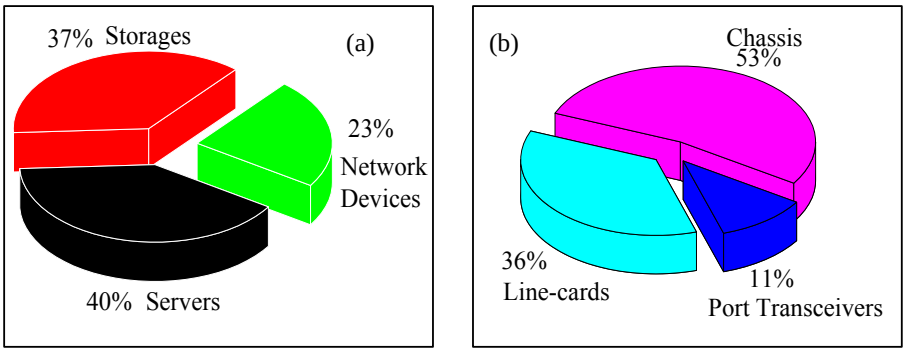

Figure 2.4: (a) Power consumption within the DC that is distributed based on the report in [20]. (b) Power consumption of a typical electrical switch in the DC [11].

OEO conversions can result in reduction of the IT power consumption and thus, can reduce the overall power consumption of the DC.

2.4 Optics for datacenter networking

As we have discussed in the previous sections, current DCs are facing many critical challenges including scalability, power consumption and end-to-end latency. To solve some of these challenges, different hardware and software technologies have been proposed and adapted, such as software defined network (SDN) in the control plane [11] and merchant switch silicon in the architecture [17]. Moreover, several optical network schemes have been presented to provide high bandwidth, reduced end-to-end latency and low power consumption. Optical links using low cost multi-mode fiber (MMF) are commonly used in current DC for short range point-to-point connections between the electrical switches that have employed fiber-based small form-factor pluggable transceivers at 1 Gbit/s up to 10 Gbit/s. Even though MMFs have replaced most of the bandwidth limited copper cables, single mode fiber (SMF) optical cables are currently getting a tremendous attention for long-term solutions as they are more suitable for WDM technologies. Despite point-to-point SMFs and MMFs are playing a crucial role in current DCN as high-capacity (up to 100 Gbit/s [22]) interconnection links, the power consumption of the associated OEO conversions at the fiber-based pluggable transceivers is a major concern especially when the bit rate in-

creases [23]. These OEO conversions in the current DCN are inevitable as the data packet flexibility and routing within the DC are performed using electronic switches.

In order to reduce the power consumption by minimizing the OEO conversions, optical switching technologies have been proposed both for DCN and telecommunication networks. Telecommunication networks have already started using high-capacity optical switching technologies [24]. With the growing demand for higher bandwidth in current DCNs [12], high-capacity all-optical interconnections with switching ability in the optical domain could provide enormous benefits to the DC such as reduced power consumption and higher bandwidth. Many optical interconnection schemes have been researched, as summarized in [25], for DCN over the past years as all-optical or hybrid electronic-optical technologies using circuit or packet connection supporting single or WDM channels.

A hybrid electrical-optical network [26] has been proposed in 2010 to enhance the current DCN. The main advantage of a hybrid network is handling the bandwidth hungry data traffic using optical circuit switches while network flexibility can be achieved using electrical packet switches. However, its main drawbacks are a limited scalability and a high power consumption mainly due to the electrical switches. In [27], a reconfigurable all-optical circuit switches was proposed for high-performance computing (HPC) that can be housed within DCNs. The main advantage of the architecture is a low power consumption as the transceivers can be adjusted according to the available traffic. But, reconfiguration time of the optical circuit switch is very slow that it may not provide the much needed flexibility in the DC.

All-optical packet switching networks [28–30] have been proposed using tunable wavelength converters and all-to-all (cyclic) arrayed waveguide-grating (AWG) router. The wavelength converters were introduced to solve possible wavelength contentions and additional electrical buffer was employed in [28, 29]. In addition to the higher power consumption associated with the electrical buffering, scalability of the AWG router can be limited by the number of wavelength channels. The scalability problem has been addressed in [30] using cascaded cyclic AWG routers. However, the lack of simple wavelength converters and device costs could be the main limitations of such optical networks in DCN.

In order to deal with the current traffic pattern shift in DC, for example around 75% of the traffic flows within the DC [12], flat DCN architectures are currently proposed using the latest optical communications and silicon photonics technologies [4, 6, 31]. Figure 2.5 shows a recently demonstrated

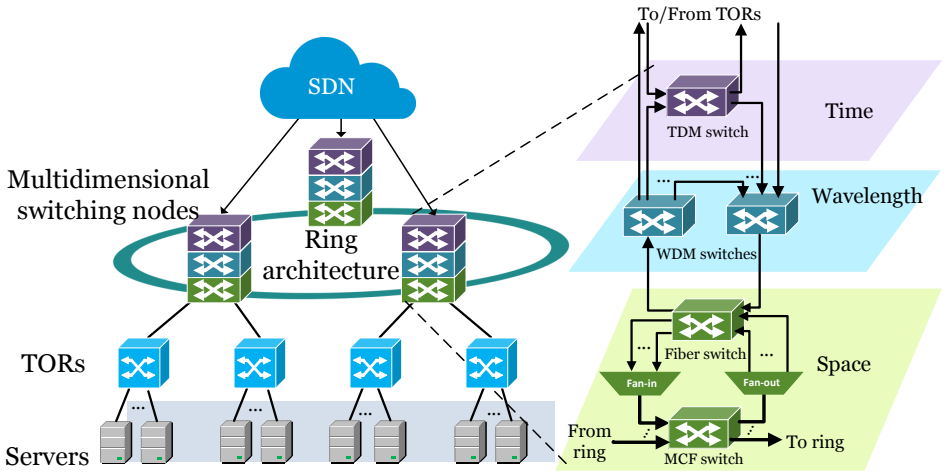

Figure 2.5: Multidimensional (space-wavelength-time) switching using ring topology. The detailed nodes structure shows the switches deployed in each dimension. Courtesy of V.Kamchevska et al [J4].

Tbit-class DC architecture [C7,J4] using the latest off-the-shelf optical devices and seven-core fibers to perform multi-dimensional switching in the space-wavelength-and time-domain. The main purpose of the hierarchical optical switching scenario is to enable each node to perform an aggregated data traffic bypassing at fiber (space) level while allowing adding/dropping of low capacity traffic using reconfigurable WDM and time-slot based optical switches. Even though the SDN controlled ring architecture suites the current traffic flow [32], the fiber and wavelength switches have very slow reconfiguration time while the time-domain optical switches need time-slot reservation before data transmission starts which may lead to large end-to-end latency and inefficient resource utilization.

Another recently proposed compact silicon-photonics based all-optical architecture for HPC nodes is depicted in Figure 2.6 [31]. The proposed network is based on optical core switch fabrics that are configured as many planes of high-port count WDM switches assisted by semiconductor optical amplifier (SOA) as gain medium [33]. Each node in the 64-node HPC machine of Figure 2.6 was proposed to support more than 10 Tbyte/s bandwidth which could be realized using 256 fiber pairs per HPC node, each fiber contained 16 WDM channels operating at 20 Gbit/s. Therefore, the 256 optical switch planes could support a very large bandwidth that can help to

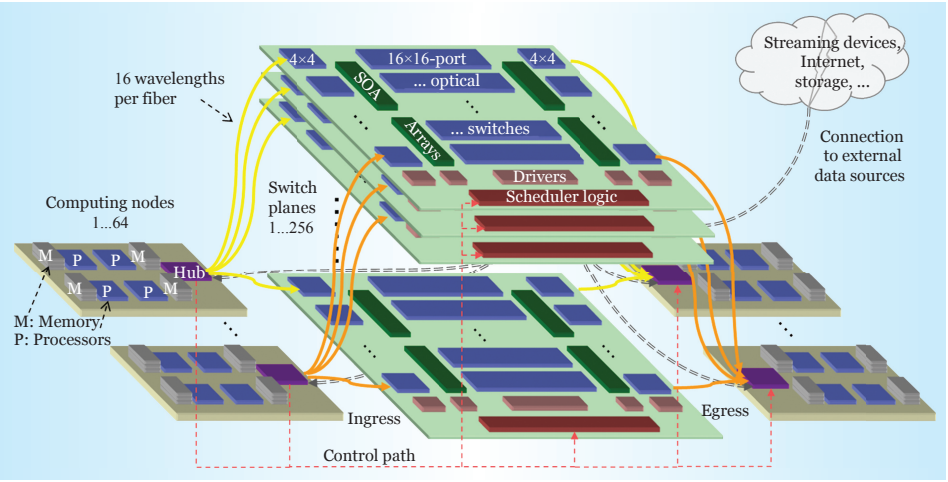

Figure 2.6: A 64-node system interconnected by 256 reconfigurable photonic-switch planes. Each switch plane contains 16 wavelength channels operating at 20 Gbit/s. Such a network could provide the enormous all-to-all bandwidth that may be required to solve large-scale graph applications in real time. Courtesy of L.Schares et al [31]

cope with ever-growing traffic within the DC. The high-radix switch can offer path diversity to minimize latency and maximize throughput by optimizing the schedulers and allocation algorithms. However, reconfiguration time of the circuit based optical network is very slow, hence it may lack the required flexibility for the current highly dynamic DC.

Optical links can easily satisfy the rapidly growing bandwidth demand in current DC. However, the DC traffic demand has two main requirements: high capacity and flexibility. Optics is not mature enough to provide highly flexible services like its electrical counterpart regardless of the ongoing research. To add flexibility in the optical domain, optical buffering is mandatory but it is still at its infancy stage and acquiring the flexibility using OEO is not attractive solution especially for high-capacity data packets. Hence, the current research direction is focusing on bringing the optics to the core switch to deal with the aggregated high-capacity data while electrical technologies are still used at low levels, as TOR for instance, to add flexibility to the aggregated data at much reduced power consumption.

This PhD thesis has addressed the capacity and flexibility demands of short range networks in general, DCs in particular, using serial optical communication based technologies (see Section 3.2). High-capacity (up to

Tbit/s) optical switching scenarios with very-fast reconfiguration time, typically around 10 ns, are proposed and experimentally demonstrated based on the following two assumptions:

- Buffering: Due to the lack of mature optical buffers, we have assumed that electrical buffering technologies can be employed at both ends of the network scenarios: before the high capacity data packets are aggregated and after each high-capacity packet is demultiplexed into lower bit rate tributaries.
- Synchronization: Addressing networking scenarios of a few km range, we have assumed that all devices are well synchronized. Furthermore, optical switching of the high-capacity data packets is performed asynchronously, thus resource reservation and packet synchronization are not required.

Compared to the previously discussed optical network architectures, the serial optical communication based networking scenario can add flexibility to the aggregated high-capacity packets in the optical domain by employing few components that may lead to power consumption and cost savings.

Chapter 3

OTDM packet generation and reception

3.1 Introduction

Since early 90s, OTDM has been extensively researched in parallel with WDM systems, which have been successfully commercialized in the telecommunication industry, for high-speed high-capacity optical communications [34–38]. OTDM has attracted considerable research interests to demonstrate high-capacity transmission systems, high-speed signal processing and monitoring techniques at serial data rates well beyond the speed of the current bandwidth limited electronics. Figure 3.1 summarizes the evolution

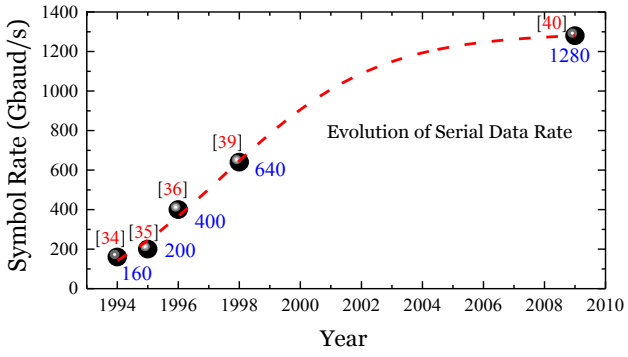

Figure 3.1: Capacity evolution of single polarization serial optical data rates. The results are extracted from published papers [34–36, 39, 40].

of the total capacity of single channel single polarization OTDM systems over the last three decades based on different publications. A 160 Gbit/s serial data generation and reception has successfully demonstrated as early as 1994 in [34]. Impressive error-free experimental results have successfully demonstrated for 200 Gbit/s [35] and 400 Gbit/s [36] OTDM data over transmission distances of 100 km and 40 km, respectively.

The first single polarization 640 Gbit/s serial data transmission over 60 km fiber span has been reported in 1998 [39]. However, highlight of the evolution is reaching the record-high symbol rate of 1.28 Tbaud/s which has been reported for the first time in [40]. Even though scaling the symbol rate of a single polarization serial data beyond 1.28 Tbaud/s remains a challenge up-to-date, the capacity has been further increased up to 2.56 Tbit/s [41], 5.1 Tbit/s [42] and even 10.2 Tbit/s [43] by using polarization-division multiplexing (PDM) and advanced modulation formats. Besides capacity upgrade, spectral efficiency of OTDM systems has also attracted noticeable research interest. Recently, 1.28 Tbaud Nyquist optical time-division multiplexing (N-OTDM) serial data transmission have been demonstrated over 100 km single mode fiber (SMF) [44] and 67 km 7-core fiber [C4], enabling both high-capacity and highly spectral efficient. In [C3], 43 Tbit/s single laser data generation using space-, wavelength-, time- and polarization-division multiplexing and transmission over 67 km 6-core fiber has been performed in which each core consists of 6-WDM×1.2 Tbit/s N-OTDM - PDM - quadrature phase-shift keying data.

In addition to the capacity and spectral gain, OTDM based optical networks have the potential to offer a genuinely flexible bandwidth on demand like their counter-part electrical time-division multiplexing (ETDM) based networks, but up to at burst symbol rates of Tbaud/s [37, 38] which is well beyond the electronics. In this chapter, we start our discussion with an optical network scenario for high-capacity short range networks using ultra-high speed serial data packets where lower bit rate tributaries are aggregated into a high-capacity packet, optically switched based on an optical header and converted back into lower bit rate tributaries. This network scenario, presented in Section 3.2, can be advantageous to reduce switching-energy-per-bit at the optical switch as all lower bit rate data packets are switched as one high-capacity packet.

In Section 3.3, we discuss generation of the high-capacity data packets using an ultra-short optical pulse source based standard OTDM transmitter. 640 Gbit/s and 1.28 Tbit/s serial data packets are optically generated corresponding to an aggregate data traffic of 64 and 128 tributary channels

at 10 Gbit/s bit rate, respectively. Section 3.4 investigates how the high-capacity serial data packets can be optical time demultiplexed into their lower bit rate channels using pulse-by-pulse switching and serial-to-parallel conversion techniques. The second technique holds an attractive features in terms of power efficiency because of its unique ability to convert the serial data packet into many lower bit rate packets simultaneously.

3.2 High-capacity optical network scenario

An optical network scenario of high-capacity serial data packets is depicted in Fig. 3.2 which is referred to as straw-man architecture of our work in this thesis. We envisage an optical networking system consists of M high-capacity optical networks acting as transmitters (senders), N

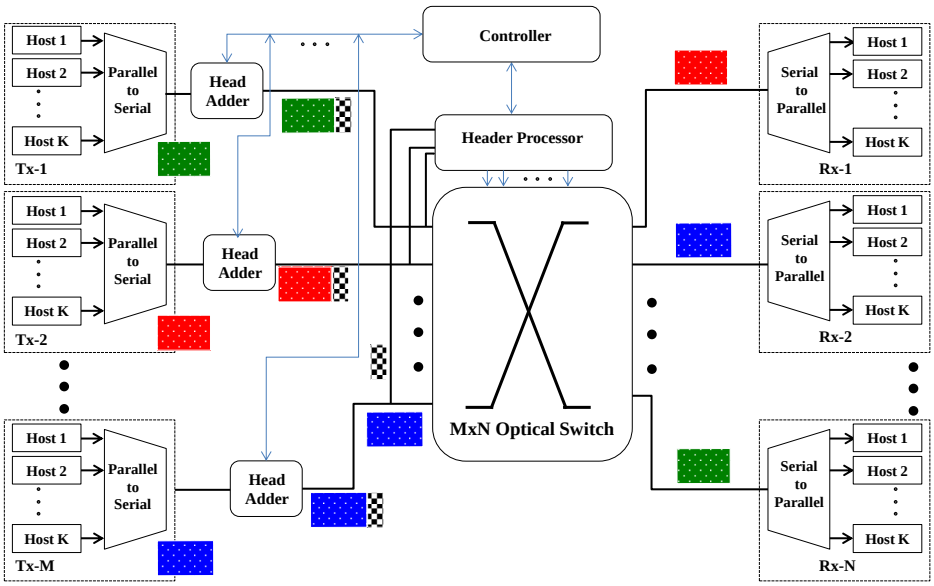

Figure 3.2: Sketch of an envisaged optical network scenario for short range networks using high-capacity serial data packets. M transmitter networks (Tx) are interconnected with N receiver networks (Rx) using a M×N high-capacity switch. Lower bit rate tributaries data from K hosts are aggregated into a high-capacity packet at each transmitter network, optically switched based on an optical header, transmitted to their receiver network and converted back into K lower bit rate tributaries.

optical networks as receivers (Rx) of the high-capacity data packets and a M×N optical switch to interconnect them. Five main functionalities are required to fully realize the optical network scenario. They include parallel-to-serial conversion (multiplexing), scalable optical packet-header addition, fast packet-header processing, high-capacity optical switching and serial-to-parallel conversion (demultiplexing). A global control layer, compatible with a dynamic software defined network (SDN) controller, manages the reconfigurable head adder and header processor modules.

Each M high-capacity Tx networks is composed of K source hosts followed by time division multiplexing (TDM) based parallel-to-serial converter module which generates high-capacity packets by aggregating the lower bit rate data of the K sources based on their final destinations. An optical header is appended to each high-capacity data packets using a head adder module. The optical header of each M high-capacity packets is a unique address information which is very helpful to the optical switch to differentiate one high-capacity packet from others. After such high-capacity serial data packets arrive at the optical switch, their optical header is extracted using a header processor module and it generates switch control signals. Each high-capacity serial data packet is then switched based on its extracted switch control signal of the header processor applied to the optical switch. Once the switched data packets are forwarded to their respective Rx networks, they are time demultiplexed into lower bit rate packets using serial-to-parallel converters and finally, received by their destination hosts.

The main advantages of the envisaged optical network scenario are reduced switching-energy-per-bit and the need for fewer components beside its attractive feature to reduce the end-to-end latency. At the optical switch, the power consumed to forward a given data packets is independent of the bit rate [23]. Hence, as the bit rate of the data packets increases, switching-energy-per-bit decreases. Furthermore, serial communication needs fewer components compare to parallel communication. Even though data aggregation at the TDM module may not be straight forward due to a random arrival time of the lower bit rate data, treating them as one high-capacity data packet can overcome congestion at the optical switch and thus may lead to low end-to-end latency.

As a final remark, the PhD work implements the high-capacity serial optical communication based network scenario as follows. The high-capacity data packet generation is investigated in Section 3.3 whereas Section 3.4 explains experimental demonstrations of time demultiplexing techniques. The head adder module is implemented, both in simulation and experimental

demonstrations, in Chapter-4 while the header processor module and optical packet switching are experimentally demonstrated in Chapter-5 and Chapter-6. Hence, this thesis has covered almost all the functionalities of the optical network scenario sketched in Figure 3.2 except the M×N optical switch is experimentally demonstrated only for M=1. For M≥ 2, a packet collision can occur when two or more data packets want to use the same output port at the optical switch and handling such scenario is beyond the scope of this thesis.

3.3 OTDM packet generation

A conventional OTDM transmitter is illustrated in Figure 3.3 where a high-capacity serial data is bit-interleaved at single carrier wavelength from K tributaries working at a base rate (B). The OTDM transmitter basically consists of three parts: a short pulse source, parallel data modulators and passive delay-lines based bit multiplier. The transmitter needs a single pulse source to generate a single wavelength optical pulses, thus enables a given serial optical system to acquire fewer components. Assuming that the pulse source and data modulator modules are synchronized, the symbol rate of the aggregated high-capacity data packet is equivalent to K×B.

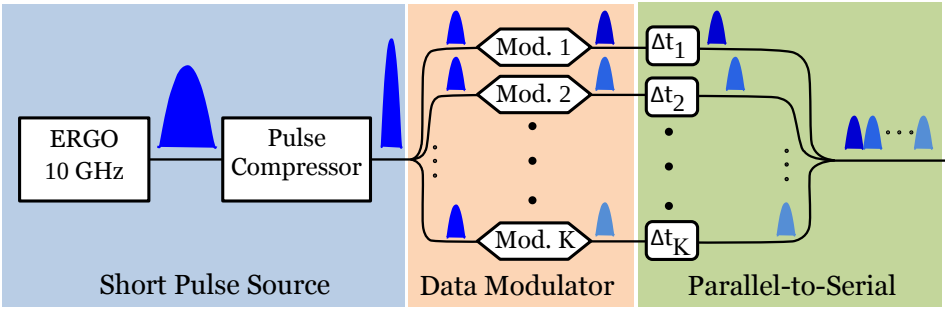

Figure 3.3: Basic OTDM transmitter: a pulsed light source generates short optical pulses at base rate (B) and the pulse duration is further reduced using a pulse compressor. The narrow optical pulses are divided into K arms emulating K independent hosts and data modulated with different user defined pattern. After the modulation, the pulses are precisely delayed by Δt_n for n=1, 2, ..., K and bit-interleaved to constitute a high-capacity (K×B) serial data.

Short pulse source

High quality short pulse sources are essential to generate transform limited, chirp-free and narrow optical pulses with low time jitter. The most popular pulsed light sources that can be applied in the OTDM transmitter are semiconductor mode-locked laser [45], mode-locked fiber-ring lasers [46], gain-switched distributed feedback lasers [47], erbium glass oscillator pulse generating laser (ERGO-PGL) [48] and electroabsorption modulator (EAM) bases optical pulse sources [49]. As shown in Figure 3.3, a 10 GHz ERGO-PGL is used as a pulsed light source in the convectional OTDM transmitter and all the experimental demonstrations of this thesis are carried out using commercially available ERGO-PGL lasers. The ERGO-PGL is a passively mode-locked solid-state laser which relies on a laser diode pumping an erbium-doped glass and a semiconductor saturatable absorber mirror to start and stabilize the pulse forming process.

A standard high-capacity optical systems like Tbaud/s testbeds needs a very narrow optical pulses with handers of fs at full-width at half-maximum (FWHM) of the pulse intensity. Since the sub-picosecond pulses of the ERGO-PGL are too broad for the Tbaud systems, a pulse compressor is often used to reduced the pulse width up to hundreds of fs. The pulse compression is a laborious task due to the burden associated with keeping the original pulse quality unaffected while the initial pulse width should be reduced to the required level. In this thesis, we use an optimized pulse compression module [40, 42, 44] which is constructed using a highly nonlinear fiber (HNLF) to generate a super-continuum by exploiting a nonlinear process called self-phase modulation (SPM) [50] in the HNLF.

Data modulator

The generated ultra-short optical pulses are split into K separate tributary channels and each channel can be return-to-zero (RZ) modulated at bit rate of B with a user defined data. The user data is originated, for example, from each K hosts of a given Tx network shown in Figure 3.2. The data modulation can be performed using an electro-optic based $LiNbO_3$ Mach-Zehnder modulator (MZM) which is the most widely used data modulator albeit being bulky compared to compact EAM [51]. MZM, which works by the principle of interference, can be applied to modulate the optical pulse in amplitude, phase, polarization and carrier frequency [52]. In many laboratory works, the user defined data of each K host is emulated by generating pseudo-random binary sequence (PRBS) bits from a bit pattern

generator (BPG). PRBS is essentially a random sequence of binary numbers which are generated using a linear feedback shift registers. It is "random" in a sense that the value of a given bit of the sequence is independent of the values of any of the other bits. It is "pseudo" because it is deterministic and after 2^n -1 bits it starts to repeat itself, unlike real random sequences, where n is the number of the shift registers. Hence, a sequence of consecutive 2^n-1 bits comprise one data pattern, and this pattern will repeat itself over time. All experimental demonstrations in this thesis are performed using a 2^7-1 PRBS bits generated by a 10 GHz BPG.

Parallel-to-serial converter

As shown in Figure 3.3, each modulated optical pulses are bit-interleaved or time multiplexed to constitute the aggregated high-capacity serial data after they are delayed using K passive delay lines. The passive delay lines can be constructed using an optical fiber or an integrated planner lightwave circuit [53]. In most laboratory works, the parallel-to-serial converter is performed using a bit multiplier module in which only one data modulated tributary channel is enough to generate the high bit rate data. As shown in Figure 3.4, several replicas of the modulated tributary channel are combined together with specific relative delays in cascaded interferometric structures. Each interferometer is constructed using two standard 3 dB (50:50) couplers, a delay line followed by a VOA in the upper arm and adjustable free space optical delay line in the lower arm. The VOA and free space delay line are very useful for precise amplitude equalization and relative delay adjustment of the multiplexed signal at output of each interferometer.

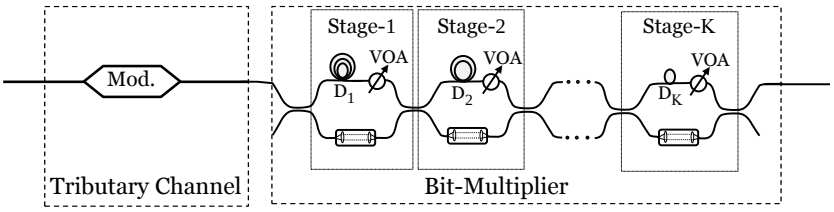

Figure 3.4: A standard bit-multiplier for laboratory works. A high bit rate data packet is generated from a single tributary channel at base rate using K interferometric stages. Each interferometric stage is constructed using delay lines (D_1,D_2,..., D_K) and VOAs at the upper arm, and tunable free space delay lines in the lower arm.

K stages of the time multiplexer sketched in Figure 3.4 multiples the base rate tributary data by 2^K. For example, K=7 multiplexer stages are enough to generate an aggregated 1.28 Tbit/s serial data starting from 10 Gbit/s tributary channel. By introducing a relative delay time longer than the one bit period, a strong decorrelation can be achieved between the adjacent multiplexed bits at the output of each interferometer. Thus, if the modulated data sequence has a specific PRBS pattern, the pattern can also be preserved at all bit-multiplier stages by employing relative delay time equals to half of the pattern length of the PRBS at the input of each stage. For example, to preserved 2^7-1 PRBS pattern of a 10 Gbit/s tributary channel, the relative delays at stage-1 equals to (127/2)·T=6.35 ns where T is 100 ps (1/10 Gbit/s), at stage-2 equals to 3.175 ns ((127/2)·T where T is 1/(20 Gbit/s)=50 ps) and so on. To achieve such relative delays, length of D_2 at stage-2 is set to half of D_1 at stage-1 and so on.

3.3.1 640 Gbit/s data packets

As previously mentioned, a standard OTDM transmitter is made-up of an optical pulse source, a pulse compressor, a data modulator and a bit-multiplier modules. Figure 3.5 shows the experimental setup of a high bit rate transmitter that generates 640 Gbit/s serial data packets. An ERGO-PGL at 1542 nm is used to generate optical pulses at a repetition rate of 10 GHz and a FWHM pulse width of 1.5 ps. After the optical pulses are amplified, they are filtered using a 5-nm wide optical band-

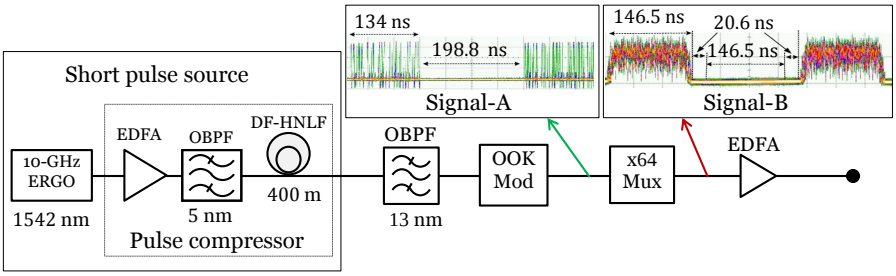

Figure 3.5: Experimental setup of a 640 Gbit/s transmitter. 10 GHz optical pulses are OOK modulated with PRBS bits followed by sequence of zero after their pulse width is reduced in a pulse compressor. The 10 Gbit/s data is then bit-interleaved using a 2^7-1 PRBS preserving multiplexer to constitute a 640 Gbit/s serial data packet.

pass filter (OBPF) to remove out-of-band noise. The pulse width is further reduced using a super-continuum generation based pulse compression in a 400 m of dispersion-flatten highly nonlinear fiber (DF-HNLF) [50]. The super-continuum generation is performed by exploiting SPM in the DF-HNLF which has a dispersion of -0.45 ps/nm/km and dispersion slope of 0.006 ps/nm^2/km at 1550 nm and a nonlinear coefficient of 10.5 W^{-1}km^{-1}. The FWHM duration of the compressed pulses is reduced to 560 fs after off-carrier filtering using a 13-nm wide OBPF centered at 1552 nm.

The spectrum of the optical pulses at the output of the ERGO-PGL is shown in Figure 3.6(a) which also depicts the super-continuum spectrum before and after off-carrier filtering. Autocorrelation traces of the optical pulse before and after compression are depicted in Figure 3.6(b) using the solid and dotted lines, respectively. The autocorrelation traces are generated based on second-harmonic generation (SHG) [50, 54].

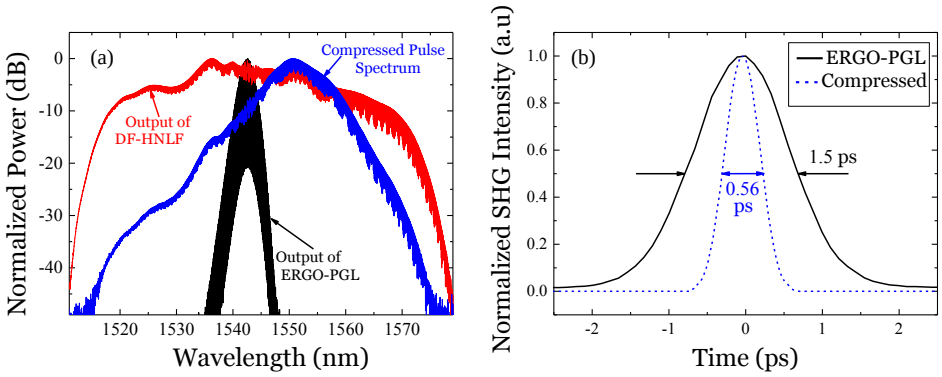

Figure 3.6: (a) Spectra of an optical pulse at the output of the ERGO-PGL (black) and after the pulses are broaden in the DF-HNLF (red). The spectrum of the compressed pulses (blue) is achieved by off-carrier filtering the super-continuum. (b) Autocorrelations of the ERGO-PGL optical pulses (solid line) and the compressed pulses (dotted line).

The ultra-short pulses are encoded using a OOK modulation format with a 10 Gbit/s custom pattern in a $LiNbO_3$ MZM. The custom pattern is provided by a BPG which is programed to generate a certain number of 2^7-1 PRBS bits as data payload followed by a fixed sequence of zero bits. Amplitude modulation using such custom pattern enables generation of optical data packet as shown in the inset of Figure 3.5 (signal-A). The sequence of zero bits are introduced to reserve the free-time slot for

inter-packet gaps and packet multiplexing. The OOK modulated pulses are multiplexed using a 2^7-1 PRBS preserving bit interleaver (see Figure 3.4) to constitute the 640 Gbit/s serial data packet. Duration of the multiplexed data packet is increased by 12.5 ns from 134 ns at 10 Gbit/s to 146.5 ns at 640 Gbit/s (refer signal-B in Figure 3.5) due to the large relative-delays introduced in the bit-multiplier stages to preserve the 2^7-1 PRBS sequence. For instance, the first stage of the bit multiplier introduces a relative delay of (127/2)·T=6.35 ns where T is 100 ps (1/10 Gbit/s), hence the packet length at 20 Gbit/s is 6.35 ns longer than at 10-Gbit/s.

Duration of the optical packet can be quite flexible as it solely depends on the total number of the PRBS bits. In all experiments, duration of the data packets are adapted from IEEE 802.3 standard [55] for 10 Gbit/s which states that the normal frame size have to be in the ranges 51.2-1214.4 ns. In [C2], duration of the data is defined using 1340 PRBS bits corresponds to 134 ns (see Signal-A in Figure 3.5). Burst Internet traffic have a duration that varies from very short control signal to very large jumbo packets. In order to emulate such traffic, a variable length custom patterns are generated using 2304 bits 2^7-1 PRBS followed by 4444 zero bits and 1024 bits of 2^7-1 PRBS followed by 8576 zero bits in [C5]. Durations of the two data packets after being bit-interleaved using the 2^7-1 PRBS preserving multiplexer are 234 ns and 115 ns.

3.3.2 1.28 Tbit/s data packets

Until now, 1.28 Tbaud is the highest achieved symbol rate in serial optical communications. As all the 1.28 Tbaud/s works have been reported based on continuous optical pulses, it can be interesting to generate Tbaud data packets to experiment high-capacity highly flexible optical networks. Figure 3.7 shows an experimental setup of a 1.28 Tbit/s transmitter which is constructed in similar way as the 640 Gbit/s transmitter.

A 10 GHz ERGO-PGL generates an optical pulses centered at 1557 nm with FWHM of 1.5 ps which is too broad for Tbaud packets. FWHM of the optical puses is then reduced using the pulse compressor to 0.4 ps after they are filtered at 1548 nm using a 16-nm wide OBPF. The ultra-short pulse is then data modulated using OOK with a 10 Gbit/s custom pattern of 1411 bits of 2^7-1 PRBS bits as data payload followed by 2173 zero bits, which are used to reserve a free time slot for packet multiplexing and inter-packet gap. A 1.28 Tbit/s serial data packet is then generated using a 2^7-1 PRBS preserving bit interleaver. The 1.28 Tbit/s data packets corresponds to aggregated data traffic of 128 tributary channels working at

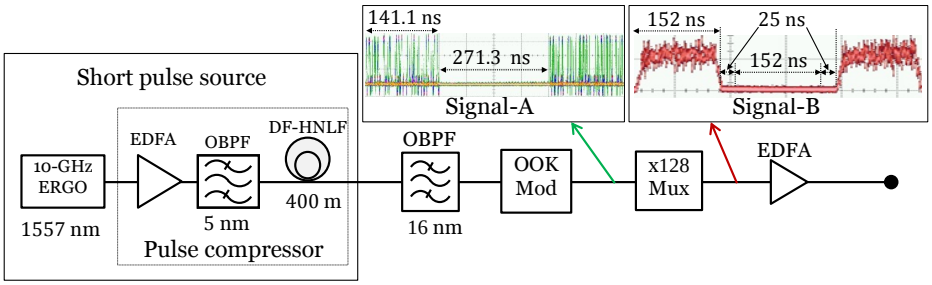

Figure 3.7: Experimental setup of a 1.28 Tbit/s transmitter. 10 GHz ultra-short optical pulses are OOK modulated and bit-interleaved using a 2^7-1 PRBS preserving multiplexer to constitute a 1.28 Tbit/s data packet.

base rate of 10 Gbit/s. In Figure 3.7, inset signal-A and signal-B represent oscilloscope traces of a 141.1 ns long 10 Gbit/s and a 152 ns long 1.28 Tbit/s data packets, respectively. Section 4.5.2 deals with optical labeling of the generated 1.28 Tbit/s data packet while Section 6.5 presents an optical switching scenario of the labeled Tbit data packets.

3.4 OTDM packet reception

After transmission and switching, the high-capacity serial data packets should be successfully received and processed. Even though enormous effort has been made to increase the speed of photodiodes (PDs), for example >100 GHz [56], it is still well below the required bandwidth to receive such a high-capacity serial data. Normally, successful reception of a given high-capacity serial data packets is achieved using a typical OTDM receiver sketched in Figure 3.8. The high-capacity serial data, aggregated from K tributary channels, is converted back into M ($1 \leq M \leq K$) lower base rate channels and successfully received by M receiver hosts. A clock recovery circuit extracts a base rate control signal from the high-capacity serial data and uses it to synchronize the demultiplexer and receiver hosts.

Converting a given high-capacity serial data into many lower bit rate parallel channels perfectly matches the network scenario depicted in Figure 3.3. However, in contrast to the parallel-to-serial converter of the OTDM transmitter which relies only on passive delay lines, the serial-to-parallel converter of the OTDM receiver is a more challenging task as it needs a recovered control signal. Moreover, all the tributary channels of the high-

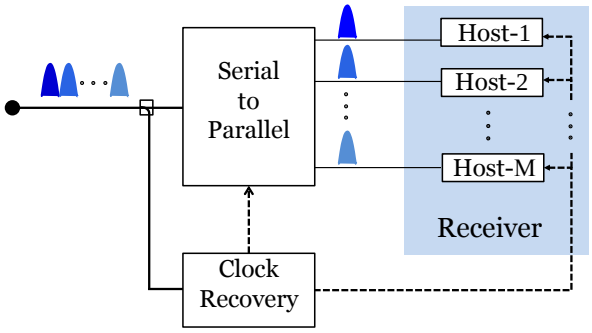

Figure 3.8: Basic OTDM receiver: high-capacity data aggregated from N tributary channels is converted back to M lower base rate tributaries using an optical demultiplexer and detected by M receivers. A clock recovery circuit extracts the base rate control that can be used to synchronize the demultiplexer and receiver.

capacity data may not be converted at once mainly due to fiber bandwidth limitation and working principle of the serial-to-parallel converter.

Extracting a base rate channel from 640 Gbit/s and 1.28 Tbit/s serial data needs a very narrow switching gate that opens for very short duration (typically <1 ps) covering only a single pulse. The serial-to-parallel converter should work based on processes that have a very fast response time, making Kerr-effect based non-linear processes the first candidate due to their instantaneous (<10 fs) response time [50]. The non-linear optical loop mirror (NOLM) [39, 57] and Kerr shutters [58] are the two well-know fiber-based switches employed to demultiplex a given high-capacity serial data down to its tributary channels. In addition to silica fiber based switching, time demultiplexing experiments have been demonstrated using a semiconductor optical amplifier (SOA) [59], semiconductor laser amplifiers [60] and chalcogenide waveguide [61]. These demultiplexing techniques can only extract a single tributary channel from the high-capacity serial data because of their work principles. Considerable effort has been made to simultaneously demultiplex several tributary channels using a number of schemes. Time lens base serial-to-parallel converter is one of the widely used techniques for simultaneous demultiplexing by applying parametric processes such as four-wave mixing (FWM) [62].

In Section 3.4.1, we employ a pulse-by-pulse switching using the NOLM to demultiplex a 640 Gbit/s serial data packet into its 10 Gbit/s tributary

channels that are successfully detected using a direct detection receiver. In Section 3.4.2, a 1.28 Tbit/s serial data packet is dempltiplexed into many simultaneous 10 Gbit/s tributary channels using a time lens based serial-to-parallel converter. Addressing short range networks of a few km range, we assume that clock recovery module is not required. The control signal of the serial-to-parallel converter is either taken directly from the short pulse source or co-propagated with the data packet.

3.4.1 Pulse-by-pulse switching

Demultiplexing techniques that extract a single tributary channel out of the high-bit rate serial data can be referred as pulse-by-pulse switches. In this section, a simplified working principle of the NOLM is presented followed by an experimental demonstration of the NOLM as pulse-by-pulse switch to demultiplex 640 Gbit/s serial packets into 10 Gbit/s tributary channels.

Working principle

The working principle of the NOLM is based on a nonlinear Sagnac interferometer switch [63]. As shown in Figure 3.9, the NOLM is constructed by connecting output ports of a standard 3-dB coupler into a fiber loop with a nonlinear medium such as HNLF which acts as phase-shifting element. The fiber loop is also composed of an additional standard coupler as a base rate control signal inlet to the loop and a polarization controller to control the polarization state of the signal circulating in the loop.

A high-capacity serial data, denoted by its field $\mathbf{E}_{data}$, is injected into the standard 3-dB coupler of the NOLM shown in top of Figure 3.9. The 3-dB coupler splits the serial data into two signals: a clock-wise ($\mathbf{E}_{cw} = \sqrt{1/2}\mathbf{E}_{data}$) and a counter clock-wise ($\mathbf{E}_{ccw} = i\sqrt{1/2}\mathbf{E}_{data}$) signal, which traverse the fiber loop in opposite direction. $\mathbf{E}_{cw}$ and $\mathbf{E}_{ccw}$, which defer by $\pi/2$ due to nature of the coupler, will be recombined by the same coupler after the round trip and will accumulate an extra by $\pi/2$ difference. The two output fields of the NOLM can expressed as:

$$\mathbf{E}_r = \sqrt{1/2}\mathbf{E}_{ccw} + i\sqrt{1/2}\mathbf{E}_{cw} = i\mathbf{E}_{data} \tag{3.1}$$

$$\mathbf{E}_t = \sqrt{1/2}\mathbf{E}_{cw} + i\sqrt{1/2}\mathbf{E}_{ccw} = 0 \tag{3.2}$$

where $\mathbf{E}_r$ and $\mathbf{E}_t$ are reflected and transmitted fields, respectively. Without any external source, the two counter prorating will interfere constructively and destructively at each input of the 3-dB couplers in such a way that the

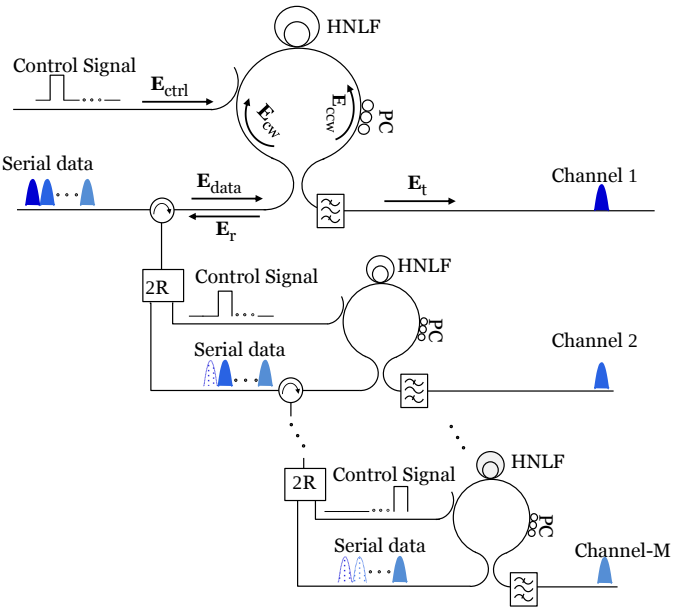

Figure 3.9: The NOLM as serial-to-parallel converter. The first stage depicts working principle of the NOLM as pulse-by-pulse switch. M NOLM stages are cascaded to demultiplex M tributaries.

entire signal will be reflected, $\mathbf{E}_r$, as shown in Equation 3.1 and 3.2. The word "mirror" in the NOLM is coined from this working principle.

In the presence of a high intensity base rate control signal, $\mathbf{E}_{ctrl}$, at different carrier wavelength, the unidirectional $\mathbf{E}_{ctrl}$ creates a phase shift on one tributary channel of the $\mathbf{E}_{cw}$ signal[1] via cross-phase modulation (XPM) in the HNLF. Assuming that the $\mathbf{E}_{cw}$ and $\mathbf{E}_{ctrl}$ signal have the same group velocity to neglect walk-off effect and are in the same linear polarization state, the XPM induced phase shift on $\mathbf{E}_{cw}$ from $\mathbf{E}_{ctrl}$ can be written as:

$$\Delta\phi = 2\gamma L P_{ctrl} \tag{3.3}$$

where γ and L are nonlinear coefficient and length of the HNLF whereas P_{ctrl} is the temporal power profile of the control signal. $\mathbf{E}_r$ and $\mathbf{E}_t$ can be rewritten, after XPM induced phase shift, as:

$$\mathbf{E}_r = \frac{i}{2}\mathbf{E}_{ccw}[exp(-i\Delta\phi) + 1] \tag{3.4}$$

[1] $\mathbf{E}_{ccw}$ can also experience a phase shift [63] that may affect the switching performance but such phase shift is neglected [64] in our discussion.

$$\mathbf{E}_t = \frac{1}{2}\mathbf{E}_{ccw}(exp(-i\Delta\phi) - 1) \tag{3.5}$$

The transmissivity: T=$|\mathbf{E}_t|^2/|\mathbf{E}_{data}|^2$ and reflectivity: R=$|\mathbf{E}_r|^2/|\mathbf{E}_{data}|^2$ of the NOLM at the inputs of the 3-dB (50:50) coupler can defined as:

$$T = \frac{1}{2}(1 - cos(\Delta\phi)) \tag{3.6}$$

$$R = \frac{1}{2}(1 + cos(\Delta\phi)) \tag{3.7}$$

When $\Delta\phi = 0$ (in the absence of the control signal), T=0 and R=1 which means all tributaries of the serial data will be reflected. Whereas, when $\Delta\phi = \pi$, the tributary channel overlapping with $\mathbf{E}_{ctrl}$ will be transmitted (as T=1 and R=0) while the other channels will be reflected. As shown in Equation 3.3, $\Delta\phi$ is directly proportional to the P_{ctrl} and by adjusting the input power of $\mathbf{E}_{ctrl}$, it is possible to achieve $\Delta\phi = \pi$ and demultiplex the tributary of our interest for example channel-1 at the first NOLM shown in Figure 3.9.

As pulse-by-pulse switch, the NOLM can be used to drop a signal tributary channel at a time from the high-capacity serial data. To demultiplex M simultaneous tributary channels, it is inevitable to employ M cascaded NOLM stages. Figure 3.9 shows a block diagram of a serial-to-parallel converter using M NOLM stages connected in series. After the first NOLM takes the serial data and the control signal, the first tributary is demultiplexed as channel-1. The remaining serial data and the control signal are reflected at the NOLM and guided by an optical circulator to the second NOLM. The second tributary is demultiplexed at the second NOLM after the serial data and control signal are amplified, re-timed, delayed[2] and split using a 2R optical module and so on. Finally, the last tributary is demultiplexed using the last NOLM as channel-M. Compared to time lens based serial-to-parallel converter, the NOLM as serial-to-parallel converter is bulky as it is fiber based. However, single NOLM is enough for our experimental demonstrations as all tributary channels can be received one by one using a tunable delay line.

Experimental demonstration

The experimental setup shown in Figure 3.10 is the NOLM based optical time demultiplexing of a 640 Gbit/s serial data packet to 10 Gbit/s tribu-

[2]The control signal is delayed by one-time, for example 1.56 ps for 640 Gbit/s data packet, so it will overlap with the second tributary.

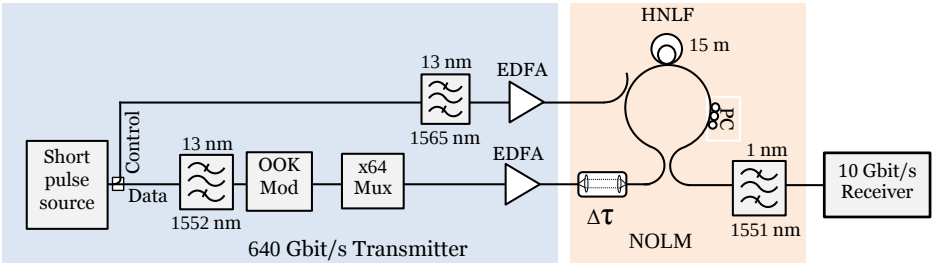

Figure 3.10: Experimental setup for optical time demultiplexing of 640 Gbit/s serial packet into 10 Gbit/s tributary channels using the NOLM.

tary channels. A high-capacity serial data with packet duration of 146.5 ns is generated by bit-interleaving a OOK modulated 0.56 ps wide optical puses at the 640 Gbit/s transmitter. After amplification, the 640 Gbit/s data packet is launched into the NOLM. A 10 GHz control pulse is taken from the control arm of the 640 Gbit/s transmitter module and coupled to the NOLM after it is filtered using a 13-nm wide OBPF centered at 1565 nm. The control pulse is used as gating window by introducing a proper phase shift to one tributary channel of the clock-wise propagating data signal using XPM inside a 50 m of HNLF. The HNLF has a γ =10.5 $W^{-1}km^{-1}$, zero dispersion wavelength λ_0=1551.8 nm and a dispersion slope of 0.018 ps/(nm^2.km) at 1550 nm. The dempltiplexed 10 Gbit/s data, is filtered out at 1551 nm using a 1-nm wide OBPF and sent to a 10 Gbit/s receiver for bit-error ratio (BER) measurement.

An autocorrelation trace of the 640 Gbit/s serial data packet and control signal are shown in Figure 3.11(a) using a solid and dotted lines, respectively. Figure 3.11(b) shows spectra of the 640 serial data packet centered at 1552 nm, the 10 GHz control signal centered at 1565 nm and a demultiplexed 10 Gbit/s channel centered at 1551 nm. Using a tunable free space delay line at the input of the NOLM, all the 64 tributary channels can be demultiplexed by introducing the right amount of delay in the range of $0 \leq \Delta\tau \leq$100 ps and time-overlapped with the control pulse.

Figure 3.11(c) shows eye diagrams of a 10 Gbit/s optical time demultiplexed channel using the NOLM from the 640 Gbit/s serial data packet. System performance of the OTDM transmitter and receiver is investigated using BER measurements of the 64 tributary channels in which they all achieve a BER $\leq 10^{-9}$. Figure 3.11(d) shows receiver sensitivity of all demultiplexed channels measured at BER $\leq 10^{-9}$. The average receiver sensitivity of all the channels is -33.75 dBm whereas the maximum variation

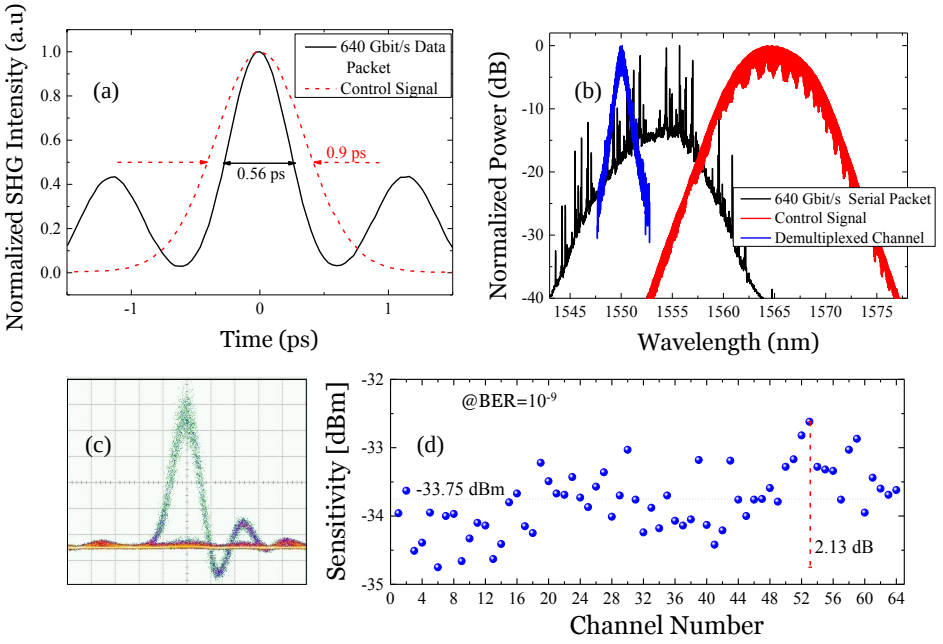

Figure 3.11: (a) Auto-correlation traces of a 640 Gbit/s serial data packet (solid line) and a control signal (dotted line). (b) Spectra of a 640 serial data packet, a 10 GHz control signal and a demultiplexed 10 Gbit/s channel centered at 1552, 1565 and 1551 nm, respectively. (c) An eye diagram trace of a 10 Gbit/s demultiplexed channel. (d) Receiver sensitivity, at BER of 10^{-9}, of all 64 tributary channels of a 640 Gbit/s serial data packet after it is time demultiplexed using the NOLM.

in sensitivity is 2.13 dB. The time traces of each demultiplexed tributary channel is similar to the signal-A trace shown in Figure 3.5 which consists of 134 ns data followed by 198.8 ns empty time slot. Almost all the optical power of each channel is carried by the data which accounts for 40% of the total duration. Hence, the receiver sensitivity is calibrated by 4 dB which corresponds to 40% duty cycle. Such calibration is applied for all experiments that involve the NOLM.

3.4.2 Serial-to-parallel conversion

A bit rate and modulation format independent serial-to-parallel converter is a key functionality to fully receive and process each high-capacity serial

data packets in optical packet networks, for example, the network scenario depicted in Figure 3.2. A WDM grid [65] compatible time lens based serial-to-parallel converter has been proposed for simultaneous demultiplexing of all channels of a 320 Gbit/s [66], most channels of a 640 Gbit/s [66, 67] and several channels of a 1.28 Gbaud [44] serial data via FWM in nonlinear devices. The main attractive features of the time lens based optical time demultiplexing technique are a reduced complexity and lower power consumption due to its ability to convert a given high-capacity serial data into many lower bit rate parallel tributary channels. In this section, we discuss the working principle of the time lens based serial-to-parallel converter and present an experimental demonstration of a serial-to-parallel conversion of a 1.28 Tbit/s data packet into many 10 Gbit/s data packets.

Working principle

Space-time duality [68], based on a mathematical analogy between paraxial diffraction of a space-confined beam and the propagation of an optical pulse in a dispersive medium, has been employed as a promising technique to implement ultra-fast optical signal processing functionalities such as pulse compression [69] and temporal imaging [70]. The envisaged serial-to-parallel conversion which is also called time-to-frequency conversion [44,67], can be demonstrated using this concept. Extending the duality to lenses, the equivalent of thin lens effect on a spatial beam is a quadratic phase modulation on the temporal profile of an optical pulse. The device that imparts a quadratic phase on the optical pulses is often referred as "time lens" [62]. A serial-to-parallel conversion can be achieved by introducing an accumulative dispersion D on a given waveform in a dispersive element followed by quadratic phase modulating it with a linear chirp rate C=1/D [67]. Hence, the time profile of a bit interleaved pulses spaced by a time interval Δt can be mapped into frequency interleaved WDM channels spaced by $\Delta\omega = \Delta$tC (as detailed in [67]). In principle, the frequency spacing of the WDM channels $\Delta\omega$ can adjusted according to our interest by introducing a proper D and C on the serial data.

Accumulated dispersion can easily introduced using very dispersive media, for example dispersion compensating fiber (DCF), whereas quadratic phase modulation can be imparted on the optical pulses using a quadratic voltage driven phase modulator [68] and parametric processes such as FWM [62] and sum-frequency generation [70]. The chirp rate induced by the phase modulator is inadequate because of the limitation on the maximum driving voltage that can applied on the modulator. Unlike sum-frequency

generation that can happen using second-order nonlinearity, FWM occurs by exploiting third order Kerr nonlinearity in a well know devices such as silica glass and silicon.

Figure 3.12 shows a working principle of the time lens based serial-to-parallel conversion which is implemented using FWM-based quadratic phase modulation. First, the OTDM serial data and the control signal (running at base rate equivalent to the repetition rate of each OTDM tributary channel), are propagated though dispersive media to accumulate dispersion D_{data} and D_{ctrl}, respectively. While propagating through the dispersive media both the data and control pulses become broader in the time domain and gain a linear chirp at rates of $1/D_{data}$ and $1/D_{ctrl}$ as shown in the horizontal axis of Figure 3.12. Then, the FWM-based quadratic phase modulation is imparted to the broadened data pulses at a rate of $C_{data}=1/D_{data}$ to cancel the dispersive chirp. During the FWM process in a nonlinear medium, the high-capacity serial data is converted into lower bit rate parallel tributary (WDM) channels which combine the phase of the control signal and the complex conjugate of the serial data [67]. In FWM processes, the field of converted channel, also called idler, is directly proportional to the square of the control field. So, the following condition should be fulfilled in order

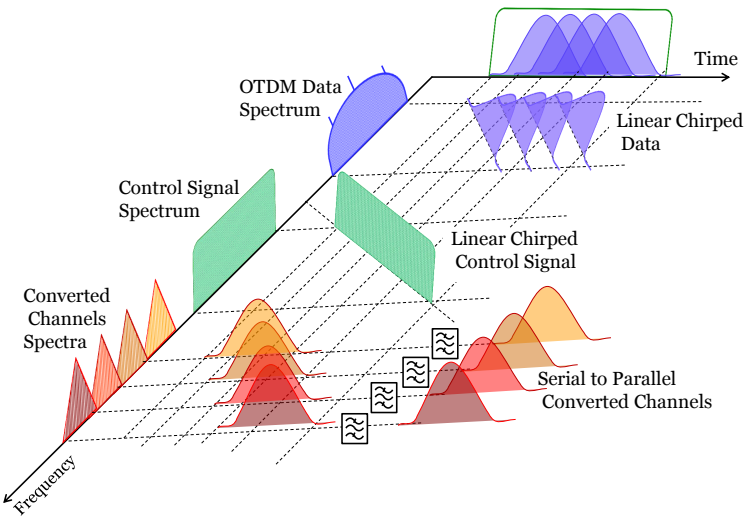

Figure 3.12: Time lens based serial-to-parallel conversion using FWM in a HNLF. A dispersed high-capacity serial data packet is launched together with a linearly chirped control signal to convert the serial data into parallel WDM channels. Sketch is kindly adapted from [71].

to achieve a successful time lens based time to frequency conversion:

$$C_{ctrl} = C_{data}/2 \quad \Leftrightarrow \quad D_{data} = D_{ctrl}/2 \tag{3.8}$$

where C_{ctrl} is the linear chirp rate of the control signal. Equation 3.8 states that the control signal should be broadened twice as much as the data pulses before the quadratic phase modulation is applied. The FWM-based quadratic phase modulation is achieved over the temporal broadening of the control pulse. Hence, the number of convertible tributary channels is related to temporal extension of the broadened control pulses.

Experimental demonstration

Figure 3.13 shows a 1.28 Tbit/s serial data packet reception using the previously discussed time lens based serial-to-parallel converter after the Tbit data packet is generated (refer Section 3.3.2) and co-propagated with a 10 GHz control signal over an optical link. The control signal, centered at 1565 nm, is used in the time lens based serial-to-parallel converter module. The dispersion compensated short optical link is made up of 3 km of SMF followed by a 500 m of DCF.

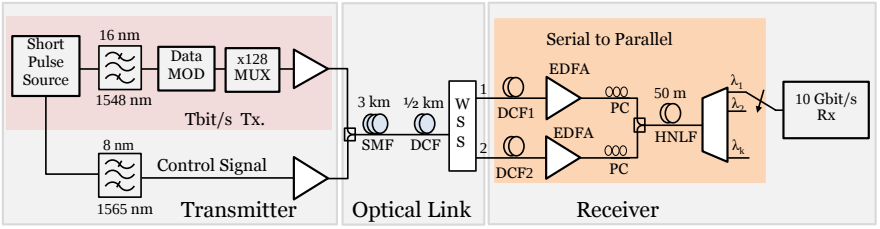

Figure 3.13: Experimental setup for time lens based serial-to-parallel conversion where a 1.28 Tbit/s serial data packet is optical time demultiplexed into K 10 Gbit/s tributary channels simultaneously.

After the Tbit data packet and control signal are separated using a wavelength selective switch (WSS), they are sent into the time lens based serial-to-parallel converter. The 1.28 Tbit/s packet can be optically time demultiplexed into many parallel 10 Gbit/s tributary channels using the effect of a second order chromatic dispersion (β_2) followed by a FWM - based quadratic phase modulation [44]. Hence, the Tbit data packet is passed through a DCF1 with D= $\beta_2 L_{DCF1}$= 1.243 ps^2 while the optical control pulse is dispersed using DCF2, $\beta_2 L_{DCF2}$=2.486 ps^2. L_{DCF1} and L_{DCF2} are length of the DCF1 and DCF2, respectively.

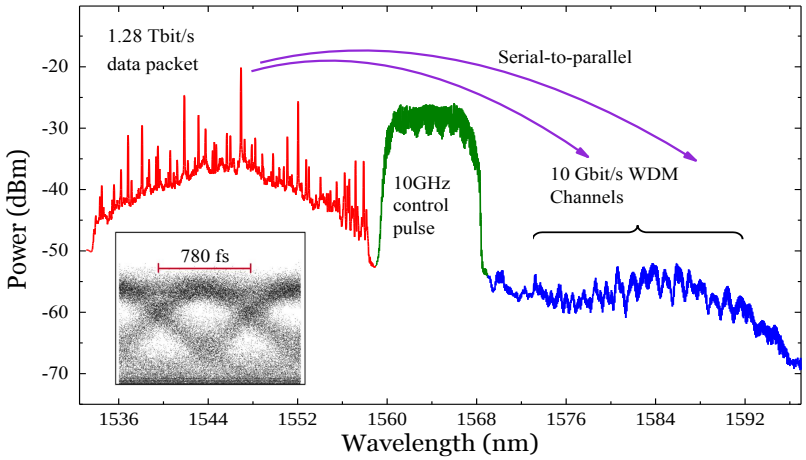

Figure 3.14: Power spectra of a 1.28 Tbit/s data packet, an optical control pulse and generated idler at the output of the HNLF. Inset shows an optical eye diagram of the 1.28 Tbit/s.

To map the demultiplexed 10 Gbit/s channels into a 100 GHz frequency spacing ($\Delta\omega$), compatible with a standard WDM grid [65], the required chirp rate for the 1.28 Tbit/s data is K=1/D= $\Delta\omega/\Delta$t; where Δt is a bit-slot time. The optical control pulse is also linearly chirped with a rate of K/2 as it is dispersed twice of the Tbit data packet. Inset of Figure 3.14 shows an optical eye diagram of the 128 Tbit/s data using a sampling oscilloscope with a timing resolution of 1 ps. The 1.28 Tbit/s bit-slot (Δt) is 0.78 ps, thus the eye appears slightly distorted. The dispersed data packet and control pulse are now amplified and launched together into a 50 m of HNLF: λ_0=1565 nm and γ =10 $W^{-1}km^{-1}$. FWM is exploited inside the HNLF to map the individual 10 Gbit/s data channels to different wavelengths by mixing the phases of the linearly chirped control pulse and the dispersed Tbit data packet. Figure 3.14 shows the spectra of the 1.28 Tbit/s serial data, optical 10 GHz control pulse and converted parallel 10 Gbit/s channels at the output of the HNLF. The control signal is filtered using a super-Gaussian transfer function in the WSS and the resultant spectrum is top flat [67]. Finally, the 10 Gbit/s WDM channels are filtered out using a 40 GHz wide tunable OBPF.

Performance of all the time demultiplexed tributary channels is evaluated through BER measurements. The optical signal-to-noise ratio (OSNR) of the Tbit input data signal to the HNLF is fixed to 36 dB which is

a theoretical limit of RZ-OOK data to achieve error free performance at 1.28 Tbit/s [52]. Like in the NOLM, all the 128 tributaries of the Tbit packet are first demultiplexed by introducing the right amount of delay using a tunable free space delay line at the input of the serial-to parallel converter. The BER measurements of all the tributary channels is shown in Figure 3.15(a). All the 128 demultiplexed 10 Gbit/s channels achieved BER performance well below the forward error correction (FEC) of 3×10^{-3} which corresponds to 6.6% overhead, resulting in a bit rate of 1.2 Tbit/s.

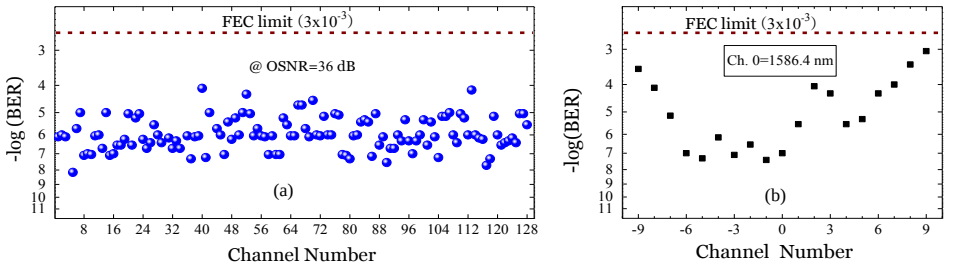

Figure 3.15: (a) BER measurements of all the 128 tributary channels of the 1.28 Tbit/s data packet. (b) BER measurements of simultaneously demultiplexed 19 tributary channels.

Furthermore, Figure 3.15(b) shows the BER measurements, all below FEC limit, of nineteen 10 Gbit/s channels of the 1.28 Tbit/s serial data packet which are simultaneously optical time demultiplexed. The average channel spacing between the nineteen channels is 100 GHz, allowing for commercial arrayed waveguide-grating (AWG) to be used for filtering. In principle, all tributaries may be converted to individual WDM channels simultaneously. In this experiment, however, only 19 channels are converted because we are limited by the fiber bandwidth[3] and the large frequency spacing of the converted WDM channels. However, the large spacing can help to reduce the effect of crosstalk between the converted channels. As shown in Figure 3.15(b), BER performance of the two furthest tributaries (with respect to channel-0 centered at 1586.4 nm) is deteriorated because they may not be fully overlapped with the dispersed control signal.

Introducing FEC for short range networks may not be the best solution as it needs a power hungry digital signal processing (DSP) modules at each M receivers of Figure 3.8. However, considering the practical challenges

[3]we use a narrow (8 nm at 3-dB bandwidth) control signal which is not enough to cover the whole Tbit data spectrum.

associated with bit-interleaving of 128 data modulated ultra-short pulses within 100 ps to constitute a 1.28 Tbaud/s, it remains ultimately difficult task, up-to-date, to receive all tributaries of the Tbaud successfully without the help of DSP.

3.5 Summary

This chapter has described serial optical communication based network scenario for high-capacity data packets, that has been referred as strawman architecture of this PhD thesis. After brief explanation of a standard OTDM transmitter main functional blocks, 640 Gbit/s and 1.28 Tbit/s data packets have been generated using the OTDM transmitter by aggregating data traffic of 64 and 128 tributaries each at 10 Gbit/s, respectively. The 10 Gbit/s tributary data has been packetized using OOK modulation with a certain number of 2^7-1 PRBS bits followed by a fixed sequence of zero bits. Amplitude modulation using such custom pattern has enabled generation of high-capacity serial data packets with flexible durations as it depends on the number of 2^7-1 PRBS bits. A successful reception of the packetized 640 Gbit/s and 1.28 bit/s serial data packets have been investigated using two well known optical demultiplexer schemes. System performance including the high-capacity data packatization and demultiplexing have been measured using BER. After the working principle of the NOLM has been illustrated as pulse-by-pulse switch, it has been employed to demultiplex the 640 Gbit/s data packet into its lower bit rate (10 Gbit/s) tributaries. All 64 tributary channels have achieved error free performance, i.e., BER $\leq 10^{-9}$. Whereas, the 1.28 Tbit/s serial data packet has been demultiplexed into its 10 Gbit/s tributaries using time lens based serial-to-parallel converter. The main advantage of this technique is its ability to demultiplexed many (nineteen in our case) tributary channels at once which makes it more power efficient than the NOLM. All the demultiplexed 128 tributary channels have achieved BER performance well below the FEC of 3×10^{-3}, resulting in a bit rate of 1.2 Tbit/s. The FEC could be performed using DSP modules that increase power consumption of the Tbit system. However the only successful way, up-to-date, to receive all tributaries error free is performed with help of DSP.

Chapter 4

Optical packet labeling

4.1 Introduction

Optical networks which consist of high-capacity optical links and WDM technologies [72], are the main building blocks of the current telecommunication industry. High-capacity optical networks up to a bit rate of 100 Gbit/s [24] have been already deployed and the Ethernet alliance is currently standardizing 400 Gbit/s technologies [8] using high speed links such as optical fibers. Recently, 100 Gbit/s active optical links [22] are receiving a considerable interest for datacenter network (DCN) and high-performance computing (HPC) interconnections. However, the high-capacity optical data is streaming over these optical technologies in continuous mode namely optical circuit switching (OCS)[1]. In this case, network flexibility is achieved with the help of electrical technologies such as Ethernet commodity switches [26].

The high-bit rate optical data is converted, at each input port of the electrical switch, into electrical data thus the network flexibility such as buffering and switching are preformed in the electrical domain. Finally, the switched electrical data is converted back into optical domain. Despite its flexibility and higher degree of functionalities, electrical switching demands high electrical power during the optical-to-electrical-to-optical (OEO) conversions [73]. Moreover, slow processing speed and unfavorable scalability of electrical switches may be among the main fundamental limitations of such high-capacity optical networks [23]. Data format independent all-optical packet/flow based switching technologies [74–77] can be a potential solution for high-capacity optical networks because of their ability to pro-

[1] A dedicated channel (optical link) has to be established. The channel is reserved to that specific user no matter whether it has data to be sent or not.

cess the optical data in the optical domain, replacing some OEO conversions. Driven by the continual growth of IP data traffic [1, 12], optical packet switching (OPS) [75,77] and optical burst switching (OBS) [76,77] technologies have been actively researched over many years to switch and route chunks of data stream optically. Like electrical packet switching, OPS can help to utilize the network resources more effectively than OCS. Compared to its electrical counter part, OPS can handle burst traffic at ultra-high bit rate (up to Tbaud [C6]) with sub-picoseconds switching time [78].

Scalable optical switches are one of the key infrastructures of OPS technologies to ensure the successful delivery of a high-capacity optical data from a given source to its final destination. Like electrical switch, the main task of the optical switch is to direct the optical data carried by a single or multiple wavelengths from an input port to an output port. To perform this simple task, the switch needs: (i) an optical control information to make the switching decision, (ii) a fabric or back plane to physically interconnect the input and output ports and (iii) an optical buffer to hold the data until switching decision is made and the output port is ready to use. In electrical packet switching technologies, the switch control information are sent as part of the data packets, for example, IP addresses in IP/TCP packets and media access control addresses in Ethernet frames. Using the same analogy, an optical address (label) is required to fully realize the OPS functionalities and perform low latency packet routing and forwarding.

In this Chapter, we present detailed characterizations of a scalable in-band optical labeling technique based on notch-filtering of the broad data spectrum of a given high-capacity packet. After different types of optical labeling schemes are reviewed in Section 4.2, a detailed numerical characterization of the proposed optical notch-filter labeling technique is discussed in Section 4.3. Based on a notch-filtering effect on data and recovered label qualities, the filter is designed as a 0.3-nm wide, 30-dB deep 4^{th} order super Gaussian filter. Notch-filtering effects on the quality of high-capacity data packet are charactered in Section 4.4 using eye-opening penalty (EOP). In Section 4.5, the in-band notch-filter labeling scheme is experimentally demonstrated, based on the simulation results, for 640 Gbit/s (Section 4.5.1) and 1.28 Tbit/s (Section 4.5.2) serial data packets. Scalability of the labeling scheme is investigated by applying up to eight and sixteen optical notch-filters (ONFs) on the 640 Gbit/s and 1.28 Tbit/s data spectra, respectively. The notch-filtering effects is investigated using bit-error ratio (BER) measurements.

4.2 Optical labeling schemes

OPS technologies have the capability to process optical data packets directly at the optical layer using a switch control information that is appended to the data packet as an optical header or optical label[2]. To reduce the complexity of the OPS, the optical header should be easily encoded at the source and detached/attached at a given OPS node using simple optical or electrical modules. Easy header detachment/attachment at intermediate OPS nodes increase flexibility of the over all optical network architecture. Other characteristics of a good optical labeling scheme includes small network overhead, minimal effect on the optical data (for instance, low crosstalk) and high signal fidelity across the optical link and associated nodes [77].

Several optical labeling schemes have been demonstrated over the last three decades in which the optical header has been inserted mainly using two approaches: bit-serial [79–81] and parallel [82–94] to the optical data payload. In the bit-serial approach, the optical label is placed bit-serial to the data payload and transmitted on the same wavelength. In addition to the inter-packet guard time (gap), another guard time is applied between the optical label and the data payload allowing for easy header detachment/attachment at intermediate switching nodes. However, this approach is suitable for OPS working with synchronous and fixed length data packets as it needs a strict control of the timing. For instance, in a 1.646 μs fixed time slot of KEOPS OPS system demonstration [79], a 180 ns optical header at 622 Mb/s has been appended as bit-serial to a 1.35 μs data payload (at variable bit rate up to 10 Gbit/s [80]) with around 26 ns guard time separation and another 64 ns guard time as inter-packet gap. Even though the low bit rate optical label could easily be processed using simple electronics, the system throughput may be reduced due to the unused guard time between the packet payload and the optical header.

In the parallel approach, the optical header is placed in a separate frequency, wavelength, modulation format or code facilitating parallel processing of the optical label and switching of variable-length data packet, arriving asynchronously. The frequency-domain optical labeling can be performed using a widely utilized subcarrier multiplexing [82–85] and a wavelength multiplexing [86, 87] techniques. Subcarrier multiplexing has been originally demonstrated in [82] using an optical header inserted as a double-sideband of a baseband data payload. The quality of the optical header on the double-sideband signal can be affected (for example,

[2]In this thesis, both names are used interchangeably.

as researched in detail for microwave subcarrier multiplexing [95]) due to the coherent interference between the sideband signal and the baseband signal. To overcome the drawback of the two-sideband technique, single-sideband [83] and carrier suppressed [84,85] have been studied to carry the optical header. Detection of the optical header of any of the three subcarrier multiplexing techniques has been achieved using an optical filterer like a fiber Brag grating (FBG) or arrayed waveguide-grating (AWG). However, the optical header in subcarrier multiplexing techniques has to be encoded in separate wavelength or frequency which can lead to spectral inefficiency.

The second frequency-domain based optical labeling has been studied in [86] using a wavelength multiplexing header technique. This technique can have the easiest label extraction method as the optical header can be appended at a separate wavelength[3], for example at 1510 nm or 1410 nm [87]. Simple all-optical module can be employed to detach and attach the optical label at the OPS node but chromatic dispersion induced time mismatch can be created specially if the wavelength spacing between the header and payload is large. Despite its simplicity, this scheme is not spectrally efficient.

Various OPS scenarios have been proposed by encoding both the header information and data payload at the same optical carrier but with orthogonal modulation formats in the amplitude, phase or polarization domains. This innovative optical label technique has been demonstrated for OPS with on-off keying (OOK) modulated payload using phase [88] or frequency [89] encoded optical header. Another work has been reported in [90] demonstrating OPS of phase modulated optical data using OOK-encoded optical header. Both reported techniques are exposed to payload and optical header crosstalk effects as it can be extremely difficult to maintain orthogonality between the amplitude modulated data and phase/frequency optical label, for instance due to frequency chirp introduced by the amplitude modulation, or vice versa. To overcome such crosstalk effect, electroabsorption modulator (EAM) with negligible frequency chirp has been used in [91] to amplitude modulate a 2.5 Gbit/s label into a phase-encoded 40 Gbit/s optical payload while orthogonal polarization modulation has been embedded with amplitude modulated data payload in [92]. This scheme has a better spectral efficiency and an easy header detection using simple electronics.

Another type of OPS networking have been pursued in [93, 94] by encoding/decoding a set of optical code using optical code-division multiple access as optical labels which are mainly a combination of time and wavelength attributes. The decoding process in such labeling technique is typi-

[3]Wavelength that is reserved for control and management plane in WDM networks.

cally performed with matching optical codes in which the matched optical label shows a strong peck intensity. Albeit its very fast optical process that eliminates the need of timing consuming table lookup, decoding of multiple optical labels needs many parallel optical devices which adds complexity to the OPS node.

As a final remark, it is worth-mentioning that all the aforementioned labeling schemes have been thoroughly investigated only in the research environments and OPS technology is still in the very early stage even though it has been actively researched with considerable efforts. In 1997 [96], an optical optical label switching (OLS) technology has been proposed to fully realize OPS, OBS and OCS using an optical header and associated contention resolution methods in the wavelength, time and space domains [97, 98]. OLS has been proposed in the same year, by chance, with the same objectives as multiprotocol label switching (MPLS) [99] which has later adopted MPLambdaS for WDM networking and generalized multiprotocol label switching (GMPLS) as a signaling technology to unify the time, space, and wavelength domain multiplexing of packet and circuit technologies [100]. However, GMPLS supports neither OPS nor OBS directly on the optical layer. Moreover, GMPLS has not gained the required commercial success as a unified control plane of the current photonic networks. Recently openFlow/software defined network (SDN) [101] has been proposed as a better unified control plane technologies due its significant advantages over MPLS for dynamic interaction between electrical packet and optical circuit networks. Therefore, the need for innovative optical labeling technology is still an open area of research that has kept receiving considerable attention to add flexibility to the optical data in the optical domain.

4.3 In-band optical notch-filter labeling

Generally, all the frequency-based labeling techniques [82–87] can be categorized as in-band or out-of-band based on the way how the information is embedded with respect to the data spectrum. In-band optical labeling techniques encode the label information within the data spectrum whereas out-of-band optical labeling schemes send the information outside the data spectrum bandwidth. Compared to out-of-band labeling, in-band optical labeling is more bandwidth efficient because of its ability to embed the label information inside the data spectrum. One key requirement of a standard OTDM system is having an ultra-short optical pulses source typically achieved using super continuum generation. During our discussion in

Section 3.3, a 640 Gbit/s and a 1.28 Tbit/s serial data packets are generated using ultra-short return-to-zero (RZ)-optical pulses. Thus, the signal spectrum bandwidth of these high-capacity packets is very broad that an in-band optical labeling technique can be an attractive method to add an optical header by utilizing the larger bandwidth with minimum impact on the data quality.

OPS of 640-Gbit/s OTDM packets, the highest bit rate data prior to our work, has been demonstrated in [7] using optical label information inserted as two in-band frequency components in the broad data spectrum. The labeling scheme has been first proposed in [102] for different modulation formats and its scalability has been studied in [103] using six labels where continuous wave (CW) sources and FBGs have been used to generate and insert/extract labels from a 160-Gbit/s OTDM data spectrum. In this section, we propose an in-band optical labeling scheme based on notch-filtering of the broad data spectrum of a given high-capacity packets

4.3.1 Working principle

The working principle of the optical switching scenario shown in Figure 3.2 can be simplified to the sketch shown in Figure 4.1 using the envisaged optical labeling scheme. Four networks: A, B, C and D are interconnected using a high-capacity 2×2 optical switch. Both Network-A and Network-B prepare high-capacity data packets by aggregating lower bit rate data packets from N source hosts using a parallel-to-serial converter module (see Section 3.3). Aggregated packet-1 and packet-3 of Network-A and aggregated packet-2 and packet-4 of Network-B are forwarded to their corresponding optical labeling module. The main function of the optical labeling module is to insert a control information inside the data spectrum of each packet so that the 2×2 optical switch can easily differentiate packets going to network-C and network-D. The label information of a packet going to network-D is added by making a narrow band spectral hole in the right side of the spectrum whereas a packet going to network-C is labeled with no hole in its spectrum. Hence, packet-1 and packet-3 of network-A are labeled with none (‘0’) and one (‘1’) spectral hole in their spectra, respectively. Similarly, the optical labeling module of network-B labels packet-2 with ‘1’ notch and packet-4 with ‘0’ notch. Finally, all four packets are forwarded to the 2×2 switch.

Once the packets arrive at the switch, the optical labels are extracted using a label detection module, which is shown as the top part of the optical switch in Figure 4.1. The label detection module first checks for

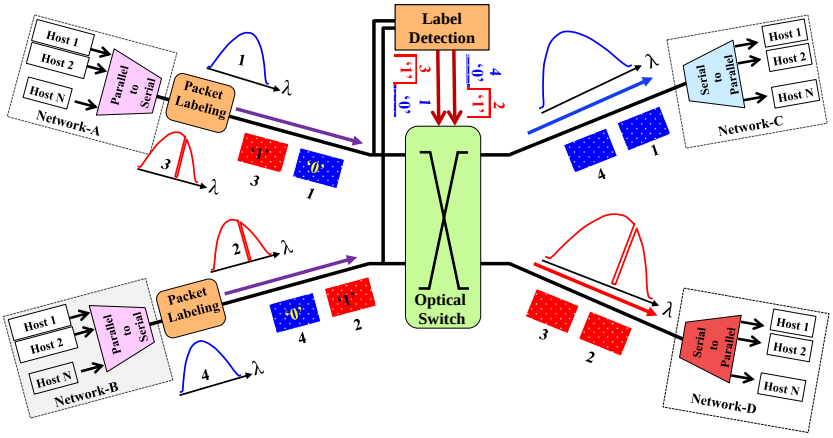

Figure 4.1: Working principle of a high-capacity OPS using the proposed in-band notch-filter labeling scheme. High-capacity network-A, -B, -C and -D are interconnected using a 2×2 switch. High-capacity packets are aggregated from N hosts of Network-A and -B, labeled using a packet labeling module, optically switched by extracting the optical label, converted back into lower bit rate packets and received by N hosts of Network-C and -D.

the presence of a spectral hole on the right side of each data spectrum by filtering out the optical power. Then, it generates a switch control signal based on the extracted optical power. The control signal is at high voltage level if a hole is detected in the data spectrum otherwise at low voltage level. The extracted control signals are shown below the label detection module for packets of network-A (left side) and network-B (right side).

Addressing high-capacity networks of a few km range, we assume that the optical switch and hosts are well synchronized. Based on the extracted label information from each packet, the 2×2 optical switch can swiftly forward the data packet optically. Hence, packets with low voltage level, i.e. packet-1 and packet-4, are sent to network-C, whereas packets with high voltage level, packet-2 and packet-3, are forwarded to Network-D. Following the switching, each high-capacity data packet is converted into many parallel low bit rate data streams using, for instance, the optical time lens based serial-to-parallel conversion (see Section 3.4.2).

In recent years, migration of IP addressing from 32-bit IPv4 to 128-bit IPv6 took place mainly to cope with the exponential growth of the Internet and the impending of the IPv4 address space [104]. As one of the

fundamental requirements of any packet switched network, a given optical packet labeling scheme should generate abundant addresses (unique labels) allowing interconnection of as many networks as possible. The proposed optical notch-filter labeling scheme can be made scalable, for example, by increasing the number of spectral holes in both side-lobes of the data spectrum. Using N spectral holes, up to 2^N unique labels can be generated, which paves the way for $2^N \times 2^N$ OPS operation. In [C1], we increased the number of spectral holes to eight so that up to 2^8=256 labels can be created for 640 Gbit/s serial data packets. The number of the spectral holes can be further increased using very narrow ONFs or by increasing the symbol rate of the data packet. One can increase N by applying very narrow ONFs in order not to distort the signal quality significantly but applying narrow filters can be very challenging in practice. Doubling the bit rate of the packet, for example from 640 Gbit/s to 1.28 Tbit/s [C6], allows scaling of N considerably.

Figure 4.2 shows block diagrams of an optical labeling of 640 Gbit/s serial data packet using the proposed in-band notch-filtering technique. In simulation, 33% RZ-optical pulses with full-width at half-maximum (FWHM) duration of 0.515 ps are generated at a repetition rate of 640 GHz and OOK modulated with a 2^7-1 pseudo-random binary sequence (PRBS) pattern. The modulated data emulates a payload of a 640 Gbit/s serial packet whose spectrum is shown in Figure 4.2(a). The high bit rate packet is labeled using an optical packet labeling module, which consists of eight 0.3-nm wide 4^{th} order super-Gaussian ONFs. Center frequencies of the ONFs are set at eight spectral positions; P_1, P_3, P_5 and P_7 on the lower frequency side, and P_2, P_4, P_6 and P_8 on the higher frequency side of the data spectrum as shown in Figure 4.2(b). The module labels each packet by employing up to eight ONFs so that a label word (LW) can be generated based on a permutation of the spectral position of these ONFs as:

$$LW\ (binary\ value) = P_8P_7P_6P_5P_4P_3P_2P_1 \tag{4.1}$$

where P_i is 1 if the ONF at P_i is used; 0 otherwise for i=1, 2, ..., 8. The one-byte (8-bit) LW is encoded based on how far the spectral holes are positioned from the center of the spectrum. The two least significant bits (P_2 & P_1) are the farthest positions on each side of the spectrum whereas the two most significant bits (P_8 & P_7) are the closest positions toward the center of the spectrum. The LW can be used as a network identifier in which packets with the same LW are forwarded to the same network by the intermediate optical switches.

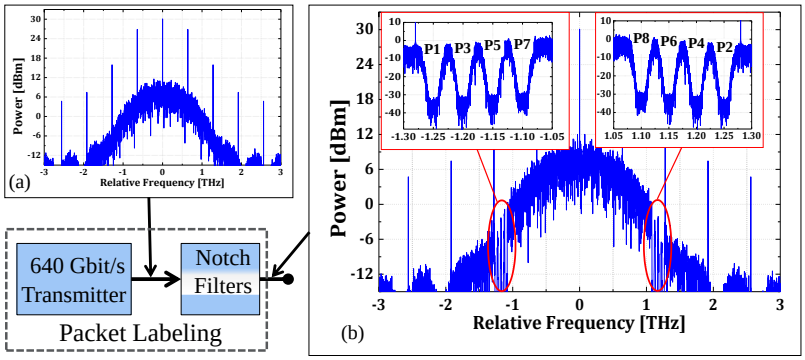

Figure 4.2: Block diagram of in-band optical labeling of a 640 Gbit/s OOK modulated serial data packet. (a) Power spectrum of the data packet. (b) Spectral positions of eight ONFs within the data spectrum.

4.3.2 Notch-filter characterization

In the proposed in-band optical labeling technique, the optical header, i.e. the spectral notches, are inserted in the data signal bandwidth. Hence, careful selection of the ONF parameters such as filter transfer function, spectral position, 3 dB bandwidth (BW), suppression ratio (SR) and total number of the ONFs is very important in order to have a stable and scalable optical labeling scheme with minimum impact on the data quality. As one can notice, for any selection of the aforementioned parameters, there exists a trade-off between the data signal quality and the label quality (scalability). In this section, we discuss selection of the filter transfer function, spectral position, 3 dB BW and SR whereas further characterization about the signal and extracted labels qualities are presented in Section 4.4 and Section 5.3, respectively.

Filter transfer function

Notch filters are suitable for applications which require strong suppression on selected narrow spectral bands while allowing maximum transmission on the remaining bands [105]. Hence, the term notch-filter indicates the availability of a hole (gap) within a broad transmission spectral range. The shape of the spectral hole or "notch" is defined by frequency response of the filter. Frequency response of the notch-filter, H_{NF}, that is used to characterize the optical labeling technique is defined by a super-Gaussian

function [106] and H_{NF} can be expressed as:

$$H_{NF}(\omega) = 1 - SR \cdot exp\Big[- ln(2)\Big(\frac{2(\omega - \omega_{0f})}{\Delta\omega_f}\Big)^{2m}\Big] \tag{4.2}$$

where m is any positive integer referring to order of the super-Gaussian and SR, ω_{0f} and $\Delta\omega_f$ are suppression ratio, center frequency and 3 dB BW of the ONF, respectively. In the label detection module of the optical switch shown in Figure 4.1, the optical label is extracted using an optical band-pass filter (OBPF) with a super-Gaussian transfer function, H_{BF}. For large suppression ratio (SR$\approx$ 1), H_{BF} can be defined as a reciprocal of the ONF, $H_{BF} = 1 - H_{NF}$ and can written as:

$$H_{BF}(\omega) = exp\Big[- ln(2)\Big(\frac{2(\omega - \omega_{0f})}{\Delta\omega_f}\Big)^{2m}\Big] \tag{4.3}$$

Assuming SR=0.999 (30-dB deep), a normalized ω_{0f} and $\Delta\omega_f$=37 GHz, frequency response of both H_{NF} and H_{BF} for m=1, 2 & 4 are shown in Figure 4.3(a) and Figure 4.3(b), respectively. For m=1, both equations are reduced to normal Gaussian functions whereas for higher orders, m=2 and m= 4, the shape of all transfer functions are top flat (bottom-flat for the ONF) resembling to rectangular windows. A good profile match between ONF and OBPF is essential in order to detect a good-quality label at the optical switch and to reduce filtering effect on the signal quality. Figure 4.3(c) shows the profile matching between the ONF and OBPF for m=1 whereas the profile matching for m= 4 is shown in Figure 4.3(d). It is clearly noticeable that the 4^{th} order Gaussian profiles have a very small non-overlapping areas: small A1, A2, A3 and A4 compared to the 1^{st} order profiles. Therefore, we characterize the optical labeling scheme using higher order super-Gaussian functions both in simulation (m=4) and experimental demonstrations (m=8).

Notch filter spectral position

The spectral positions of the ONFs are chosen based on two main criteria: signal and extracted label qualities. The ONFs are carving notches in the data spectrum by removing optical power from specific spectral components leading to signal quality degradation. So, the ONFs should be positioned as far as possible from the center frequency of the broad data spectrum to minimize their effect on the signal quality. On the other hand, in order

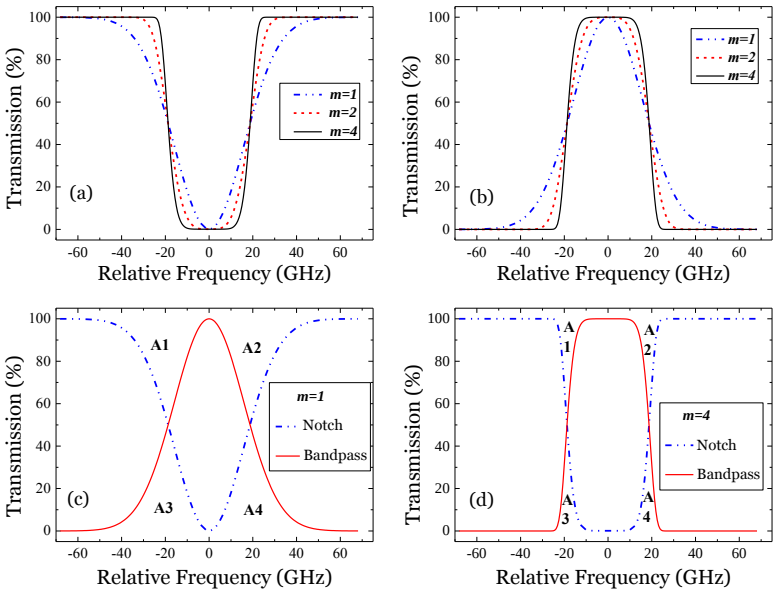

Figure 4.3: (a) Frequency response of a super-Gaussian ONF for SR=0.999, $\Delta\omega_f$=37 GHz and for different super-Gaussian order (m=1, 2 & 4). (b) Transfer function of super-Gaussian OBPF for $\Delta\omega_f = 37\ GHz$ and for different super-Gaussian order (m=1, 2 & 4). Profile matching of both the ONF and OBPF with non-overlapping areas: A1, A2, A3 and A4 for (c) *m=1* and (d) *m=4* that has very small non-overlapping areas.

to minimize the effect of noise on the extracted label quality, the position of the ONFs should be placed as close to the center frequency of the data as possible. Hence, there exists a trade-off between signal and extracted label qualities. To address this trade-off, we set, as a rule of thumb, two boundaries based on a chirp-free transform limited Gaussian pulse[4]. In the case of amplitude modulated pulses, the spectral lines (spikes) mostly at multiples of the bit rate are not considered when the two boundaries are applied. The first boundary states that every notch filter has to be positioned outside the 3 dB BW of the data spectrum in order to minimize the signal quality degradation. The second boundary is defined in such a way that each notch filter has to be centered inside the 20 dB bandwidth of the data spectrum to ensure a certain signal-to-noise ratio of the extracted labels. When more than one ONFs are applied in either side of the data

[4] Chirp free transform limited pulses have the minimum time-bandwidth product and the two boundaries are, thus, set to the minimum values.

spectrum, the frequency spacing between the filters at each side is set to 50 GHz to allow practical filtering, for instance, using an AWG.

Filter suppression ratio and 3 dB bandwidth

Beside the position, other parameters of the notch filter that can affect the label and signal qualities are the 3 dB BW and SR. Section 5.3 discusses the detail characterization of the 3 dB BW and the SR of the ONF with respect to label quality. Based on that, we use a 30-dB deep ONF for simulations while the maximum SR achieved during the experiment is 20 dB. Whereas, considering the practical implementation and quality of the signal, we use 0.3-nm wide ONFs and OBPFs both in simulations and experimental demonstrations.

4.4 Impact of notch-filtering on data quality

In this section, we present a detailed numerical characterization to investigate the effect of optical notch-filtering on the quality of the data signal. Using MATLAB®, we generate a 640 Gbit/s serial data packet and optically label it by employing up to eight ONFs centered at the same spectral positions as shown Figure 4.2. The data packet is simulated using chirp free Gaussian pulses whose time-bandwidth product is 0.44 [2]. We study the effect of the ONF for a single Gaussian pulse in which the notch-filtering effects is quantified using pulse-to-tail extinction ratio (PTER). Then, we investigate the effects of the labeling technique on the 640 Gbit/s using EOP.

Single Gaussian pulse

We simulate a single Gaussian pulse at repetition rate of 640 GHz that gives a pulse period (bit time) of 1.5625 ps. To model RZ-Gaussian pulse, the FWHM of the intensity profile is set to 0.515625 ps which corresponds to 33 % duty cycle. Using the minimum time-bandwidth product of chirp-free Gaussian pulse [2], the FWHM of the power spectrum is set to 0.853 THz. The Gaussian spectrum is filtered using eight ONFs which are simulated using the previously defined parameters: m =4, SR= 0.999 (30 dB) and 3 dB BW of 0.3 nm. Figure 4.4(a) shows power spectra of the Gaussian pulse before (dashed line) and after (solid line) the ONFs are applied. The intensity profile of the normal (dashed line) and the 8×notched (solid line) Gaussian pulses are shown in Figure 4.4(b). The 8×notched Gaussian pulse

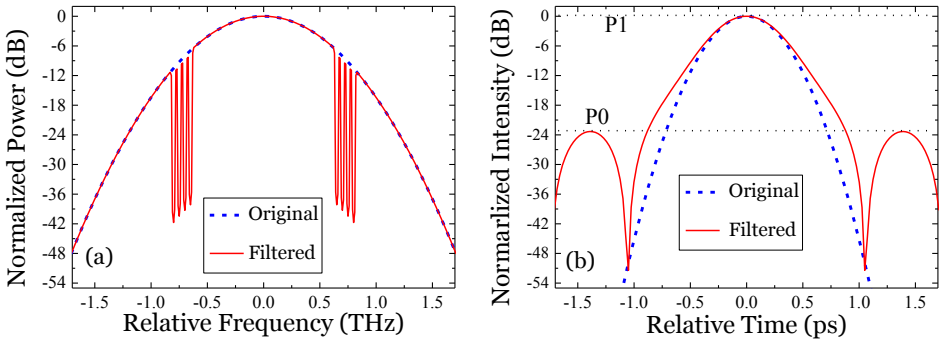

Figure 4.4: (a) Normalized power spectra of a chirp-free 33% RZ-Gaussian optical pulse before (dashed line) and after (solid line) eight optical ONFs (see Figure 4.2(b)) are applied. (b) Normalized intensity profiles of the Gaussian pulse before (dashed line) and after (solid line) notch-filtering.

is clearly distorted due to the notch-filtering effects. Temporal duration of the notched pulse is increased while new pedestals (tails) are generated in both side of the pulse. The second effect can be quantified using a PTER which can be defined as:

$$PTER_{dB} = 10.log(P1/P0). \tag{4.4}$$

where P1 and P0 are the peak value of the intensity of the Gaussian pulse and peak value of the newly generated tail. The PTER value is increased to -24 dB, as shown in Figure 4.4(b), as consequence of the employed ONFs. The observed pulse broadening and trails generation effects can lead to inter-symbol-interference between the ultra-short pulses of a high-capacity serial data packets.

OOK modulated data packet

Using the previously characterized 33% RZ-optical pulse, trains of Gaussian pulses are simulated at a repetition rate of 640 GHz with FWHM of 0.515 ps. High-capacity 640 Gbit/s serial data is generated by OOK modulating the ultra-short RZ-optical train pulses with a 2^7-1 PRBS pattern emulating a data payload. Considering the limited extinction ratio of a practical intensity modulator, for example Mach-Zehnder modulator (MZM), the ratio of the peak intensity of bit-one and peak intensity of bit-zero is set to 15 dB. After the OOK modulated data packet, is generated, it is optically labeled

using multiple ONFs centered at different spectral positions of the data packet as shown in Figure 4.2.

Applying ONFs to the data spectrum means removing small portion of optical powers from the different spectral position which undoubtedly degrades the signal quality in general and its amplitude in particular. An eye-diagram or eye pattern can be a useful tool for understanding the notch-filtering effects, and quantifying the amplitude and time distortions that degrades the signal quality [107]. Focusing on solo notch-filtering effects, we simulate an ideal high-capacity transmitter using MZM intensity modulator with a limited extinction ratio set to 15 dB. The 640 Gbit/s optical data packet is photo-detected using an ideal photodiode (PD) and its eye-diagram is displayed using an ideal time sampling oscilloscope. Figure 4.5 shows eye-diagrams of a 640 Gbit/s RZ-OOK data packet before (a) and after (b) eight ONFs are applied on the data spectrum. One can clearly see that the filtered data packet has closed eye which can relate to amplitude jitter due to the notch-filtering effects.

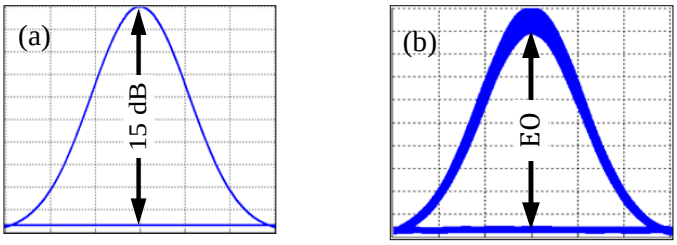

Figure 4.5: Eye diagrams of a 640 Gbit/s RZ-OOK serial data: (a) with EO of 15 dB, and (b) after eight ONFs (refer Figure 4.2(b)) are applied on the data spectrum that leads to EO $<$ 15 dB.

For OOK modulated data packets, the notch-filtering effects is characterized using an EOP which can be quantified as:

$$EOP\ (dB) = 15\ dB - EO\ (dB) \tag{4.5}$$

where 15 dB is the extinction ratio of the OOK modulator and EO is calculated as the distance between the inner-most traces in the eye diagram. When the 640 Gbit/s data spectrum is not notch-filtered, the EO is 15 dB as depicted in Figure 4.5(a), which means there is no EOP. Whereas, the notched-filtered 640 Gbit/s data (see Figure 4.5(b)) has an EO less than

15 dB due to the filtering effect, which leads to EOP. During the simulation, transmitter imperfections, link impairments and receiver effects are neglected in the EOP calculation leaving notch-filtering effects as the only source of signal quality degradation.

Figure 4.6 shows the EOP for the 640 Gbit/s packet that is labeled using different LWs, generated based on Equation 4.1. The 8-bit LW is represented in its equivalent decimal value ranging from 0 (00000000) up to 170 (10101010) above which the EOP remains $>$ 1.12 dB but below 2.2 dB. The top part of Figure 4.6 shows eye diagrams (with their LW and EO) corresponding to specific EOP points. As expected, the EOP increases when the most significant bits are '1', i.e. when there are spectral holes at positions close to the center frequency of the data. However, the EOP is not steadily increasing with decimal value as it also depends on the total number of notches in addition to their spectral position, for instance, as one can see from the EOP values corresponding to LW 60 (00111100) and 128 (10000000). LW 60 is created using four ONFs centered at P_6, P_5, P_4 and P_3 whilst LW 128 is generated using single ONF centered at P_8 and understandably that yields to lower EOP compared with LW 60.

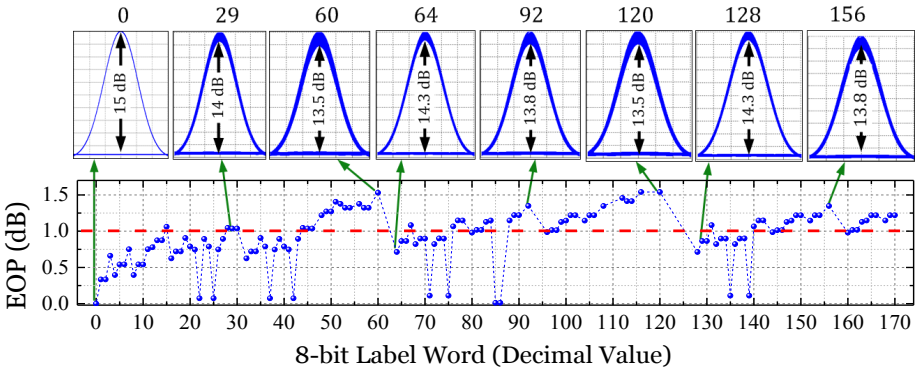

Figure 4.6: The low part shows EOP of the longest packet for LWs up to decimal value of 170, above which the EOP remains >1.12 dB but below 2.2 dB. The upper part shows eye diagrams of selected LWs with their EO.

As a rule of thumb and reference for our discussion, we set EOP of 1 dB as the maximum tolerable penalty to achieve error free performance. Hence, more than 60 LWs for high-capacity 640 Gbit/s serial data packets can be generated at the expense of <1-dB EOP whereas 76 and 92 LWs can be achieved with EOP of <1.1 dB and <1.12 dB, respectively. We have

found that all LWs, generated by employing up to four ONFs at the same time, can achieve an EOP below or close to 1 dB. As a final remark, it is important to note that the EOP is used as a rule of thumb for the effects of notch filtering on the signal quality but does not directly predict the receiver sensitivity changes in the final system performance. Hence, there is no straight forward relationship between EOP as it is used here and the experimental BER results of Section 4.5.

4.5 Experimental demonstration

In this section, we present an experimental demonstration of the proposed in-band optical labeling scheme based on the previous numerical characterizations. In Section 4.5.1, five 640 Gbit/s serial data packets are generated using a standard OTDM transmitter and optically labeled by employing up to eight ONFs demonstrating the scalability of the labeling scheme for possible 1×256 switching operation. Further experimental demonstration of the in-band optical labeling scheme is presented in Section 4.5.2 for a record-high 1.28 Tbit/s serial data packets. A maximum of sixteen ONFs are applied to the Tbit/s spectrum that leads to 65.536 unique labels. Effect of the optical labeling is investigated using the BER measurements.

4.5.1 640 Gbit/s packet labeling

Experimental setup

Experimental setup of the proposed optical labeling scheme for 640 Gbit/s packets is shown in Figure 4.7. The setup is constructed using three modules: a 640 Gbit/s transmitter module based on a standard OTDM transmitter (refer Section 3.3.1), an optical packet labeling module and the nonlinear optical loop mirror (NOLM) as pulse-by-pulse switch to demultiplex the 640 Gbit/s serial into its 10 Gbit/s tributaries as explained in Section 3.4.1. The short pulse source generates a 10 GHz ultra-short optical train pulse with very broad spectrum. The optical pulses are split in two paths: a data signal and a control signal which is used in the NOLM. FWHM of the optical puses of the data signal is 540 fs after they are filtered using a 13-nm wide at 3 dB OBPF centered at 1552 nm.

The filtered optical pulses are OOK modulated with a 10 Gbit/s pattern, which consists of 1340 bits of 2^7-1 PRBS followed by 1988 zero bits. The amplitude modulation enables creation of optical packets shown as Signal-A in Figure 4.7. The modulated pulses are then time multiplexed using

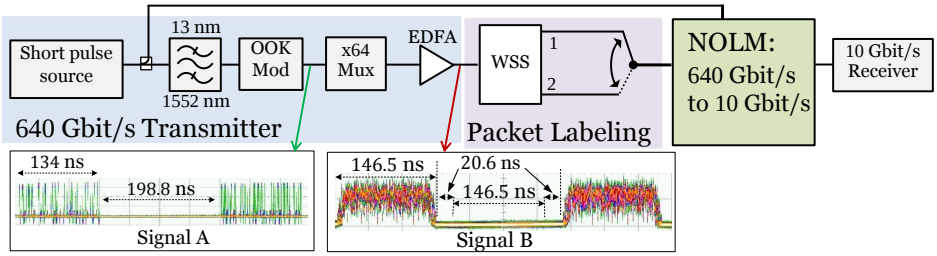

Figure 4.7: Experimental setup of the proposed notch-filter labeling scheme using 640 Gbit/s serial data packets.

a 2^7-1 PRBS preserving bit interleaver to constitute 640 Gbit/s serial data packets. The packet length is increased by 12.5 ns from 134 ns at 10 Gbit/s to 146.5 ns at 640 Gbit/s (see Signal B in Figure 4.7), due to the delay introduced in the bit interleaver to preserve the 2^7-1 PRBS sequence. Signal B has a 146.5 ns duration of data packet followed by 20.6 ns inter-packet gap and a 146.5 ns sequence of zero bits is used to reserve a free time slot for another data packet followed by another 20.6 ns inter-packet gap.

The 640 Gbit/s serial data packet is labeled using the proposed in-band labeling scheme in the packet labeling module using a commercialized programmable wavelength selective switch (WSS) [108]. In this experimental demonstration, the multi-purpose WSS provides three main functionalities. The first task of the WSS is to broadcast the whole spectrum of the 640 Gbit/s data packet into two ports which gives the freedom to treat the data packet at each port independently. The data packet at port-1 is referred as Packet-1 whereas Packet-2 represents the data packet at port-2. As we have explained in Section 4.3.2, the ONF is characterized using an ideal transform limited Gaussian pulses in order to achieve the minimum time-bandwidth product. Therefore, the WSS is also used as wave-shaper to emulate transform limited Gaussian pulses by shaping the optical spectra of both Packet-1 and Packet-2. Figure 4.8(a) shows the unshaped data spectrum input to the WSS whereas Figure 4.8(b) depicts the shaped data spectrum of Packet-1 after the WSS is used as wave-shaper by applying amplitude and phase filtering profiles. The shaped and unshaped spectra are compared with an ideal transform limited Gaussian pulse as shown in Figure 4.8 using a dashed line. As expected, the shaped spectrum shows good agreement with the transform limited Gaussian pulse.

The third functionality of the WSS is to label the shaped data spec-

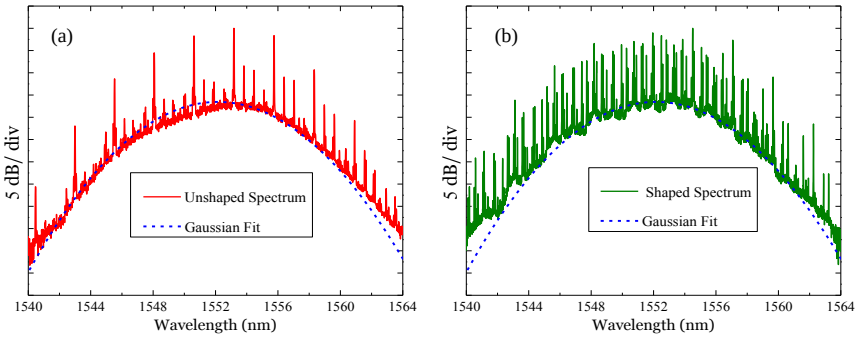

Figure 4.8: (a) Power spectrum of a 640 Gbit/s serial data input to the WSS. The data spectrum is fitted with a transform limited Gaussian pulse (dashed line). (b) Power spectrum of the 640 Gbit/s serial data after it is shaped using the WSS to emulate transform limited pulses and shows a good agreement with the ideal transform limited Gaussian pulse.

tra optically using the proposed in-band notch-filtering scheme. The ONF parameters are selected based on characterization results of Section 4.3.2. Ideally, the filter is designed as a 0.3-nm wide 30-dB deep 4^{th} order super-Gaussian filter even though it is challenging to practically achieve all these parameters. For example, it is difficult to achieve super-Gaussian filer with sharp transition due to limited resolution of the WSS[5] [109]. Figure 4.9(a) shows frequency response of the ONF after the WSS is programmed with the aforementioned ONF parameters. Frequency response of the ideal 4^{th} order super-Gaussian filter shown in Figure 4.3(a) is used as a reference (fit) of the WSS generated frequency responses in Figure 4.9(a). For m=4, the SR is 26 dB which is not as deep as the fit and the filter shape also resembles to a normal Gaussian function.

Then, the WSS is reprogrammed with m=8 where the SR is close to 30 dB but the shape of the ONF still resembles to a normal Gaussian function. By introducing a π phase change (phase filtering effect) on the higher frequencies i.e., from 0 up to 20 GHz, the SR and shape of the ONF are further improved as shown in Figure 4.9(a) which shows a good agreement with the fit. For all experimental demonstration we apply the 8^{th} order super-Gaussian filter with the introduced π phase change. Figure 4.9(b) shows portion of Packet-1 (black) and Packet-2 (red) data spectra after a 0.3-nm wide ONFis applied on Packet-2 at 1559 nm. Even though more

[5]Frequency resolution of the commercialized WSS is limited to 1 GHz

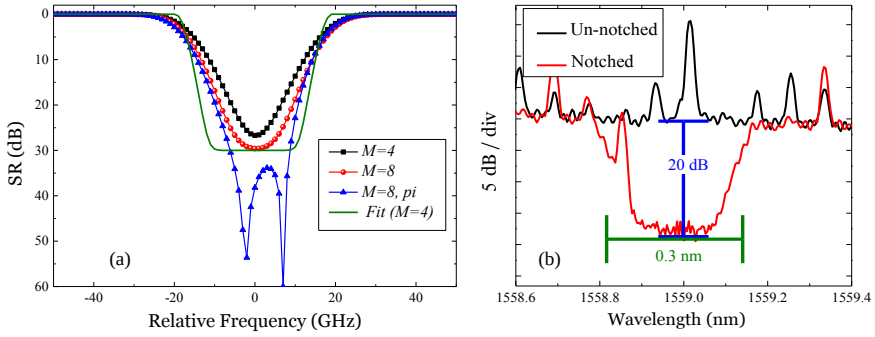

Figure 4.9: (a) Frequency responses of WSS generated 4^{th} and 8^{th} order super-Gaussian ONFs that are fitted with ideal 4^{th} order super-Gaussian filter. (b) 3 dB BW and SR of the ONF after it is employed on a 640 Gbit/s data spectrum.

than 30 dB of SR is shown in Figure 4.9(a), the applied ONF is only 20-dB deep because the WSS attenuates the specific spectral position with respect to the peak power of the whole data spectrum.

The WSS labels the shaped data spectrum by employing up to eight ONFs centered at different spectral positions which are outside the 3 dB but inside the 20 dB bandwidth of the data spectrum. Like in the simulation part, the 3 dB and 20 dB bandwidth boundaries are defined without considering the scattered spectral lines shown in Figure 4.8. Packet-1 is labeled without making any notch while Packet-2 is labeled by making one spectral hole at 1559 nm as shown in Figure 4.10(a). Further more, three different labels are applied on Packet-2 by making two (centered at 1546.1 nm and 1559 nm), four (centered at 1545.7 nm, 1546.1 nm, 1559 nm and 1559.4 nm) and eight (centered at 1544.9 nm, 1545.3 nm, 1545.7 nm, 1546.1 nm, 155 nm, 1559.4 nm, 1559.8 nm and 1560.2 nm) spectral holes at both sides of their spectra as shown in Figure 4.10(b)-(d). In total, five data packets are labeled using the optical labeling module and up to a maximum of eight ONFs are employed at once.

Each labeled data packet is launched into a 640 Gbit/s to 10 Gbit/s time demultiplexer built using the NOLM. A 10 GHz control pulse with pulse duration of 900 fs FWHM is taken from the control arm of the 640 Gbit/s transmitter module and coupled to the NOLM after it is filtered at 1565 nm using a 13-nm wide optical filter. The control pulse is used as gating win-

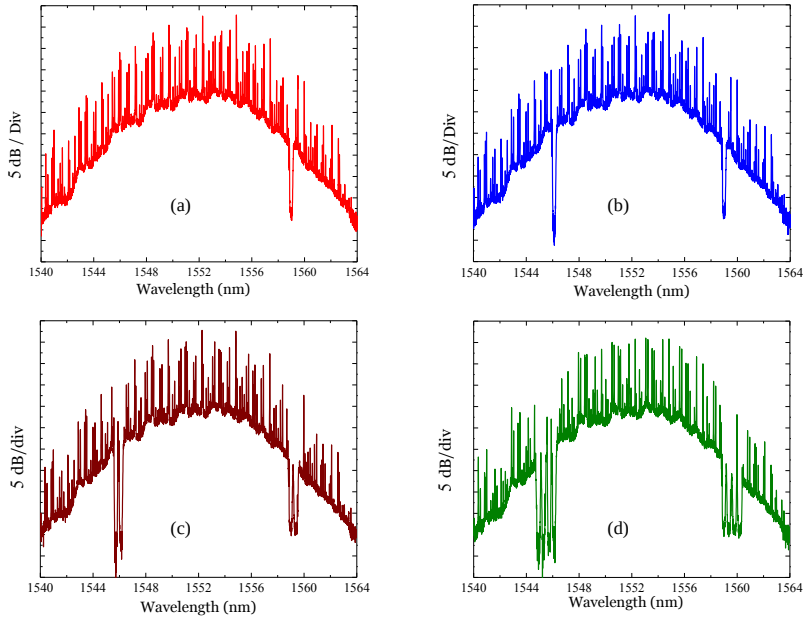

Figure 4.10: Power spectra of 640 Gbit/s data packets after they are optically labeled using (a) one, (b) two, (c) four and (d) eight ONFs.

dow of the NOLM which works as a pulse-by-pulse switch. The resulting demultiplexed 10 Gbit/s data channel, is filtered out at 1551 nm using a 1 nm OBPF and sent to a receiver for BER measurement.

Result and discussion

Figure 4.11(a)-(e) show eye diagrams of an extracted 10 Gbit/s channel from five different 640 Gbit/s data packets which are labeled using zero, one, two, four and eight spectral holes. The effect of the proposed in-band labeling scheme on the quality of the five data packets is investigated by measuring BER performance of all the demultiplexed 10 Gbit/s tributary channels. All channels of the five data packets have achieved error free performance, i.e. BER $\leq 10^{-9}$. Figure 4.11(f) shows receiver sensitivities, at a BER of 10^{-9}, of all the 64 channels of the data packet with no, one, two, four and eight spectral holes.

The difference in receiver sensitivities between the best and worst channels of each data packet is less than 3 dB. As expected, the un-notched data packet has the best receiver average sensitivity (-33.75 dBm), which

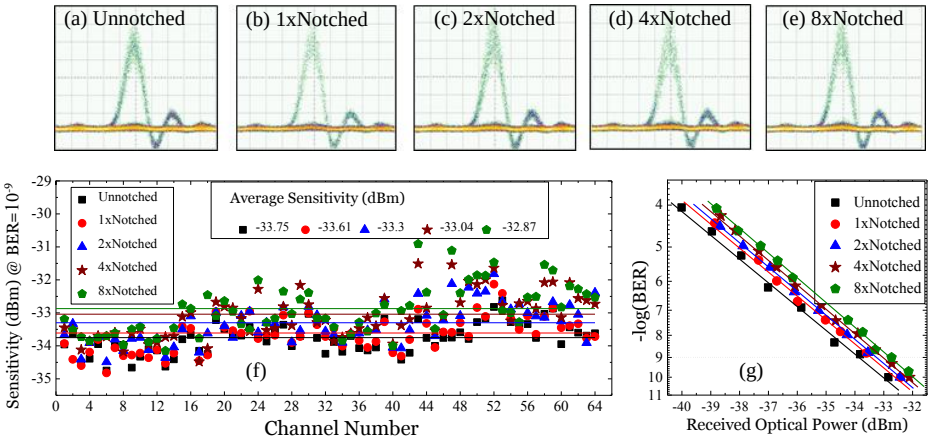

Figure 4.11: Eye diagram of demultiplexed 10 Gbit/s data signals of (a) unnotched, (b) 1×notched, (c) 2×notched, (d) 4×notched and (e) 8×notched data packets. (f) Receiver sensitivities of all channels of zero (rectangular), one (circle), two (triangle), four (star) and eight (pentagon) times notched packets. (g) Full BER curves of 10 Gbit/s data signals with zero (rectangular), one (circle), two (triangle), four (star) and eight (pentagon) spectral holes.

is 0.14 dB less than the data packet with one spectral hole. On the other hand, the data packet with eight spectral holes has the worst average sensitivity (-32.87 dBm), which is 0.17 dB and 0.43 dB higher than the data packets with four and two spectral holes, respectively. The average sensitivity of the data packet with eight notches is only 0.88 dB higher than the average sensitivity of the un-notched packet and this demonstrates the scalability of the labeling scheme allowing 1×256 switching operation as up to 256 different labels can be created with a system penalty of less than 1 dB. Finally, Figure 4.11(g) shows full BER performance of a single channel of the five data packets: unnotched, one spectral hole, two spectral holes, four spectral holes and eight spectral holes.

4.5.2 1.28 Tbit/s packet labeling

The proposed notch-filter labeling scheme is very suitable for high symbol rate data packets while it may incur in substantial system penalty for lower bit rate packets. In serial communication, the high symbol rate data is

achieved using ultra-short optical pulses. Very short optical pulses has a very broad spectrum which means a 1.28 Tbaud data packet can a handle large number of ONFs with low penalty compared to a 640 Gbit/s data. Therefore, doubling the symbol rate can enable the labeling technique to generate high number of distinct labels by employing more than eight ONFs. Here, we experimentally demonstrate scalable optical packet labeling for 1.28 Tbit/s data packets. A maximum of sixteen ONFs are applied to the Tbit/s spectrum that leads to generation of 65.536 unique labels. Effect of the sixteen ONFs is investigated using the BER measurements.

4.5.3 Experimental setup

Figure 4.12 shows an experimental setup of the 1.28 Tbit/s optical packet generation, Tbit/s packet labeling, transmission and reception. The main building blocks of the experimental setup are a Tbit/s transmitter, packet labeling and a serial to parallel converter. The Tbit/s transmitter module, as previously discussed in Section 3.3.2, is built using the same procedure as the 640 Gbit/s transmitter except for some small details. The short pulse source module consists a 10 GHz erbium glass oscillator pulse generating laser (ERGO-PGL) centered at 1557 nm whereas the signal pluses are filtered

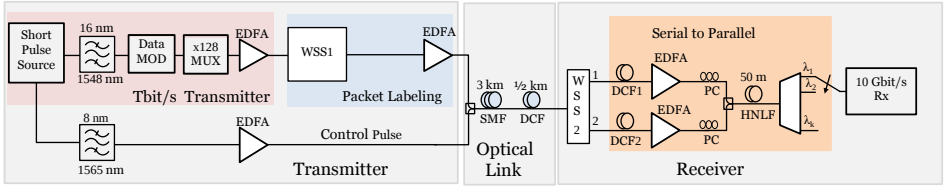

Figure 4.12: Experimental setup of a 1.28 Tbit/s optical packet generation, label allocation, transmission and reception.

at 1548 nm using a 16-nm wide OBPF. The optical pulses after filtering have a FWHM duration of 400 fs which corresponds to 50% duty cycle as the bit time for 1.28 Tbit/s is 780 fs. The ultra-short pulse is then data modulated using OOK format with a 10 Gbit/s custom pattern of 1411 bits of 2^7-1 PRBS followed by 2173 zero bits, which are used to reserve a free time slot for packet multiplexing and inter-packet gap. A 1.28 Tbit/s serial data packet is generated using a 2^7-1 PRBS preserving bit interleaver.

In-band optical labeling of the 1.28 Tbit/s packet is performed using a WSS1 which shapes the Tbit/s data spectrum and insert label information by carving spectral holes outside 3 dB but within 20 dB bandwidth

of the data spectrum. Figure 4.13(a) shows the shaped Tbit/s data spectrum emulating a chirp-free transfer-limited Gaussian pulses. Then, the WSS1 is reconfigured to apply a 0.3-nm wide ONF (see Figure 4.8(b)) and Figure 4.13(b) shows the Tbit/s data spectrum with one spectral hole at

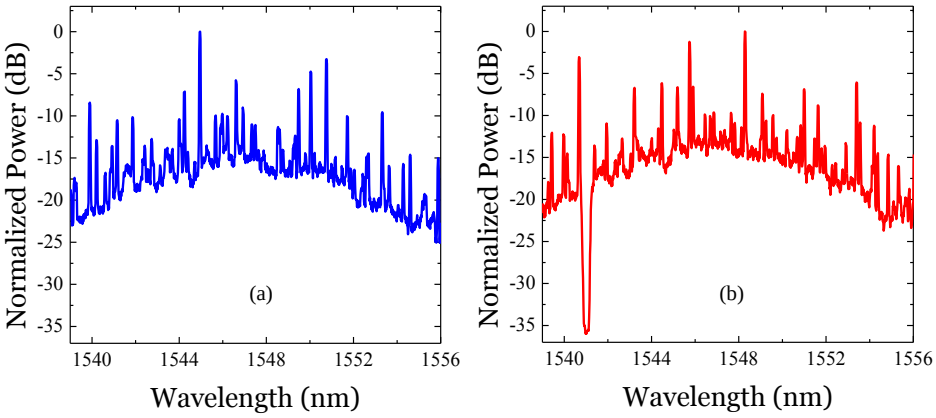

Figure 4.13: Tbit/s data spectra: (a) with no spectral hole and (b) with a 0.3-nm wide spectral hole at 1541 nm.

1541 nm. Furthermore, a total of sixteen ONFs are employed on the Tbit/s data spectrum, as shown in Figure 4.14(a), to demonstrate the scalability of the in-band labeling scheme. Figure 4.14(b) shows eight ONFs centered at position: P_1, P_3, P_5, P_7, P_9, P_{11}, P_{13} and P_{15} on the lower wavelength side of the Tbit/s spectrum whereas the remaining eight ONFs centered at P_2, P_4, P_6, P_8,P_{10}, P_{12}, P_{14} and P_{16} on the higher wavelength side are depicted in Figure 4.14(c). The eight spectral holes at each side of the data spectrum are separated by 50 GHz spacing to relax filtering challenges during label detection. Using the sixteen ONFs, a 16-bit LW can be generated in binary value as:

$$LW = P_{16}P_{15}P_{14}P_{13}P_{12}P_{11}P_{10}P_9P_8P_7P_6P_5P_4P_3P_2P_1 \tag{4.6}$$

where P_i is 1 if the notch filter at P_i is used or 0 otherwise for i=1, 2, ..., 16. Like the one byte LW that is given by Equation 4.1, the two byte (16-bit) LW is encoded based on how far the spectral holes are positioned from the center of the spectrum. The two least significant bits are the farthest positions (on each side of the spectrum) whereas the two most significant bits are the closest positions toward the center of the spectrum. The maximum number of unique LWs that can be generated using the sixteen ONFs is $2^{16} = 65.536$.

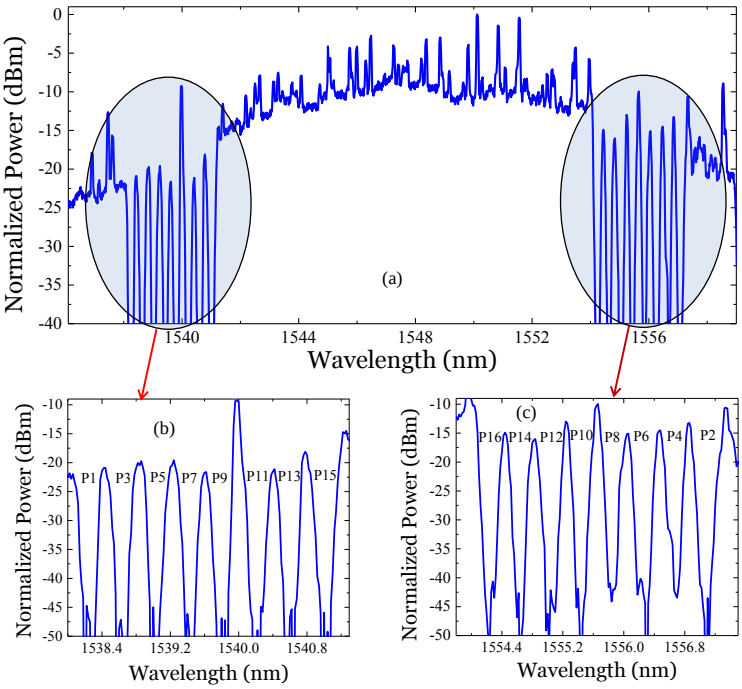

Figure 4.14: (a) Tbit/s spectrum of 16×notched packet using: (b) eight ONFs centered at lower wavelength side and (b) eight ONFs centered on the higher wavelength side.

In total, the WSS1 labels three Tbit/s data packets with zero, one and sixteen spectral hole(s). The labeled data packets and a 10 GHz optical control signal are launched together into a 3 km of single mode fiber (SMF) followed by a 0.5 km of dispersion compensating fiber (DCF). After transmission, a second WSS filters the Tbit/s data and control signal out to port-1 and port-2, respectively. The Tbit/s data packet is sent into the time lens based serial-to-parallel converter together with the transmitted control pulse. As previously explained in Section 3.4.2, both the data and control pulses are linearly chirped [44] to allow for chirped-pulse four-wave mixing (FWM) in a 50 m long highly nonlinear fiber [66], which ensures an optical serial-to-parallel conversion to a 100 GHz frequency spaced WDM grid. The converted WDM data channels are filtered out using a 40 GHz tunable OBPF on a 100 GHz.

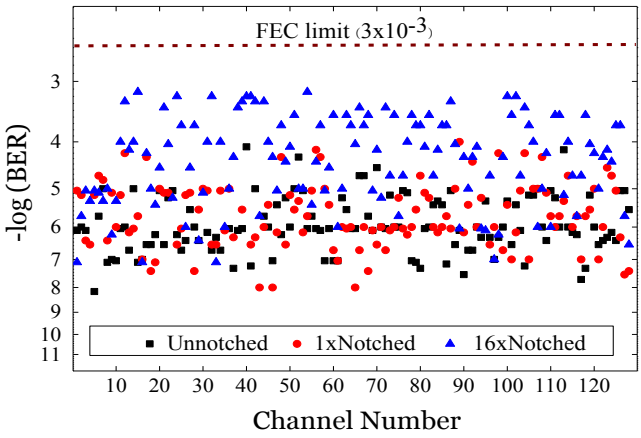

Figure 4.15: BER performance of all demultiplexed tributary channels of unnotched (rectangle), 1×notched (circle) and 16×notched (triangle) Tbit/s serial data packets. BER is measured at OSNR of 36 dB.

Result and discussion

Performance of all the time demultiplexed tributary channels is evaluated using BER measurements. The OSNR of the Tbit/s input data signal to the highly nonlinear fiber (HNLF) is fixed to 36-dB which is a theoretical limit of RZ-OOK data to achieve error free performance at 1.28 Tbit/s [52]. The BER measurements of unnotched and 1×notched and 16×notched data packets are shown in Figure 4.15. All the measured 384 channels achieve BER performance well below the forward error correction (FEC) limit of 3.3×10^{-3}. This demonstrates scalability of the labeling technique to be compatible with up to 1×65.536 OPS using sixteen ONFs. As expected, the 16×notched Tbit/s data packet has the worst system performance due to the presence of the sixteen ONFs on its spectrum. Nevertheless, the penalty is acceptable as the BER measurements of all the 10 Gbit/s tributary channels are below the FEC limit.

4.6 Summary

In this chapter, we have proposed a new in-band notch-filter labeling technique for high-capacity serial optical data packets. Detailed characterization of the optical labeling scheme has been presented in simulation using

4^{th} order super-Gaussian ONFs whose 3 dB BW and SR have been set, based on data packet and extracted label qualities, to 0.3 nm and 30 dB, respectively. Scalability of the optical labeling technique has been illustrated by employing up to eight ONFs inside the data spectrum of a 640 Gbit/s data packets and a maximum of 256 LWs have been generated based on permutation of the eight spectral position. As the optical labeling has been performed by filtering out optical power from selected spectral components of the data spectrum, the data quality has been affected by the number and position of the ONFs. Hence, we have investigated the notch-filtering effects on OOK modulated data signals using EOP. We have found that 60, 72, and 92 LWs for 640 Gbit/s serial data packets can be generated, by employing up to four ONFs simultaneously, at the expense of <1-dB, <1.1-dB and <1.12-dB EOPs, respectively.

Furthermore, the in-band optical labeling has been experimentally demonstrated, based on the simulation results, for 640 Gbit/s and and 1.28 Tbit/s serial data packets and the notch-filtering impact has been thoroughly investigated using BER measurements. A maximum of eight ONFs have been applied to the data spectrum of 640 Gbit/s packets to verify scalability of the in-band notch-filter labeling scheme for possible 1×256 OPS operation. It has been found that the difference on average sensitivities (at BER $\leq 10^{-9}$) between the data packet with no notch and with eight notches is only <1 dB. Finally, the optical labeling technique has been applied for 1.28 Tbit/s serial data packets and its scalability has been experimentally demonstrated by employing sixteen ONFs as the same time leading to generation of 65.536 unique LWs. Impact of notch-filtering on the Tbit/s data quality has been quantified using BER measurements and all tributaries of the Tbit/s data packet have achieved BER below the FEC limit of 3×10^{-3}.

Chapter 5

Optical label detection

5.1 Introduction

In Section 4.2, we have discussed various optical labeling techniques that have been employed to add an optical header to the data payload. The appended optical header is a switch control signal containing the information on where to route the optical packet in a given OPS network scenario. At each OPS node, the optical packet header is extracted using an optical header processing module that can be implemented using all-optical or opto-electronic blocks. The main attractive attributes of any header processor are speed, scalability and robustness. All-optical header processors have been actively studied mainly due to their ultra-fast processing speed [110–114]. In [111], the label information has been optically decoded after the packet header has been tapped in to the label detection module. The optically decoded label can directly control the OPS operation [115] or it can be converted into the electrical domain and drive an electro-optic based OPS node [111]. Albie to the ongoing research to develop optical processing modules such as all-optical flip-flop [112] and optical logic gate [113], the all-optical header processioning approach is still limited by the lack of flexible, stable and robust optical bit-level processing technologies.

Opto-electronic based header processing modules has been implemented, in most optical labeling techniques, using the matured, flexible and stable electronic processing technologies. Typically, the header processing module is constructed using optical module to separate the optical header from the data payload, an optical-to-electrical converter and a label processor to decode the label information. Complexity of this label detection module depends on how the label information is appended to the

data payload. The label information can be sent as a digital bit sequence that are appended serially to the data payload [79–81] or using out-of band wavelength multiplexing [83, 87]. Appending digital information as an optical header adds flexibility and high-degree of functionalities to the optical label detection module at the expense of higher complexity and larger label processing time that an optical memory may be needed to buffer the data payload. The label processing time can be reduced by increasing the symbol rate of the optical header and receive it using high-speed electronics (for example, at repetition rate of 10 GHz which corresponds to 100 ps per bit) but the higher the symbol rate the more bandwidth it requires.

A very fast and simple opto-electronic based label detection module can be employed to process an optical header that is sent as an analog signal and perform OPS operation of the data payload. In section 4.3, an in-band notch-filter labeling technique is introduced to send an analog switch control information in the optical spectrum of a given high-capacity serial data. The main role of the control information is to act as an address (similar to IP address) of the given optical data packet. The OPS node should have the means to detect the label control information, interpret it correctly and apply it to forward each data packet to its respective destination. The optical label detection module is the responsible block for extracting the switch control information from each data high-capacity serial packets as show in Figure 4.1.

In Section 5.2, we start our discussion with detailed illustration of the opto-electronic based optical label detection in simulation. The optical label information is successfully decoded from 640 Gbit/s data packets using an experimental demonstration. Furthermore, stability of the label detection is experimentally demonstrated by decoding the optical information from sixteen spectral positions of 1.28 Tbit/s serial data packets. The impact of notch-filter parameters such as 3 dB bandwidth (BW), suppression ratio (SR) and offset in center frequencies of the ONF and OBPF, on the decoded switch control information is discussed in Section 5.3 using label contrast (LC), calculated as the ratio between optical power of a given spectral position before and after the notch filter is applied. A mismatch between central frequencies of the two optical filters leads to a penalty in LC. Moreover, packet length independence of the optical labeling and label detection modules is experimentally verified by extracting four switch control signal from 640 Gbit/s variable length data packets. Finally, we discuss scalability of the optical label detection module to extract switch control signal from more than one spectral positions.

5.2 Label detection

In Chapter 4, the in-band notch-filter labeling technique is introduced to send a switch control information in the optical spectrum of a given high-capacity data packet. The switching control information is embedded within the signal bandwidth using ONFs. At an OPS node, the control information has to be extracted using a label detection module. In this section, we discuss the optical label detection module which is constructed with a narrow OBPF, an optical-to-electrical converter, and a simple electronic circuit. The module is explained using a numerical analysis followed by experimental demonstrations.

5.2.1 Numerical analysis

The numerical analysis is developed using MATLAB® based on the block diagram shown in Figure 5.1 which is an extension of Figure 4.2. Two high-capacity optical data packets are simulated using the 640 Gbit/s transmitter which are referred as Signal-A in Figure 5.1. Similar to the numerical work of Section 4.4, the data packets are generated using 33% RZ-OOK modulated optical pulses at a repetition rate of 640 GHz. The packet labeling module shown in Figure 5.1(a) labels packet-1 and packet-2 by turning on/off an ONF centered at f1. Packet-2 has a notch at the right side of the data spectrum centered at f1 while packet-1 is labeled by turning off the ONF as shown in Signal-B of Figure 5.1.

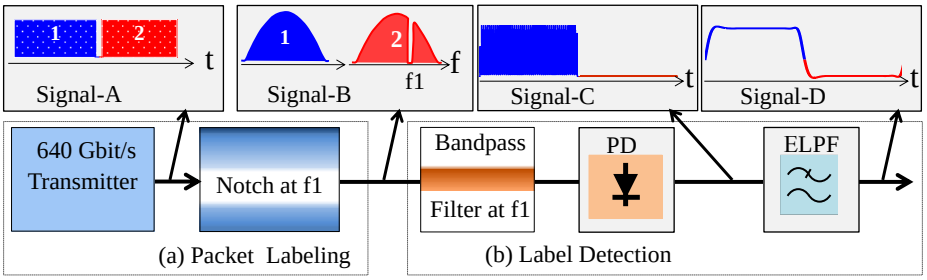

Figure 5.1: (a) Schematics of the in-band notch-filter labeling of two 640 Gbit/s serial data packets, optically labeled by turning on/off the notch at f1. (b) Block diagram of the proposed label detection module where the label information are extracted, photo-detected and low-pass filtered to generate the rectangular like electrical control signal.

The label extraction module shown in Figure 5.1(b) has an OBPF connected to an opto-electronic module consisting of a photodiode (PD) followed by a electrical low-pass filter (ELPF). Like the ONF, the OBPF is 0.3-nm wide 4^{th} order super Gaussian filter centered at f1. The main function of the OBPF is to check for a notch (switch control information) made by its corresponding ONF in the packet labeling module and sends the output to an ideal PD converting it to an electrical signal. Signal-C of Figure 5.1 shows the switch control information of both data packets at the output of the PD.

Due to the availability of a notch at f1, packet-2 has smooth low voltage control signal. On the other hand, packet-1 has a distorted control signal with strong ripples in the entire duration mainly due to bit-pattern dependence of the optical power at f1. Since the bandwidth of an ideal PD is infinite, optical power (amplitude modulation leads to high power for 1-bit low power for 0-bit) of all the bits can be detected by the PD. In order to detect the envelope of packet-1, the electrical signal at the output of the PD is filtered using a 400-MHz wide 4^{th} order Bessel ELPF. As shown by signal-D in Figure 5.1, the output of the ELPF is a rectangular like electrical signal where its slow rising and falling time is inherited from the bandwidth-limited ELPF.

The label detection module is further characterized by scaling the number of ONFs to eight which are centered at eight different spectral positions (see Figure 4.2). The ability of the notch-filter labeling scheme to control OPS operation is verified using five variable length 640 Gbit/s serial data packets as depicted at the top in Figure 5.2. The duration of each packet from left to right is: 300 ns, 26 ns, 128 ns, 240 ns and 70 ns, respectively, whereas the inter-packet gap is set to 10 ns. All the high bit rate data packets are labeled by employing their corresponding notch filters in which the five label words range from 38 (P_2, P_3 and P_6 are used) up to 233 (P_1, P_4, P_6, P_7 and P_8 are used).

After all labels of each packet are extracted as high/low voltage levels from each data spectrum as shown in the middle part of Figure 5.2, the label word (LW) which is defined using Equation 4.1, is reconstructed by decoding the voltage level of each extracted label, L_i. For instance, a LW of the shortest optical packet is decimal value 97 which consists of all L_i at high voltage level except L_1, L_6 and L_7, whereas the label word of the longest optical packet is 156 (i.e., binary 10011100) which consists of L_1, L_2, L_6 and L_7 at high voltage level and L_3, L_4, L_5 and L_8 at low voltage level as depicted bottom of Figure 5.2.

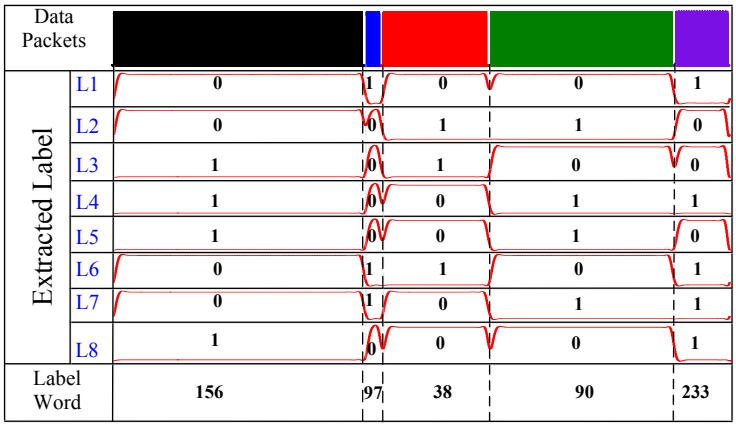

Figure 5.2: The top shows five labeled variable length 640 Gbit/s serial optical packets with 10 ns gap. The middle shows voltage levels of eight extracted labels for each packet. The bottom shows reconstructed label words in decimal value for each packet.

Due to power differences between the eight selected spectral positions, the extracted control signal may not have the same voltage levels. Moreover, the falling/rising time between the voltage levels is not sharp as clearly seen from the shortest packet in Figure 5.2. From practical perspective, duration of the control signal should match with the packet length in order to switch the whole data packet successfully. Furthermore, depending on the type of the optical switching, the high voltage level should be set to the optimum value to drive the switching operation properly. The voltage level can be regulated to the required value, for instance, using an electrical amplifier. However, sharpness of the rising/falling time and smoothness of the control signal should remain unaffected during the amplification. All these practical issues are addressed in Section 5.2.2 using experimental demonstrations.

5.2.2 Experimental demonstration

Any optical switch requires a stable control signal to perform packet based data forwarding within a given time interval. In most cases, the control signal is recovered at the optical switch from a specific information set by the sender along with the data packet or separately. In our case, the control signal is encoded within the signal bandwidth at the sender using notch-filter labeling. In this section, we address how the switch control

signal is experimentally regenerated from the specific spectral position of a given data packet using the proposed label detection module. We start characterizing the label detection technique using 640 Gbit/s serial data packets. Then, we scale the symbol rate of the data packets to 1.28 Tbit/s where sixteen switch control signals are successfully recovered from the Tbit/s data spectrum.

640 Gbit/s data packets

Based on the numerical characterization, an experimental demonstration is performed using the setup shown in Figure 5.3. The setup is made-up of a 640 Gbit/s transmitter, optical labeling and label extraction modules. The 640 Gbit/s transmitter, as detailed in Section 3.3.1, generates a high-capacity data with packet duration of 146.5 ns followed by inter-packet gaps and free time slot for packet multiplexing as shown using packet-1 trace in Figure 5.3. In the optical labeling module, the data packet is split into two arms and multi-casted to port-1 and port-2 of a WSS that treats the data packet at each port independently. The data packet at port-1, referred as packet-1, is labeled without any spectral notch while the data at port-2 (packet-2) is labeled by inserting a notch at 1559 nm using a 0.3-nm wide ONF. After packet-2 is delayed using a 30 m of SMF (see packet-2 in Figure 5.3), it is time multiplexed with packet-1. The oscilloscope traces of the multiplexed packet-1 and packet-2 is shown in Figure 5.3, thus the spectrum of every second packet has a notch at 1559 nm.

The label detection module is responsible to extract an electrical control signal from the spectra of data packet-1 and packet-2. The module is

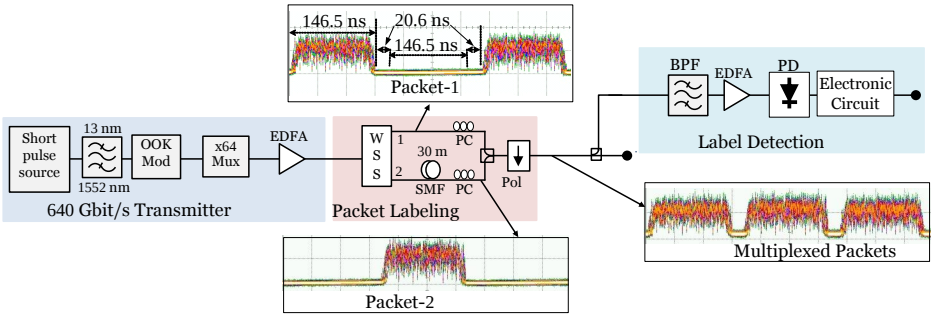

Figure 5.3: Experimental setup of the proposed optical label detection for 640 Gbit/s data packets, labeled using the in-band notch-filtering scheme.

constructed using an OBPF followed by a PD, similar to the block diagram shown in Figure 5.1(b). The OBPF has 0.3-nm wide at 3 dB BW and it is centered at 1559 nm where the notch of packet-2 is positioned. Figure 5.4(a) shows a top flat transfer function of the OBPF and a simulated 4^{th} order super Gaussian function as reference. The experimental transfer function, represented by solid line, shows a good agreement up to 3 dB BW with the simulated fit depicted by dash line. However, the experimental transfer function diverges from the fit as bandwidth increases and it can be related to slow frequency transition of the OBPF.

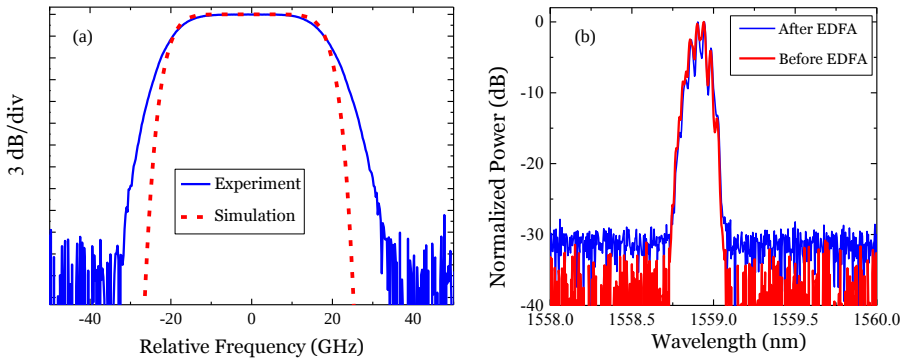

Figure 5.4: (a) Transfer function of the OBPF used in the experiment (sold line) and simulated 4^{th} order super Gaussian function (dashed line). (b) Power spectra of the extracted label before (blue) and after (red) the EDFA.

We first characterize the labeling detection scheme using packet-1 while port-2 of the WSS is disconnected. Hence, packet-2 is not time multiplexed with packet-1 which enables us to investigate effects such as amplified spontaneous emission (ASE) noise from an EDFA that is primarily used to boost output of the OBPF. As we discuss in more details in Section 5.3, EDFA introduced ASE noise which can fill-up the spectral notch and affect quality of the extracted control signal. In order to extract optical switch control information from packet-1, the OBPF filters out the optical power from the data spectra. For reference measurements, the payload of packet-1 gives high optical power whereas the padded zero bits (act as a notched spectrum) gives low optical power at 1559 nm. Figure 5.4(b) shows power spectra of the filtered control signal before and after the EDFA. Due to ASE noise from the EDFA, noise floor of the amplified control signal has increased by 5 dB and this can lead to reduction in LC. However, we expect negligible impact on the final outcome as the OSNR of the extracted label remains >30 dB.

The label detection module is further characterized by reconnecting port-2 of the WSS and the control signal is extracted from the multiplexed data packet-1 and packet-2. Figure 5.5(a) shows oscilloscope traces of multiplexed packet-1 and packet-2. Duration of both packet-1 and packet-2 is 146.5 ns while their inter-packet guard time is set to 20.6 ns. The output of the OBPF, as shown in Figure 5.5(b), has an optical power from packet-1 as there is no notch at 1559 nm. The filter optical power is then amplified using the per-amplifier EDFA and converted to an electrical voltage using a 50-MHz PD. The finite bandwidth of the PD enables it to act as a low-pass filter and additional ELPF is not required in contrary to the numerical module shown in Figure 5.1(b). Figure 5.5(c) shows an oscilloscope traces of the electrical signal at the output of the PD. Even though the electrical signal has a rectangular shape which can be employed to control switching operation, for example based on electro-optical effect [78], it is not the final outcome because of a slow rising/falling time, a ripples on the high voltage level and a short high voltage level duration.

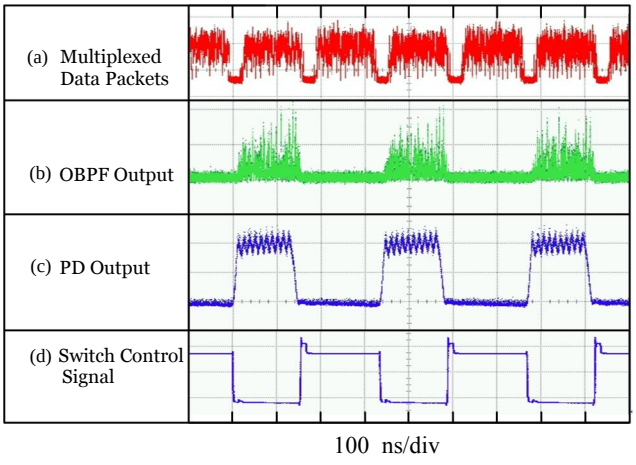

Figure 5.5: Oscilloscope traces of: (a) multiplexed packet-1 and packet-2 input to the OBPF; (b)oOptical label information that is extracted from packet-1 and packet-2 using the OBPF, centered at 1559 nm; (c) a rectangular like electrical control signal after the extracted optical power is received by the 40 MHz PD; and (d) clean and sharp electrical control signal regenerated by the electronic circuit.

The slow rising/falling time of the electrical control signal originates from the bandwidth-limited PD whereas the ripples on the high voltage

level can be related to a bit pattern dependence of the power spectrum of packet-1 which leads to power fluctuation of the optical signal after the OBPF. At best, duration of the high voltage level is 140 ns long which is 7 ns shorter than the duration of packet-1. This is the most critical issue as the switch control signal will not stay at fixed-voltage level until packet-1 is fully switched. This issue can be related to the way the high-capacity data packet is generated at the 640 Gbit/s transmitter. As explained in Section 3.3.1, the 640 Gbit/s data packet is generated using a 2^7-1 PRBS preserving bit interleaver where each multiplexing stage introduces up to 63-bit time delay. This leads to a data packet with less number of bits (lower optical power) at its leading and trailing edges as shown in Figure 5.6 using a simulated intensity profile of OOK modulated 640 Gbit/s data packet. Hence, such profile leads to shorter high-voltage level duration.

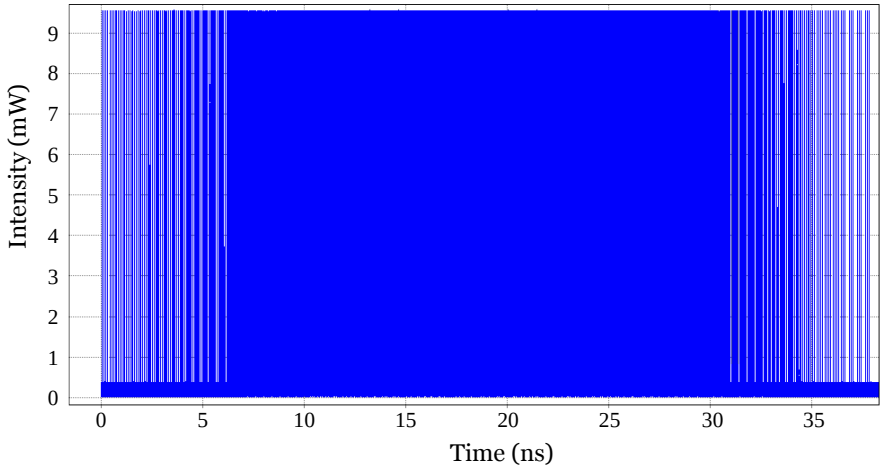

Figure 5.6: Simulated intensity profile of OOK modulated 640 Gbit/s data packet generated using a 2^7-1 PRBS preserving bit-multiplier that results in less number of bits at the leading and trailing edges of the packet.

These three practical challenges of the rectangular electrical control signal can be tackled using a very fast 1-bit analog to digital converter which is also called a comparator. The output of a comparator is a binary digital value that is generated based on a given threshold voltage. Hence, the output of the PD is fed into two comparators to get a clean control signal with two voltage levels. Figure 5.5(d) shows oscilloscope traces of the regenerated electrical control signal at the output of the electrical circuit. In order to drive the switching operation using the required electrical signal,

a field-effect transistor is used to regulate the voltage level and invert the sign of the electrical control signal in a way that if there is a notch, the switch control signal is at high voltage level otherwise it is at low voltage level. From Figure 5.5(d), it clear that the electrical circuits has smoothen the ripples and reduced the rising/falling time significantly.

The two comparators in the electrical circuit are connected in series so that an extra duration can be added to the high voltage level to make sure that the whole data packet is switched using the extracted control signal. As one can observe from the falling time of the PD and rising time of the comparator output electrical signals shown in Figure 5.5(c) and (d), the high voltage level duration of the comparator output is 10 ns longer. Nevertheless, the extra duration is not restricted to 10 ns as it can be controlled using a delay circuit between the two comparators.

1.28 Tbit/s data packet

In this section, we discuss a successful optical label detection from 1.28 Tbit/s serial packets that are packetized, optical notch-filter labeled, amplified and transmitted over 3 km of SMF. The label detection is characterized using an experimental setup shown in Figure 5.7. The Tbit/s transmitter, which is detailed in Section 3.3.2, generates a 152 ns long Tbit/s data packet followed by 25 ns inter-packet gap and 152 ns free time slot reserved for packet multiplexing. In-band optical labeling of the 1.28 Tbit/s packet is performed using a reconfigurable WSS1. The WSS1 broadcasts the Tbit/s data into port-1 and port-2 and the data at port-1 of the WSS1 (packet-1) is labeled using no notch while the data at port-2 (packet-2) is labeled by carving 0.3-nm wide notches at sixteen different

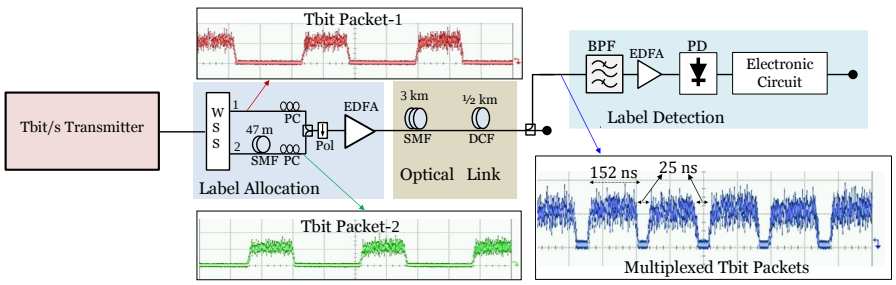

Figure 5.7: Experimental setup of an optical label detection from 1.28 Tbit/s serial data packets labeled using the in-band notch-filter scheme.

spectral position between the 3 dB and 20 dB of the data bandwidth as depicted in Figure 5.8(a). After packet-2 is delayed using a 47 m of SMF, it is time multiplexed with packet-1 on the free time slot reserved by encoding a sequence of zero bits. The multiplexed 1.28 Tbit/s data packets have a duration of 152 ns followed by 25 ns inter-packet gap as guard time. Oscilloscope traces of packet-1 and packet-2 before and after packet multiplexing are shown in Figure 5.7. After amplification using an EDFA, the packets are launched into a 3 km of SMF followed by a 0.5 km of DCF.

After the data packets are transmitted over 3 km of SMF, they are power tapped into a label detection module that extracts the optical label information from the data spectrum of each packet and generates an electrical control signal. As explained previously, the label detection module consists of an OBPF, centered at a spectral position where the label is placed; a PD to convert the optical power to an electrical voltage; and a comparator circuit to regenerate a stable electrical control signal. For a given spec-

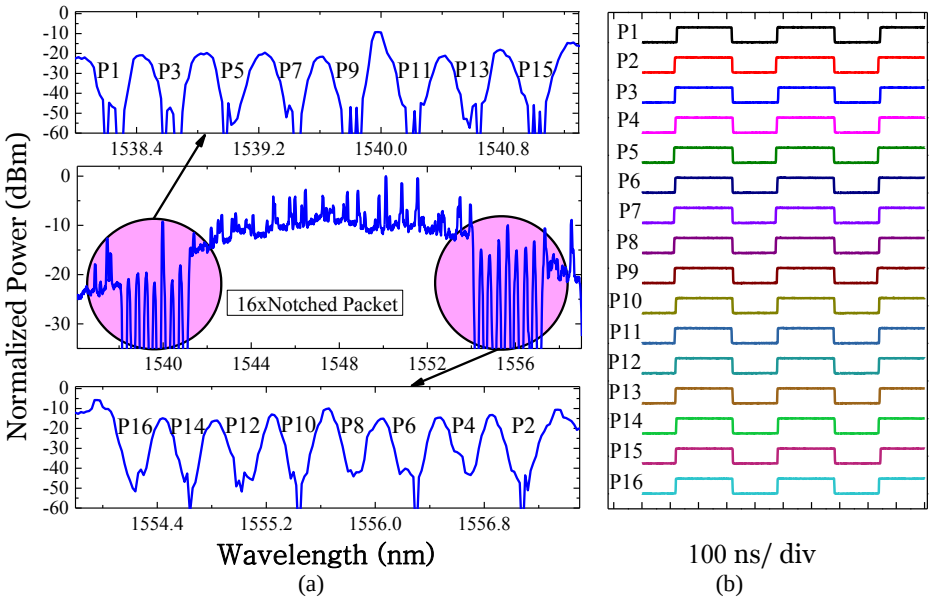

Figure 5.8: (a) Tbit/s spectrum of 16×notched packet. (b) Extracted labels of sixteen spectral positions from multiplexed 16×notched and not-labeled packets. All sixteen switch control signals are recovered by tuning the center wavelength of the OBPF to the sixteen spectral positions while the threshold voltage of the comparators is kept at a fixed value.

tral position, the switch control signal is at high voltage level if there is a spectral hole made by a notch filter otherwise it is at low voltage level.

As shown in Figure 5.8(a), the optical power filtered out from each of the sixteen spectral holes may not be the same because of their relative position from the center wavelength and due to the fact that the power spectrum of OOK modulated Tbit/s data packets is bit-pattern dependent. In order to investigate resilience of the label detection to small optical power fluctuation of a given spectral position, sixteen switch control signals of multiplexed packet-1 and 16×notched packet-2 are extracted from all spectral positions where the sixteen ONFs are centered. Threshold voltage of the comparator is kept constant for all sixteen scenarios. Figure 5.8(b) shows all the extracted labels in which the low voltage levels correspond to packet-1 whereas the high voltage levels belong to the 16×notched packet-2. The durations of the high/low voltage levels of all control signals are identical and stable regardless of their possible optical power differences.

5.3 Label quality

In Section 4.3.2, we have presented detailed characterization of the notch-filter parameters like spectral position, and filter transfer functions. The effect of the notch-filter on the high-capacity data packets is quantified in Section 4.4 and Section 4.5 using EOP and BER measurements, respectively. In this section, we discuss in simulation the effect of notch filter parameters on the extracted label quality by varying the 3 dB BW and SR of the ONF. In Section 5.2, we explain that the ONF in the packet labeling module and the OBPF in the label detection module have the same 3 dB BW and are centered at the same spectral positions. In reality, there may exist a mismatch between center frequencies of both filters which can lead to error during the OPS operation. Tolerance of the label detection module for such scenario is also presented in this section by varying center frequency of the OBPF while keeping the notch-filter position fixed.

The voltage level of the extracted electrical control signal is directly proportional to the PD input optical power. The quality of the extracted label is characterized by using the contrast between the high and low voltage levels, which means the ratio of the detected optical power when there is no notch and the optical power in the presence of a notch at the specific spectral position. Label contrast, LC, of a given spectral position can be defined as:

$$LC_i\ (dB) = 10\log(Power_{P_i=0}/Power_{P_i=1}) \tag{5.1}$$

where $i = 1, 2, ..., 8$, $Power_{P_i=0}$ is an optical power input to the PD when the ONF at P_i is off while $Power_{P_i=1}$ is an optical power input to the PD when the ONF at P_i is on.

ASE noise from optical amplifiers is one of the main link impairments that can affect the label contrast that is given by Equation 5.1. Once the data packet is labeled using the ONF(s), the carved spectral hole(s) can be filled by noise when the data packet is amplified as the OSNR of the data is also reduced, hence, it may lead to reduction in LC. Therefore, the ONFs should be positioned close to the 3 dB BW of the signal to minimize the effect of ASE by increasing the initial LC.

Other parameters of the ONF that can affect the label quality are the 3 dB BW and SR in which their effect is characterized using LC for the eight spectral positions shown in Figure 4.2. Due to symmetry of the 640 Gbit/s spectrum, notches centered at left side of the spectrum have the same LC with their corresponding (the same relative position to the center of the data spectrum) right side notches. For example, P_1 has the same LC as P_2 while P_3 has the same LC as P_4 and so on.

Suppression ratio

Beside noise and notch position, SR of the ONF can affect the quality of the extracted label. SR measures how deep the spectral hole can penetrate the data spectrum at a specific position. The optical power, $Power_{P_i=1}$, decrease as the depth of the spectral hole (SR) increases. Therefore, the LC value increases, based on Equation 5.1, as SR increases. In simulation, we investigate the effect SR on the LC for eight 0.3-nm wide ONFs which are centered at eight different spectral positions as shown in Figure 4.2.

Table 5.1 shows LC summary of the eight spectral potions for varying SR value from 6 dB to 40 dB. For SR=6 dB, the LC value of each spectral position is less than 10 dB. The LC increases by more than 5 dB when the SR value is set to 16 dB. As expected, the LC increases for all spectral positions as the SR of the notch filter increases. But the LC of the 40-dB deep ONF is only 0.6 dB higher than the LC of 16-dB deep ONF due to the fact that 16 dB SR of each ONF is deep enough to remove almost all the optical power. In our work, we use a 30-dB deep ONF in all simulations whereas the maximum SR we achieve during the experiment demonstration is 20 dB[1], which only results in 0.2 dB lower LC than for 30 dB depth.

[1]We used different SR values as the experimental demonstration is performed after the simulations.

Table 5.1: LC for different suppression ratio of eight ONFs centered at eight spectral positions as shown in Figure 4.2.

SR	LC_i (dB)			
(dB)	i=1 (2)	i=3 (4)	i=5 (6)	i=7 (8)
6	9.64	9.63	9.7	9.69
10	13.48	13.44	13.6	13.58
12	14.53	14.47	14.67	14.64
16	15.56	15.48	15.73	15.69
20	15.94	15.85	16.11	16.06
30	16.14	16.05	16.32	16.27
40	16.16	16.07	16.34	16.29

3 dB bandwidth

3 dB BW of the ONF is another important parameter that can affect the extracted switch control signal. By fixing the SR at 30 dB but varying the 3 dB BW of the eight ONFs, we measure LC of eight spectral positions (see Figure 4.2) using Equation 5.1 in the absence of noise. Table 5.2 summarizes the LC of the eight ONFs for 3 dB BW ranging from 0.225 nm (28.1 GHz) to 0.373 nm (46.6 GHz). The LC of the eight spectral positions is almost independent(with maximum variation of 0.5 dB) of the 3 dB BW because LC is a ratio of the two optical powers; $Power_{P_i=0}$ and $Power_{P_i=1}$. So, when the BW of each ONF changes, the value of the optical powers also varies but their ratio can still remain constant. The exact shape of the optical data spectrum depends on the bit pattern of the PRBS sequence. Hence, the spectrum OOK modulated data packet is full of small modulation peaks which can lead to the 0.5-dB variation in LC.

One parameter of the notch filter that does not affect the label quality considerably is the 3 dB BW because the LC is a relative value as it is a ratio of two optical powers. However, applying narrow filters with super Gaussian transfer function can be very challenging in practice. Considering the practical implementation and quality of the signal, we use 0.3-nm wide ONFs and OBPFs.

Table 5.2: LC for different 3 dB BWs of eight ONFrs centered at eight spectral positions that are shown in Figure 4.2.

BW	LC_i (dB)			
(nm)	i=1(2)	i=3(4)	i=5(6)	i=7(8)
0.227	16.25	16.29	16.23	16.31
0.251	16.28	16.49	16.17	16.25
0.275	15.94	16.11	16.32	16.41
0.3	16.14	16.05	16.32	16.27
0.324	16.23	15.99	16.35	16.3
0.348	16.12	16.02	16.19	15.9
0.373	16.05	16..05	16.26	15.94

Mismatch in center frequencies

Here we investigate the impact of a possible center frequency mismatch between both ONFs and OBPFs. First, a 640 Gbit/s serial data packets is generated in simulations by using the same procedure of Section 4.3.2 and optically labeled using eight ONFs (see Figure 4.2). Hence, the center frequency of all the ONFs is fixed at eight specific spectral positions. We evaluate the LC value of each spectral position by intentionally varying center frequencies of their corresponding OBPFs. Figure 5.9 shows the calculated LC versus offset in center frequencies of the ONF and OBPF for eight different spectral positions. As expected, the LC is maximum when the frequency offset is zero for all spectral positions whereas every $\pm$1 GHz mismatch in center frequency leads to around 1 dB reduction in LC for all eight spectral positions. Though a couple of GHz mismatch in center frequency can be tolerable, the LC is deteriorated considerably for a frequency mismatch $\geq$3 GHz.

5.4 Scalable label detection

The envisaged optical notch-filter labeling scheme is highly scalable that a maximum of sixteen ONFs are applied within the Tbit/s data spectrum as shown in Figure 5.8(a). In principle, this enables the generation of $2^{16} = 65.536$ unique labels that can be utilized by many high radix opti-

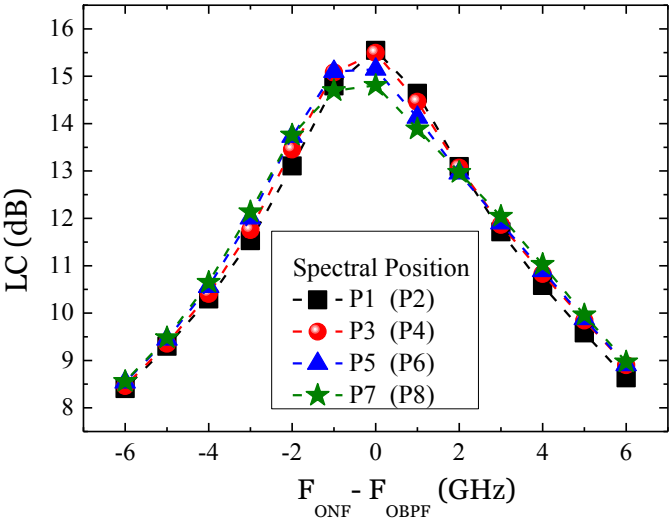

Figure 5.9: LC versus offset in center frequencies of the ONF and OBPF for eight different spectral positions that are shown in Figure 4.2.

cal switches. In order to control these switches properly, a scalable label detection module is mandatory. Here, we address how the label detection can be adapted to extract optical labels from N≥2 spectral positions.

Two spectral positions

So far, we explain the extraction of an electrical control signal from a single spectral position. Then, the decoded electrical signal can be applied to control a 1×2 optical switch. Scaling the number of spectral positions to N means up to 2^N switch control signals can be extracted and subsequently applied to control 1×N optical switching operation. For N=2, four high-capacity data packets can be optically labeled using the in-band notch-filtering technique. Here, we experimentally demonstrate extraction of four switch control signals for 640 Gbit/s serial data packets and the extracted control signal are applied in Section 6.4 to switch a variable length 640 Gbit/s serial data packets. Figure 5.10(a)-(d) shows the power spectra of the four data packets. Packet-1 is labeled with zero notches whereas packet-2, -3 and -4 are labeled by carving two, four and eight spectral notches. Highlighted areas marked L_1 (1548.3 nm) and L_2 (1560.1 nm) show where the two ONFs of our interest are positioned. The four data packets are optically labeled by turning on/off these two ONFs.

Figure 5.10(e) shows the experimental set-up of a label detection module that extracts two optical labels from L_1 and L_2. It is an extension of the label detection scheme shown in Figure 5.1. Two 0.3-nm wide OBPFs, centered at 1548.3 nm and 1560.1 nm, extract the optical power of L_1 and L_2. After each extracted optical label is amplified and converted to electrical signals using two PDs, the electrical signals are regenerated as digital values, In_1 and In_2, using two comparator modules. These two binary values are processed using a 2-bit decoder and four switch control signals are generated using logical interpretation of In_1 and In_2.

Oscilloscope trace of the variable length four data packets are shown in Figure 5.10(f). As summarized in Table 5.3, the four data packets are optical labeled by turning the two ONFs at L_1 and L_2 ON/OFF. Figures 5.10(g) and (h) shows the In_1 and In_2 binary electrical signals of each

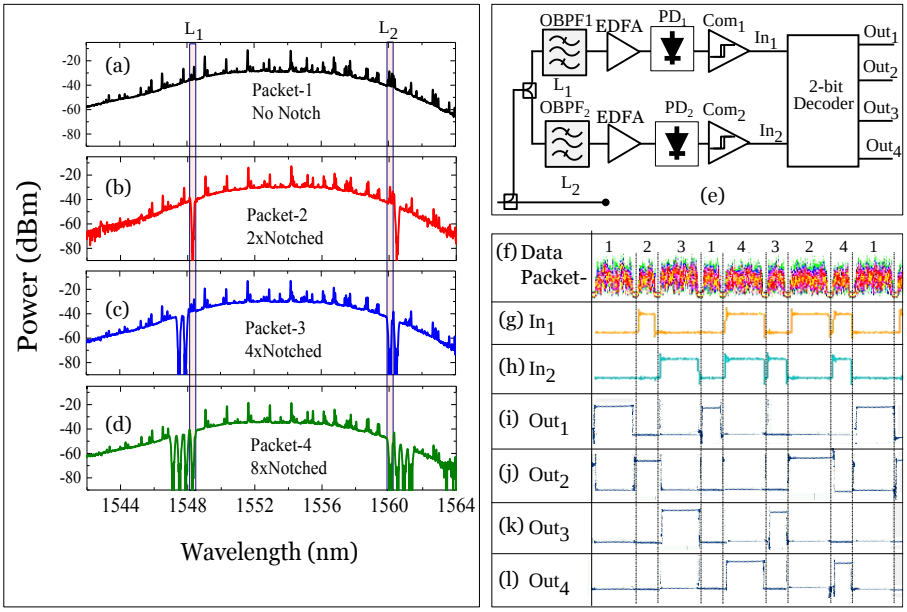

Figure 5.10: Power spectra of notch-filter labeled 640 Gbit/s data packets: (a) unnotched, (b) 2×notched, (c) 4×notched and (d) 8×notched. Highlighted areas marked L_1 and L_2 shows where the OBPFs are positioned. (e) Experimental set-up of the label detection module used to extract optical labels from L_1 and L_2. (g) In_1 and (h) In_2 are electrical control signals extracted from L_1 and L_2, respectively. Output of the 2×4 decoder when binary value of In_2In_1 is: (i) "00", (j) "01", (k) "10" and (l) "11".

Table 5.3: Generation of four electrical control signals using in-band optical label inserted in two spectral position as shown in Figure 5.10.

Data	Notch at		Voltage level at		Output Control Signal			
Packets	L_1	L_2	In_1	In_2	Out_1	Out_2	Out_3	Out_4
1	OFF	OFF	0	0	high	low	low	low
2	OFF	ON	0	1	low	high	low	low
3	ON	OFF	1	0	low	low	high	low
4	ON	ON	1	1	low	low	low	high

packet that are extracted from L_1 and L_2, respectively. As shown in Table 5.3, both In_2 and In_2 of packet-1, for instance, are at zero voltage level as there is no notch on the data spectrum (see Figure 5.10(d)). Figure 5.10(i)-(l) depicts the oscilloscope traces of the four switch control signals that are applied to a 1×4 OPS node to switch the four data packets. As summarized in Table 5.3, each electrical control signal is generated based on the presence of spectral notch(es) at L_1 or/and L_2. For example, a high voltage level control signal is generated at Out_2 of the 2-bit decoder when there is a notch only at L_1, i.e., in case of packet-2.

N spectral positions

Figure 5.11 shows two block diagrams of label detection modules that can used to extract 2^N switching control signals from N spectral positions of a given high-capacity data packets. The block diagram shown in Figure 5.11(a) is an extended version of the label detection module shown in Figure 5.10(e) in which N OBPFs are connected to N PDs followed by N 1-bit comparators. 2^N switching control signals can be generated based on the output of all N comparators using a N-to-2^N decoder. Despite the label detection module is cost-ineffective because each input port of the optical switch requires N OBPFs, N PD and N comparator modules, it is simple to implement the heart ot the optical label processing module using robust electronic circuits such as analog-to-digital converters and a N to 2^N decoder. But, the labeling module is bulky and it may introduce high splitting loss to the optical label information, especially when N is large.

In the second block diagram shown in Figure 5.11(b), the N OBPFs are replaced by one compact 1×N AWG filter while one EDFA may be enough to compensate the insertion loss of all N optical label information. Moreover,

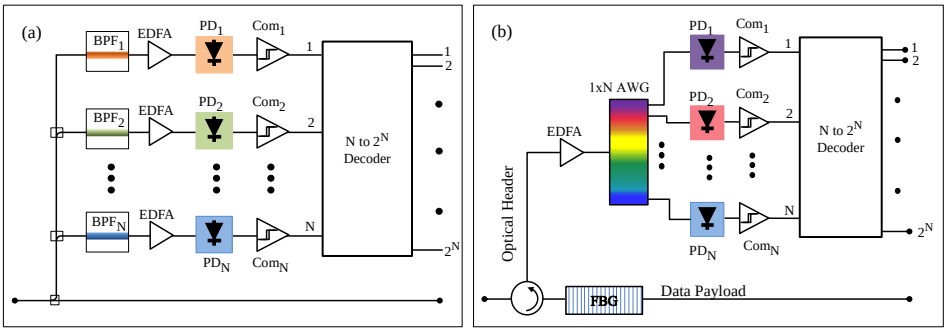

Figure 5.11: Scalable N optical label detection block diagrams. (a) An extended version of the label detection module shown in Figure 5.10. (b) A compact label detection module.

the N optical label information can be extracted from the optical data using an optical circulator and a FBG for N spectral positions of the data spectrum. By doing so, any high capacity data packet can experience the same notch-filtering effects regardless of the number of available spectral holes in its spectrum. The labeling module can also pave the way for easy header deattachment and attachment at the OPS node. Once the optical header is removed using the FBG, a new header information can be attached easily by filtering the output a broadband source according the new LW and coupling it within data signal bandwidth. However, such method need a strict timing control as duration of the newly added optical label should match with the data packet length.

5.5 Summary

This chapter has presented detailed illustration of an opto-electronic based label detection module which has been experimentally applied to regenerate stable electrical control signals using optical labels of 640 Gbit/s and 1.28 Tbit/s data packets. The opto-electronic module has been constructed using a OBPF, a PD and 1-bit comparator circuits. The optical labels have been inserted within the signal bandwidth using the in-band optical notch-filtering labeling scheme, hence, quality of the extracted label information has been investigated in LC for different parameters of the ONF including 3 dB BW and SR, and offset in center frequencies of ONFs and OBPFs. It has been found that LC is almost independent of the 3 dB BW, whilst only

0.6 dB difference in LC has been calculated when the SR has increased 16 dB to 40 dB. Furthermore, every ±1 GHz mismatch in center frequencies of eachONF and OBPF has bean observed leading to almost 1 dB reduction in LC. Finally, packet length independence of the opto-electronic module has been experimentally verified by extracting four electrical control signals from variable length 640 Gbit/s data packets while further scalability of the label detection module has been addressed by using two approaches.

Chapter 6

Optical packet switching

6.1 Introduction

Recently, the need for fast and high-capacity optical switches in short-range networks including datacenters (DCs), could computing and high-performance computing (HPC) has considerably increased. Optical switching networks can be very helpful to deal with the unprecedented growth of the DC global Internet traffic [12], because they possess the attractive feature of offering fast reconfiguration of high-capacity data at a potentially low cost and better power efficiency[1] than conventional electrical switch networks. OCS, OBS and OPS are the most popular optical networking technologies that are proposed to realize switching operation in the space, wavelength and time domains [116].

In recent years, space domain based optical switching technologies such as 3-D micro-electro-mechanical system (MEMS) have accomplished a remarkable progression compared to the other optical technologies though they are not as matured and sophisticated as the electronics counterpart yet. MEMS switches are very scalable to large number of space ports, mainly optical fibers [117], where high-capacity optical data are switched with low polarization and wavelength dependent losses. Unfortunately, they have a very slow reconfiguration time, typically in the order of milliseconds [118]. Hence, they are mainly suitable for reconfigurable OCS technologies where switching operation is performed at the granularity of a lightpath. The lightpath can be based on wavelength in which high-capacity data-streams carried by multiple WDM channels can be routed together using the MEMS switch. On the other hand, optical switching

[1] Due to the possible reduction in optical-to-electrical-to-optical (OEO) conversions.

of each individual WDM channel can be achieved in the wavelength domain using wavelength selective switchs (WSSs) [119] or a combination of arrayed waveguide-gratings (AWGs) and tunable lasers [120]. Such WDM switches are typically used in OCS networks. WDM based OPS networks have been proposed in [112, 121] as a possible solution to reduce power consumption of the current electronic packet switching technologies. However, such OPS technologies may not be full realized using the wavelength based switching due to the possible wavelength contention albeit to the ongoing efforts to handle the problem using different types of wavelength conversion schemes [122–124]. Moreover, OPS operation at the wavelength level may not be the most power efficient solution for high-capacity short-range networks as the switching-energy per bit of the OPS node may scale with the number of separately routed WDM channels.

Internet traffic in TCP/IP networks is bursty in nature mainly due to TCP self-clocking and queuing at congested bottleneck networking elements [125]. Because of the burstiness of the data traffic which is dominating the network and since OCS are not suitable for such traffic, OPS and OBS technologies have been actively researched for decades [75–77, 79, 126–129]. OBS has been mainly researched as as trade-off between OPS and OCS. Like OPS, OBS is a packet based switching technology that makes it more bandwidth and resource efficient than OCS. However, OBS needs resource reservation before the packets, which are aggregated into larger data bursts, are sent through the network. Hence, OPS offers better flexibility and resource utilization than OBS though OPS requires ultrafast switching time (typically in a ns time scale). Along side the fast reconfiguration time, scalability is another important requirement of an optical switch to perform ultra fast forwarding of high-capacity data packets with low insertion and wavelength dependent losses.

The packet forwarding at the OPS node requires an optical label to make switching decisions and an optical back plane to connect input ports with output ports. In electronic switches, the switch control information is sent inside data packets like IP address in IP/TCP packets. To realize OPS, the same analogy is proposed in Chapter 4 using in-band labeling scheme where switch control information is carried within the optical data bandwidth. The switch control signals can be regenerated, as explained in Chapter 5, to perform the OPS operation, for instance, using an electro-optic effect [78]. The highest switched data rate prior to our work is experimentally demonstrated in [7] where 1×4 OPS of 640-Gbit/s OTDM data packets has been performed using an electro-optic effect inside a $LiNbO_3$ switch.

In this chapter, we experimentally investigate an OPS of a 640 Gbit/s and a 1.28 Tbit/s serial data packets using the proposed notch-filter labeling scheme. In Section 6.2, we discuss the basic working principle of an electro-optic based OPS node, particularly using a $LiNbO_3$ based Mach-Zehnder switch (MZS). The first experimental demonstration of an OPS is carried out for 640 Gbit/s serial data packets using a 1×2 $LiNbO_3$ optical switch as detailed in Section 6.3. Modulation format and packet duration independence are among the most important features of an optical labeling scheme. In Section 6.4, we demonstrate a 1×4 OPS of variable length 640 Gbit/s serial data where four types of packets are generated with two durations: 243 ns and 115 ns. In Section 6.5, a record high 1×2 optical switching scenario is experimentally demonstrated where a 1.28 Tbit/s serial data stream is packetized, labeled using the notch-filter labeling scheme, transmitted over 3 km of single mode fiber (SMF) and optically switched. As we have discussed in Section 4.5.2, up to sixteen optical notch-filters (ONFs) are applied to the Tbit/s data demonstrating scalability of the optical labeling scheme. The switched 1.28 Tbit/s data packet is time demultiplexed into 10 Gbit/s channels using a time lens based serial-to-parallel converter [66].

6.2 Electro-optic based OPS

Despite OPS is still in its infancy stage compared to its electrical counterpart, a lot of research work has been conducted in the area of time domain based OPS using all-optical [114, 115] or electro-optic [7, 130–132] switching operations. All-OPS technologies can have ultra-fast switching time (in the order of fs scale) as they have been typically demonstrated by utilizing the instantaneous response of nonlinear processes such as cross-phase modulation (XPM) [115]. However, all-OPS can be very challenging to fully realize because generating a stable switch control signal using an all-optical label detection and performing a scalable all-OPS without possible wavelength contention (both for the data and the control signals) are very challenging tasks.

On the other hand, electro-optic based OPS technologies can be very attractive solutions as they posses the stability and flexibility of the opto-electronic based optical label detection module and a very fast switching time, for instance, using Pockels electro-optic effect [78]. Electro-optic based OPS can be performed using very fast optical switching technologies such as $LiNbO_3$ based MZS [130], silicon based MZS [131, 132], semiconductor optical amplifier (SOA) gate arrays [133] and hybrid MZS-SOA [134]. In

addition to switching time and scalability, other important characteristics of all types optical switches are insertion loss, cross talk, extinction ratio, and wavelength and polarization dependent losses while power consumption can be seen as their valuable asset compared to electrical switches. Scalability of the $LiNbO_3$ based MZS to a large port count can be a challenge as $LiNbO_3$ is sensitive to polarization hence may introduce high polarization dependent loss. Nonetheless, all of our OPS demonstration are performed using off-the-shelf $LiNbO_3$ based MZSs. Here, we discuss working principle, scalability and power consumption of the electro-optic switch.

Working principle

Like Mach-Zehnder modulator (MZM), the $LiNbO_3$ based MZS works based on the principle of interference in a Mach-Zehnder interferometric structure. To illustrate the working principle of the switch, we consider a simplified interferometric structure as shown in Figure 6.1. The Mach-Zehnder interferometer is constructed using two standard 3 dB couplers by connecting output ports of the first coupler with input ports of the second coupler while the electro-optic material, $LiNbO_3$ crystal, is inserted in the upper arm. Assuming that the standard input and output couplers have a power splitting and combining ratio of 1/2 and the optical path of the two arms are equal, the power at the two output ports of the MZS depends on the phase shift difference between the lightwave propagating in the two arm of the interferometric structure.

When an optical signal, represented by its amplitude field $\mathbf{A}_{in}$, is launched to the MZS using In1 port, it will be split into two arm of the

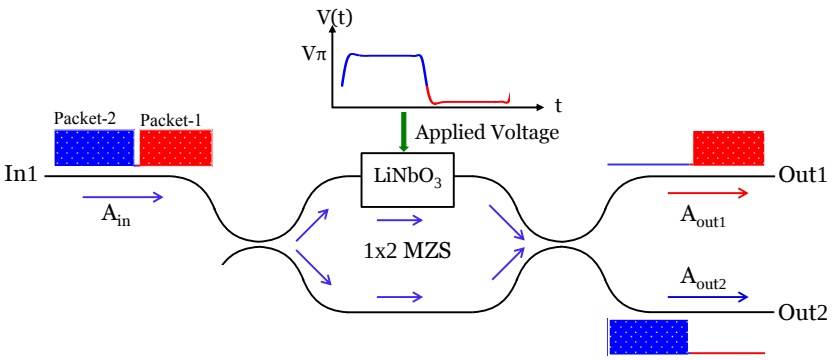

Figure 6.1: Working principle of a 1×2 $LiNbO_3$ based electro-optic switch.

interferometer using the first 3 dB coupler and recombined using the second coupler. During the recombination process, the optical signals of each arm can interfere constructively or destructively depending on their phase shift difference that is introduced by the $LiNbO_3$. If the $LiNbO_3$ introduces zero phase shift difference, the two optical fields will interfere constructively at Out1 but destructively at Out2. Hence, the total optical power will route to Out1 as $\mathbf{A}_{out1}$. Whereas, if the $LiNbO_3$ introduces a π phase shift difference, the two fields will interfere constructively at Out2 and the total field will appear as $\mathbf{A}_{out2}$. Hence, the Mach-Zehnder interferometer can be used as an optical switch to forward a given data packet from In1 to either Out1 (bar) or Out2 (cross) by controlling the $LiNbO_3$ induced phase shift. The optical properties of the $LiNbO_3$ crystal can be controlled with an external electrical signal using Pockels effect where a refractive index of the crystal changes proportionally to the applied electric field. The change in refractive index leads to a phase shift difference between the lightwaves propagating in the two arms of the interferometric structure.

In Figure 6.1, high capacity data packet-1 and packet-2 are launched into the In1 port of the 1×2 MZS while their electrical control signal is applied to upper arm of the optical switch as a time-dependent voltage, V(t). The applied electrical signal can be extracted from the optical label of the two data packets as previously illustrated in Section 5.2.1. When V(t) is applied to the MZS, the refractive index of the $LiNbO_3$ becomes time-dependent and, in turn the transmission of the MZS varies with time. An applied voltage that enables the $LiNbO_3$ to impart a π phase shift to the optical field is commonly referred as V_π. Hence, the voltage level of packet-2 is set to V_π whereas the low voltage level of V(t) corresponds to data packet-1. During the OPS operation, packet-1 cannot exhibit any phase shift effect from the $LiNbO_3$, as the applied voltage is at low voltage level hence it is switched to Out1. On the other hand, since the applied voltage of packet-2 is at V_π of the switch, the refractive index of the $LiNbO_3$ crystal changes in which packet-2 exhibits a π phase shift difference hence it is routed to Out2.

Scalability

The electro-optic switch shown in Figure 6.1 can be, in principle, scaled to large port count fabric as the interferometric structure introduces low insertion and wavelength dependent losses [135, 136]. The $LiNbO_3$ crystal makes the optical switch very suitable for OPS due to its very fast reconfiguration time. But, the crystal may increase the insertion loss of the switch

and introduce polarization dependent loss. Moreover, a large port count MZS can suffer from crosstalk mainly due to the limited extinction ratio of the switch, typically around 15 dB [130].

Scalability of the electro-optical based optical switch can be demonstrated using a "broadcast and select" concept and a cascaded approach. Figure 6.2(a) shows a 1×4 optical switch that is constructed based on "broadcast and select" switching. After the data packets are broadcasted using a 1×4 passive splitter, the OPS operation is performed using four 1×1 based optical switches. Even though such architecture has bee proposed in [135] for up to 1×16 OPS operation with low crosstalk, the high insertion loss to broadcast the high-capacity data packets to all electro-optic switches limits the scalability of the switch for higher port count. The scalability problem can be solved by cascading the optical switches as shown in Figure 6.2(b). Using cascaded approach, up to 16×16 optical switch has been proposed in [136]. The cascaded architecture can overcome the 6 dB loss of the passive splitter of Figure 6.2(a). In this thesis, we experimentally demonstrate OPS operation of high-capacity serial data packets using 1×2 and 1×4 $LiNbO_3$ based optical switches that are constructed using the "broadcast and select" concept.

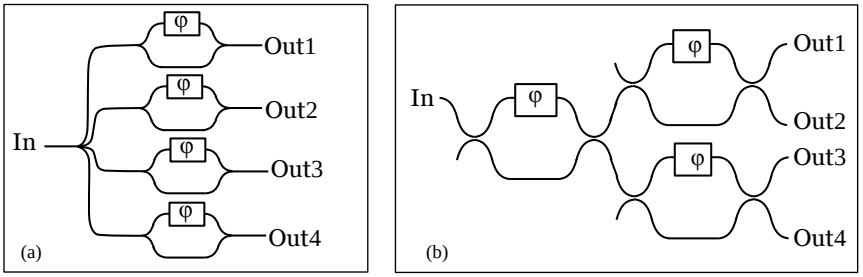

Figure 6.2: 1×4 Mach-Zehnder interferometer based $LiNbO_3$ optical switching architecture as: (a) "broadcast and select" using 1×4 passive splitter and four 1×1 parallel optical switches and (b) cascaded using three 2×2 optical switches. The phase shift difference, φ, is introduced using $LiNbO_3$ crystal.

Power consumption

The main objective of the proposed optical switching scenario in this thesis is to reduces energy consumption by minimizing if not replacing electrical-

power hungry operations like OEO conversions. The $LiNbO_3$ optical switch is capable of forwarding a given high-capacity data packets in the optical domain. However, the OPS operation of each data packet is controlled using electrical signals, hence, the electro-optic switch consumes an electrical power. The total power consumption of the electro-optic switch that have employed in the experimental demonstration can be expressed as [23, 137]:

$$P_T = P_{control} + P_{label\_detection} \tag{6.1}$$

where $P_{control}$ is the power consumed by the electrical control signal and $P_{label\_detection}$ is the total power consumed by the label detection module, for instance, the one detailed in Section 5.2.2. The electro-optic switch is usually controlled by applying the time-dependent driving voltage, V(t), (alternating between 0 V and Vπ at relatively low frequency) and a constant bias voltage, V_{cons}, to adjust V(t) to the desired operating values. Hence, the $P_{control}$ can written as :

$$P_{control} = P_{drive} + P_{bias} = \frac{(V_\pi)^2}{Z_0} + \frac{(V_{cons})^2}{Z_0} \tag{6.2}$$

where Z_0 is a total impedance which may have different valued for the two voltage levels of V(t) and the typical Z_0 value for V_{cons} is 50 Ω.

6.3 1×2 OPS of 640 Gbit/s serial data packets

In principle, the proposed in-band optical labeling scheme could be used for all-OPS by generating an optical control signal like in [115, 138] using the extracted optical labels. However, all network scenarios in this thesis are investigated using electro-optic switches. In this section, we present experimentally demonstration of 1×2 OPS of 640 Gbit/s serial data packets using a $LiNbO_3$ optical switch.

Experimental setup

The experimental setup of the 1×2 OPS of 640 Gbit/s serial data packets is shown in Figure 6.3. The setup consists of five main modules: a 640 Gbit/s transmitter, a packet labeling, a label detection, an optical switch and the non-linear optical loop mirror (NOLM) as 640 Gbit/s to 10 Gbit/s demultiplexer. The 640 Gbit/s transmitter which is similar to the standard OTDM transmitter of Figure 3.5, generates a 146.5 ns long high-capacity data packet followed by 20.6 ns inter-packet gap as its traces is shown by

Signal-B in Figure 6.3. In addition, a 146.5 ns sequence of zero bits are used to reserve free time slot for another data packet followed by another 20.6 ns inter-packet gap.

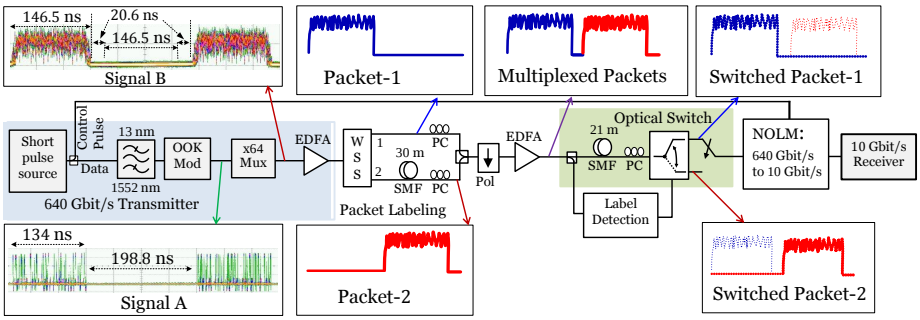

Figure 6.3: Experimental setup of 1×2 OPS labeling scheme for 640 Gbit/s serial data packets.

In the packet labeling module, a WSS takes the amplified 640 Gbit/s data packet and broadcasts the whole data spectrum in two to arms. The WSS shapes the 640 Gbit/s data at each arm so that it resembles to a transform limited signal. The shaped data packet at arm-one is sent to output port -1 and it is represented as packet-1 in Figure 6.3. Whereas, the data packet at arm-two, packet-2, is labeled by making a notch at 1559 nm using 0.3-nm wide optical notch-filter (ONF). Figure 6.4(a) shows spectra of packet-1 with no notch and packet-2 with one notch. The inset in Figure 6.4(a) depicts the 3 dB bandwidth (BW) and suppression ratio (SR) of the carved optical notch at 1559 nm. The measured SR is 20-dB deep which is 10 dB less than the simulation value. However, as summarized in Table 5.1, reducing the SR from 30 dB to 20 dB results only in 0.23-dB of penalty in label contrast (LC). Once packet-2 is forwarded to output port-2 of the WSS, it is delayed using a 33 m of SMF and placed at the reserved 146.5 ns free time slot during packet multiplexing with packet-1. The polarization state of the multiplexed data packets, shown in Figure 6.3, is aligned by a polarizer. The multiplexed data packets are fed to the packet switching and label detection modules.

As previously explained in Figure 5.3 of Section 5.2.2, the detection module is made up of an optical band-pass filter (OBPF), a photodiode (PD) and a 1-bit comparator circuit which are responsible for extracting the optical label information from the multiplexed data packets. The 0.3-nm

wide OBPF centered at 1559 nm selects the optical label and sends it to the PD which converts the optical power to a rectangular-like electrical signal. Output of the PD is fed to the comparator circuit to generate a clean electrical control signal. For a switching operation, a field-effect transistor is used to swing the voltage level between 0 V and V_π. It also inverts the sign of the control signal in such a way that if there is a notch, the control signal is at high voltage level otherwise it is at low voltage level.

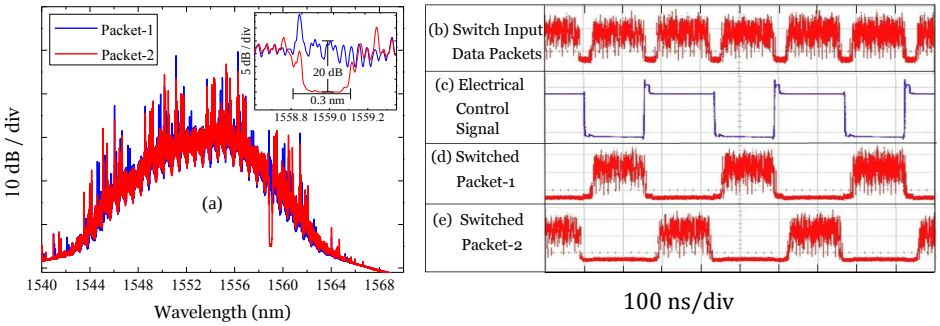

Figure 6.4: (a) Power spectra of packet-1 (with no notch) and packet-2 (with a notch at 1559 nm). Inset figure shows 3-dB BW and SR of the ONF. Oscilloscope traces: (b) multiplexed packets input to the switch, (c) electrical control signal, (d) switched packet-1 and (e) switched packet-2.

The core part of the experimental setup shown in Figure 6.3 is the optical switching module. The multiplexed packets are delayed using 21 m of SMF while the electrical control signal is extracted in the label detection module. Figure 6.4(b) shows oscilloscope traces of the multiplexed data packets whereas their corresponding electrical control signal is depicted in Figure 6.4(c). The delayed high-capacity data packets are sent to a 1×2 $LiNbO_3$ optical switch which works as "broadcast and select' using two 1×1 optical switches. The 1×2 optical switch forwards packet-1 (un-notched) and packet-2 (1×notched at 1559 nm) using their respective electrical control signal. Packet-1 is switched when the electrical control signal is at low voltage level whereas packet-2 is switched when the electrical control signal is at high voltage level (at V_π). Oscilloscope traces of switched packet-1 and packet-2 are shown in Figure 6.4(c) and (d), respectively.

Each switched data packet is sent to a pulse-by-pulse based standard OTDM receiver consisting of a 640 Gbit/s to 10 Gbit/s time demultiplexer

built using the NOLM. A 10 GHz control pulse with pulse duration of 900 fs at full-width at half-maximum (FWHM) from the control pulse of the 640 Gbit/s transmitter module is launched into the NOLM together with the optically switched packet-1 or -2. Reference measurements are made for packet-1 and -2 by feeding them directly to the demultiplexer before they are switched. The resulting demupltiplexed 10 Gbit/s data channel is filtered out at 1551 nm using a 1-nm wide OBPF and sent to bit-error ratio (BER) analyzer for system performance measurement.

Results and discussion

640 Gbit/s eye diagrams of the switched data packet-1 (upper) and data packet-2 (lower) are shown in Figure 6.5(a). Time demultiplexed 10 Gbit/s eye diagrams of data packet-1 and packet-2 before (upper part) and after (lower part) switching are shown in Figure 6.5(b). Signal quality of all the time demultiplexed channels of both data packet-1 and packet-2 before and after switching is analyzed using BER measurements. The receiver sensitivities of packet-1, packet-2, switched packet-1 and switched packet-2 at a BER of 10^{-9} are shown in Figure 6.6(a). All the 256 measured channels achieve BER below 10^{-9} and the maximum variation in receiver sensitivity of the 64 channels of each of the four packets is below 3 dB.

On average, packet-1 has -33.8 dBm, the best receiver sensitivity, which is 3.2 dB lower than the multiplexed and switched packet-1. Whereas, the labeled and switched packet-2, have the highest average receiver sensitivity (-29.7 dBm), which is 1.2 dB higher than the not-switched packet-2.

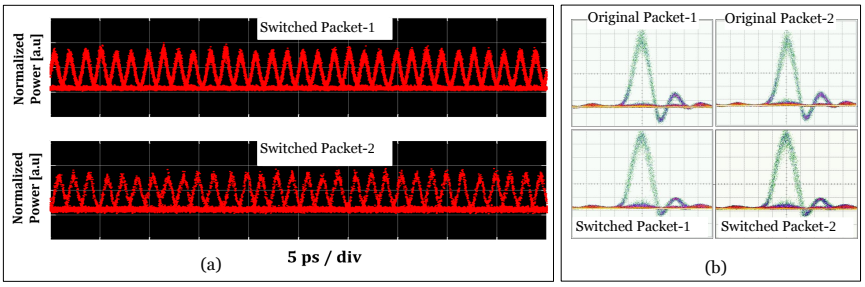

Figure 6.5: (a) 640 Gbit/s eye diagram of switched serial data packet-1 (upper) and packet-2 (lower). (b) Eye diagram of a demultiplexed 10 Gbit/s channel data signal of packet-1 and packet-2 (upper), and switched packet-1 and switched packet-2 (lower).

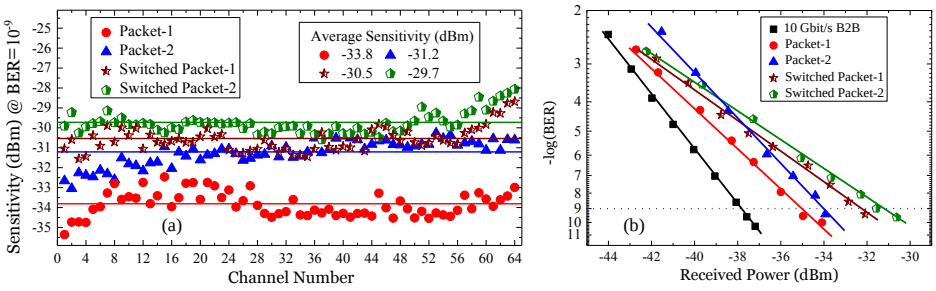

Figure 6.6: (a) Receiver sensitivities of all channels of packet-1 (circle), packet-2 (triangle), switched packet-1 (star) and switched packet-2 (pentagon). (b) Full BER curves of 10 Gbit/s back-to-back and a given channel of packet-1 (circle), packet-2 (triangle), switched packet-1 (star) and switched packet-2 (pentagon).

Therefore, the system full implementation penalty is 4.1 dB, calculated as the difference between the lowest and highest average receiver sensitivities. Finally, Figure 6.6(b) shows BER performances of 10 Gbit/s back to back, and one channel of packet-1, packet-2, switched packet-1 and switched packet-2. Comparing the slopes of the BER curves of Figure 4.11(g) and Figure 6.6(b), multiplexing of the high-capacity data packets seems to give rise to a penalty. This is expected to be due to the limited SR of the '0'-bits used to reserve free time slots for packet multiplexing, which may lead to crosstalk when the packets are placed in the free time slot.

6.4 1×4 OPS of variable length 640 Gbit/s serial data packets

In the previous section, we have experimentally demonstrated 1×2 OPS of 640 Gbit/s serial data packets using the in-band optical labeling technique. Here, we extend the work by investigating 1×4 OPS of 640 Gbit/s variable length OTDM data packets and further demonstrate scalability of the in-band labeling scheme to 1×256 OPS operation using eight ONFs.

Experimental setup

Figure 6.7 shows the experimental setup of the proposed 1×4 OPS of 640 Gbit/s variable length serial data packets. The 640 Gbit/s transmitter

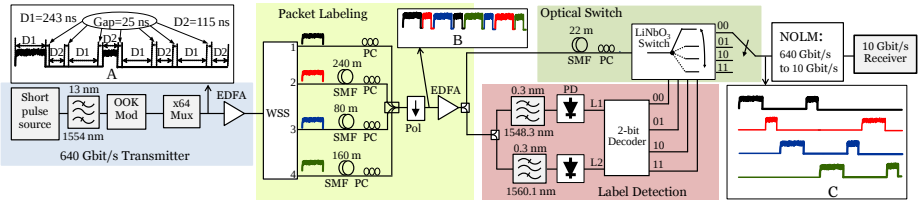

Figure 6.7: Experimental setup of 1×4 OPS of 640 Gbit/s variable length serial data packets.

module uses a short pulse source (see Figure 3.5) to generate optical pulses at 10 GHz repetition rate with pulse duration of 540 fs after the optical pulses are filtered at 1554 nm. The ultra-short optical pulses are on-off keying (OOK) modulated with a 10 Gbit/s custom pattern of 16384 bits, generated in such a way that the first 2304 bits are 2^7-1 pseudo-random binary sequence (PRBS) followed by 4444 zero bits and 1024 bits of 2^7-1 PRBS followed by 8576 zero bits. All zero bits are introduced for inter-packet gaps and to reserve time slots for packet multiplexing, performed at the packet labeling module. Here, we use two different lengths of the PRBS sequence to emulate data payloads of variable length. The modulated signal is multiplexed using a 2^7-1 PRBS preserving bit interleaver to constitute the 640 Gbit/s OTDM data packet represented as signal A in Figure 6.7. The packet durations are: D1=243 ns and D2=115 ns and the inter-packet gap is set to 25 ns.

In the packet labeling module, a WSS appends an optical label information in the variable length 640 Gbit/s serial packets by splitting the high-capacity data into four arms and applying up to eight ONFs. So, packet-1, data at output-1 of the WSS, is labeled without any spectral holes, while the data at output-2 (packet-2), is labeled by making two spectral holes (at 1548.3 nm and 1560.5 nm). Finally, Packet-3 at output-3 and packet-4 at output-4 of the WSS, are labeled by making four and eight spectral holes, respectively. Figure 6.8 shows data spectra of the four serial data packets. Highlighted areas marked as L_1 at 1548.3 nm and as L_2 at 1560.1 nm are the two spectral positions where the optical label information is inserted into/extracted from to generate four electrical control signals.

The four variable length data packets are multiplexed using a 6 dB coupler after packet-2, packet-3 and packet-4 are delayed using 240 m, 80 m and 160 m of SMFs, respectively, and placed in the reserved free time slots as shown in trace A of Figure 6.7. The multiplexed data packets, represented

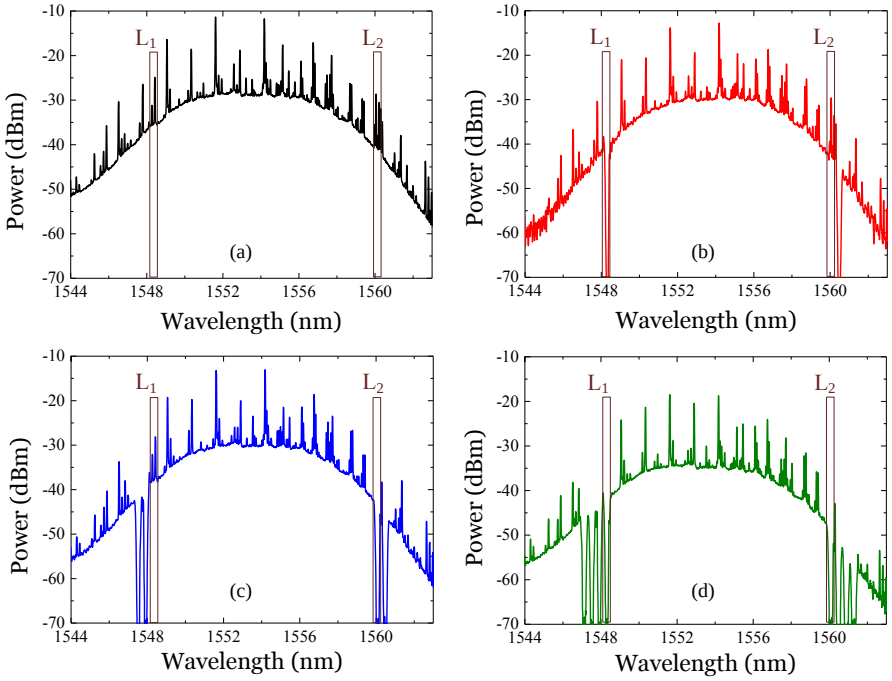

Figure 6.8: (a) Not-notched spectrum of packet-1. (b) Packet-2 spectrum with two notches. (c) Packet-3 spectrum with four notches. (d) Packet-4 spectrum with eight notches. Highlighted areas marked L_1 and L_2 are the two spectral positions where the optical labels are extracted from.

by trace B in Figure 6.7, are filtered using a polarizer so that all packets are aligned to the same polarization state. The final multiplexed signal consists of data packets with different number of notches and two different packet durations, where both packet duration and number of notches are changing for every packet in the sequence. Optical switching of the high-capacity serial data packets is carried out using four electrical control signals, which are extracted from two fixed spectral positions (L_1 and L_2) even though up to eight notches are used. The label detection is responsible of extracting the optical label and regenerate the four electrical control signals. The detailed implementation of the label detection module is illustrated in Figure 5.10. Two 0.3-nm wide OBPFs, centered at 1548.3 nm and 1560.1 nm, are used to extract the optical power of L_1 and L_2. The optical power of L_1 is low for both packet-2 and -4 due to the presence of a notch in their spectra while packet-1 and -3 have high optical power. On the other hand,

L_2 has low optical power for packet-3 and -4 and high optical power for packet-1 and -2. The output of the two OBPFs is fed to two PDs, which convert the optical power of L_1 and L_2 to electrical signals. The output of each PD is sent into two comparator modules, which smoothen the photo-detected electrical signal and generate clean electrical control signals: In_1 and In_2. The digital value of In_1 and In_2 is related to the availability of a notch or optical power at L_1 and L_2. As summarized in Table 5.3, In_1 (In_2) is binary value '0', if there is no notch at L_1(L_2) and binary value '1' otherwise. Four electrical control signals are generated by a 2-bit decoder (see Figure 5.10) using logical interpretation of the two inputs signals, In_1 and In_2. For example, a high voltage level control signal is generated at Out_1 of the label detection when there is no notch at L_1 and L_2, i.e., in case of packet-1.

The main module of the setup is the packet switching block in which the multiplexed data packets are delayed using 22 m of SMF until their respective electrical control signals are generated. Using the four electrical control signals, a specific data packet, represented as trace C in Figure 6.7, is switched to one of the four output ports of a 1×4 $LiNbO_3$ optical switch. The 1×4 optical switch works based on "broadcast and select" approach at it is depicted in Figure 6.2(a). Figure 6.9 shows the 1×4 OPS operation based on extracted optical label information from L_1 and L_2. Figure 6.9(a) shows the multiplexed data packets input to the 1×4 optical switch, while Figure 6.9(b) and (c) are In_1 and In_2 input signals of the 2-bit decoder, which are generated from L_1 and L_2, respectively. Data packet-1 is switched when both In_1 and In_2 are at low voltage level, which means no spectral hole is detected at 1548.3 nm and 1560.1 nm (see Figure 6.9(d)) whereas data packet-2 is switched when In_1 and In_2 are at high and low voltage levels, respectively, as shown in Figure 6.9(e). As depicted in Figure 6.9(f), packet-3 is switched when In_1 and In_2 are at low and high voltage levels, respectively, while packet-4, which has 8-notches, is switched when both In_1 and In_2 are at high voltage levels (see Figure 6.9(g)).

As we have discussed in Section 3.4.1, the NOLM is used as pulse-by-pulse switch to demultiplex the switched 640 Gbit/s to 10 Gbit/s tributary channels. A control pulse train with pulse duration of 900 fs and one of switched the 640 Gbit/s data packet are sent to the NOLM, which contains 50 m of highly nonlinear fiber (HNLF) to introduce a XPM induced π shift on the tributary channel of our interest. The demultiplexed 10 Gbit/s tributary channel is then filtered out at 1557 nm using a 1-nm wide OBPF and sent to the receiver for BER measurements.

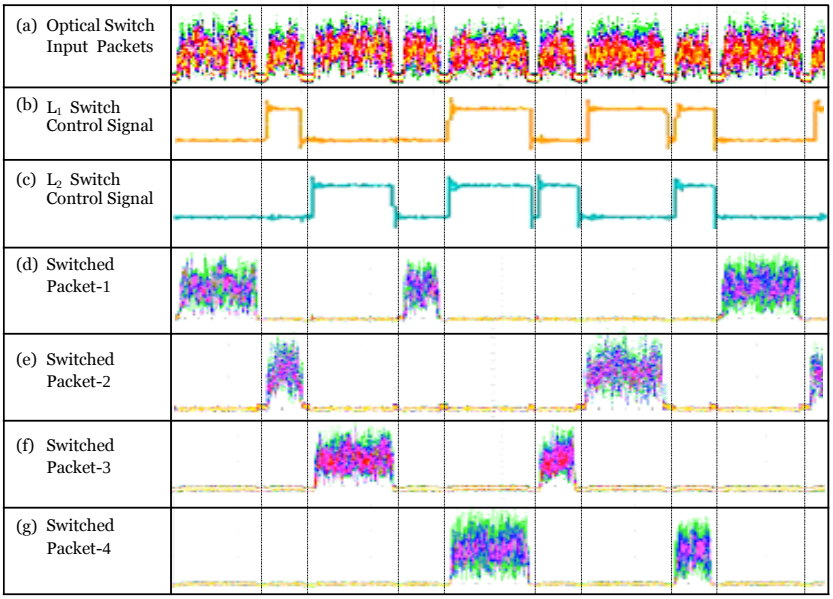

Figure 6.9: 1×4 OPS operation: (a) Variable length data packets input to the optical switch. (b) In_1 electrical control signal extracted from L_1. (c) In_2 electrical control signal extracted from L_2. (d) Switched packet-1 when both In_1 and In_2 are at low voltage levels. (e) Switched packet-2 when In_1 and In_2 are at high and low voltage levels, respectively. (f) Switched packet-3 when In_1 and In_2 are at low and high voltage levels, respectively. (g) Switched packet-4 when both In_1 and In_2 are at high voltage levels

Results and discussion

Figure 6.10(a) shows receiver sensitivities at a BER of 10^{-9} for all 64 channels of packet-1, -2, -3 and -4. All 256 channels achieve error free performance, BER$\leq 10^{-9}$. On average, packet-1 (not notched) has the best receiver sensitivity (-31.99 dBm), while packet-4, which is labeled using eight notches, has the worst sensitivity (-29.3 dBm). The difference between the best and worst sensitivity is 2.7 dB, which accounts for the full system penalty. This indicates that 1×256 OPS is possible, as the number of notches required for 256 labels is eight, just like the case of packet-4. Furthermore, Figure 6.10(b) shows BER curves of a single channel of packet-1, -2, -3 and -4. From the slopes of the BER curves, multiplexing of the four

data packets is seen to give rise to a penalty. As previously mentioned, this can be related to the limited SR of the '0'-bits used to reserve free time slots for packet multiplexing.

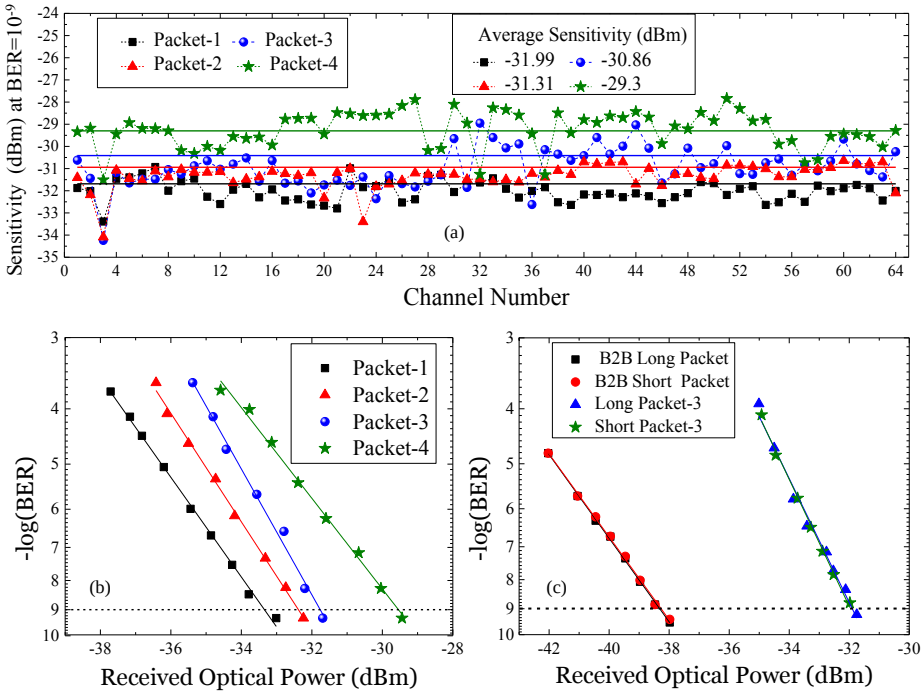

Figure 6.10: (a) Receiver sensitivities of all channels of packet-1 (rectangle), -2 (triangle), -3 (circle) and -4 (star). (b) Full BER curves of packet-1 (rectangle), -2 (triangle), -3 (circle) and -4 (star). (c) Full BER curves of long and short duration data packets for B2B and one channel of packet-3.

We also investigate the performance of the long and short data packets separately for back to back at 10 Gbit/s and for one channel of packet-3 as shown Figure 6.10(c). Both short and long data packets have almost identical BER curves. The 1×4 OPS has the capability to switch long (short) data packets, which are placed between two short (long) data packets, with the same performance. Hence, the proposed in-band optical labeling and label detection schemes are packet-length independent.

6.5 1×2 OPS of 1.28 Tbit/s serial data packets

In this section, we propose and demonstrate for the first time an optical switching scenario, where 1.28 Tbit/s serial data streams are packetized, optically labeled, transmitted over 3 km of SMF and subsequently optically switched in a 1×2 $LiNbO_3$ switch. Moreover, up to sixteen ONFs are applied to the Tbit/s data demonstrating scalability of the optical labeling scheme.

Experimental setup

The 1×2 Tbit/s OPS is demonstrated using an experimental setup shown in Figure 6.11 consisting of a transmitter, an optical link and a receiver. The main building blocks of the setup are a Tbit/s Tx and a label allocator at the transmitter. And, a label detector, an optical switch and a serial-to-parallel converter at the receiver. In the Tbit/s Tx module, a 10 GHz short pulse source generates an ultra-short optical pulse with FWHM of 0.4 ps duration after it is filtered at 1548 nm using a 16-nm wide OBPF. The ultra-short pulse is then data modulated using a OOK format with a 10 Gbit/s custom pattern of 1411 bits of 2^7-1 PRBS followed by 2173 zero bits, which are used to reserve a free time slot for packet multiplexing and inter-packet gap. A 1.28 Tbit/s serial data packet is then generated using a 2^7-1 PRBS preserving bit interleaver. This corresponds to aggregated data traffic of 128 channels each at bit rate of 10 Gbit/s. The packetized 1.28 Tbit/s data is then sent to the label allocation module.

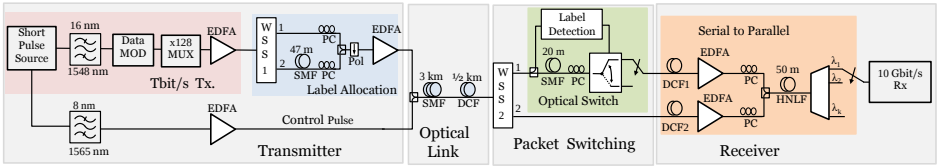

Figure 6.11: Experimental setup of Tbit/s optical packet generation, label allocation, transmission, optical packet switching and reception.

In-band optical labeling of the 1.28 Tbit/s packet is performed using a reconfigurable WSS1. The WSS1 broadcasts the Tbit/s data to two different arms namely port-1 and port-2. This gives us the degree of freedom to insert distinct label information by carving spectral holes in the Tbit data spectrum of each packet. Hence, the data at port-1 of the WSS1 (packet-1) is labeled by making zero spectral holes while the data at port-2 (packet-2)

is labeled by making one 0.3-nm wide spectral hole (refer Figure 4.9(b)) at 1541 nm as shown in Figure 6.12(a) and (b). After packet-2 is delayed using a 47 m of SMF, it is time multiplexed with packet-1 on the free time slot reserved by encoding a sequence of zero bits. Figure 6.12(c) shows the multiplexed 1.28 Tbit/s data packets which have a duration of 152 ns followed by 25 ns inter-packet gap. Finally, the Tbit/s packets and a 10 GHz optical control signal are launched together into a 3 km of SMF followed by a 0.5 km of dispersion compensating fiber (DCF). Detailed characterization of the optical labeling scheme and its scalability for 1×256 OPS of 640 Gbit/s data are presented in the previous section. Here, a total of sixteen ONFs are employed on packet-2 (see Figure 6.13) to further demonstrate the scalability of the in-band labeling scheme. Hence, three Tbit/s data packet are optical labeled: packet-1, 1×notched packet-2 and 16×notched packet-2. Using the sixteen ONF, the maximum number of unique labels that can be generated is 65.536.

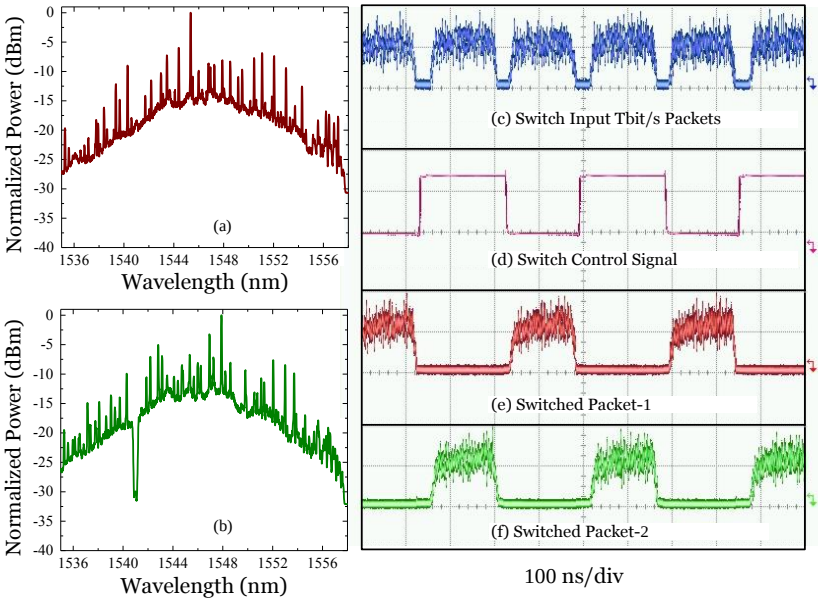

Figure 6.12: Power spectra of: (a) un-notched Tbit/s packet-1 and (b) 1×notched Tbit/s packet-2. Oscilloscope traces of: (c) Tbit/s packets input to optical switch, (d) electrical control signal, (e) switched Tbit/s data packet-1 and switched Tbit/s data packet-2.

The data packets are now transmitted over 3 km of SMF together with the optical control signal needed for the serial-to-parallel conversion. A

second WSS2 filters the Tbit/s data and control signal out to port-1 and port-2, respectively. At the optical switch module, a label detection block extracts the optical label information from the Tbit data spectrum of each packet and generates an electrical control signal. As we have explained in Section 5.2.2, the label detection module is made up of an OBPF which is centered at a spectral position where the label is placed; a PD to convert the optical power to an electrical voltage; and a comparator circuit to determine whether the detected label is at high or low level. For a given spectral position, the electrical control signal is at a low voltage level if there is no notch otherwise it is at a high voltage level. Figure 6.12(d) shows the oscilloscope traces of an electrical control signal that is extracted from the multiplexed Tbit/s data packet-1 and packet-2. As the spectrum data packet-1 does not have any notch, its control signal is at 0 V while the electrical control signals of packet-2 (both the 1×notched and 16×notched) are at V_π due to the presence of notch at 1541 nm.

At the optical switch, the multiplexed data packets are delayed using 20 m of SMF while the electrical control signals are generated from the optical label inserted at 1541 nm. Based on the electrical control signal, a 1×2 $LiNbO_3$ optical switch forwards packet-1 to port-1 and packet-2 (both 1×notched and 16×notched) to port-2. Figure 6.12(e) shows the oscilloscope traces of the switched Tbit packet-1 while 1×notched packet-2 is shown in Figure 6.12(f). A 10-ns switching time is measured from the rising/falling time of the electrical control signal that is sufficient to switch the Tbit/s packets within the 25 ns inter-packet gap. The total power consumption of the optical switch used to forward a 1.28 Tbit/s data packet, including the label detection, is 1.5 W which is calculated using Equation 6.1 and Equation 6.2. This leads to 1.25 pJ/bit switching energy [23]. For comparison with commercial Ethernet switches, we investigated the energy per bit of the Cisco Nexus 7000 and 9000 series and the Juniper EX8200 and EX9200 series. We found that for input capacities ranging from 640 Gbit/s to 10.24 Tbit/s, these Ethernet switches used from 0.6 nJ/bit [139] or 4.6 nJ/bit [140] up to 10 nJ/bit. It is important to note that this comparison is only relevant in cases where the added functionality of a full Ethernet switch is not required.

After each Tbit/s data packet is optically switched, it is sent into the time lens based serial-to-parallel converter together with the transmitted control pulse. As previously illustrated in Section 3.4.2, the serial-to-parallel conversion of the 1.28 Tbit/s packet into many 10 Gbit/s tributary channels is performed using chromatic dispersion effect followed by

quadratic phase modulation [44]. Hence, the switched packet is passed through a DCF1 while the optical control pulse is dispersed using DCF2, after it is filtered using a top-flat super-Gaussian transfer function in WSS2. To map the demultiplexed 10 Gbit/s channels into a 100 GHz frequency spacing ($\Delta\omega$) compatible with a standard WDM grid, the required chirp rate for the 1.28 Tbit/s data is K=1/D= $\Delta\omega/\Delta$t; where Δt is a bit-slot time and the optical control pulse is also linearly chirped with a rate of K/2. The dispersed data packet and control pulse are amplified and launched together into a 50 m of HNLF: zero dispersion wavelength of 1565 nm and nonlinear coefficient $\gamma = 10\ \mathrm{W}^{-1}\ \mathrm{km}^{-1}$. Four wave mixing (FWM) is exploited inside the HNLF to map the individual 10 Gbit/s data channels to different wavelengths by mixing the phases of the linearly chirped control pulse and the dispersed data packet. Figure 6.13 shows the switched spectra (with sixteen notches) of the 1.28 Tbit/s serial data packet-2, the top flat optical control pulse and converted parallel 10 Gbit/s channels at the output of the HNLF. The 10 Gbit/s WDM channels are filtered using a 40-GHz wide tunable OBPF and sent to 10 Gbit/s receiver for BER measurement.

Results and discussion

Performance of all the time demultiplexed tributary channels is evaluated using BER measurements. The optical signal-to-noise ratio (OSNR) of the

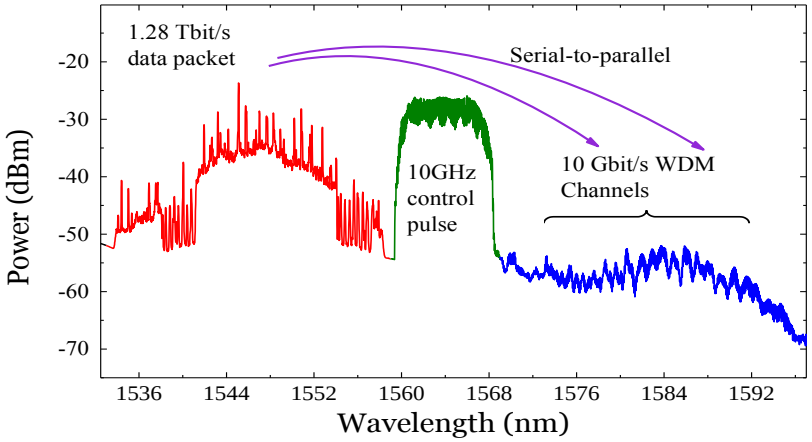

Figure 6.13: Power spectra of a 16xnotched 1.28 Tbit/s data packet-2, a top flat control pulse and generated idler at the output of the HNLF.

Tbit/s input data signal to the HNLF is fixed to 36 dB [52]. For comparison purpose, two system performance scenarios, with and without the optical switch, are investigated for not-notched packet -1, 1×notched packet-2 and 16×notched packet-2. The BER measurements of packet-1 and 1×notched packet-2 with and without the optical switch are shown in Figure 6.14. All the 512 channels achieved BER performance well below the forward error correction (FEC) limit of 3×10^{-3}. As expected, both un-switched data packets show better performance than the switched ones due to limited extinction ratio of the $LiNbO_3$ switch.

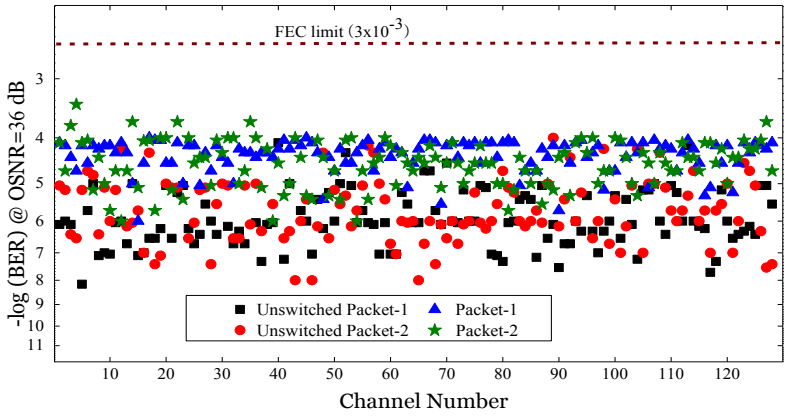

Figure 6.14: BER measurements of all tributaries of Tbit/s data packet-1 (rectangular), 1×notched packet-2 (circle), switched packet-1 (triangle) and 1×notched switched packet-2 (star).

Furthermore, Figure 6.15 shows the BER measurements of 16×notched packet-2 with and without the switch. The system performance in Figure 6.15 has a BER penalty compared to Figure 6.14 due to the sixteen ONFs applied on the data spectrum. However, the penalty is acceptable as the BER measurements of all the 10 Gbit/s tributary channels are below the FEC limit. This demonstrates scalability of the labeling technique to be compatible with up to 1×65.536 OPS using sixteen ONFs. The main attractive feature of the time lens based optical time demultiplexing technique is its ability to reduce power consumption by converting the 1.28 Tbit/s serial data into many parallel 10 Gbit/s tributary channels. As shown in Figure 3.15(b), up to nineteen 10 Gbit/s channels are simultaneously optical time demultiplexed, all below FEC limit, in to 100 GHz frequency grid,

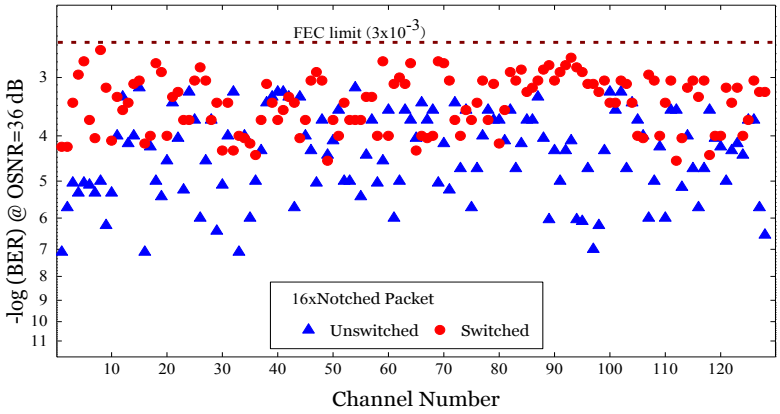

Figure 6.15: BER measurements of all tributaries of 16×notched Tbit/s data packet before (triangle) and after (circle) the optical switching. The BER is measurement is performed by setting the OSNR of each Tbit/s serial data packet at 36 dB [52].

allowing for commercial AWGs to be used for filtering. The FEC limit of 3×10^{-3} corresponds to 6.6% overhead, resulting in a bit rate of 1.2 Tbit/s.

6.6 Summary

In this chapter, three high-capacity optical switching scenarios have been demonstrated for 640 Gbit/s and 1.28 Tbit/s serial data packets using electro-optical based $LiNbO_3$ switches. Systems performance of the three network scenarios have been investigated using BER measurements. The first OPS experiment has been demonstrated for 640 Gbit/s serial data packets. After two packets have been optically labeled with/without a notch on their spectra, they have been optically switched using the 1×2 $LiNbO_3$ switch after the optical label has been extracted. All tributaries of the two switched data packets have achieved BER 10^{-9} at the expense of only 4.1-dB system penalty. On average, the packet with one notch has 0.8 dB high receiver sensitivity than the packet without notch. We have observed a non-uniform BER curves of a selected tributary channels of the two switched packets mainly due to the limited SR of the '0'-bits used to reserve free time slots for packet multiplexing.

The second network scenario has dealt with the experimental demonstration of 1×4 OPS of 640 Gbit/s variable length serial data packet. Four packets, with two durations, have been labeled by carving up to eight notches using ONFs and switched using a $LiNbO_3$ switch. Error free operation, i.e. BER $\leq 10^{-9}$, has been achieved at the expense of only 2.7-dB system penalty. Using the eight ONFs scalability of the optical labeling for 1×256 OPS has been suggested. The OPS has showed similar performance for the short and long packet durations.

Finally, we have reported an experimental demonstration of 1.28 Tbit/s OPS using the scalable in-band notch-filter labeling scheme for short-range networks including a transmission distance of 3 km. The 1.28 Tbit/s data packets have been labeled and optically switched using a 1×2 $LiNbO_3$ switch. Up to sixteen ONFs have been applied to the 1.28 Tbit/s data spectrum to demonstrate scalability of the in-band labeling scheme for 1×65.536 OPS operation. The BER performance of all the demultiplexed 10 Gbit/s data packets have been measured below the FEC limit of 3×10^{-3}, suggesting OPS of 1.2 Tbit/s packets using only 1.25 pJ/bit switching energy. Thus, introducing high-capacity optical switching in parts of a network, where simple switching functionality is sufficient, can deliver significant energy saving and reduced complexity.

Chapter 7

Conclusion

As datacenters (DCs) today remain the fastest growing part of the Internet, efficient resource utilization (energy, space, complexity and latency) is paramount. Contemporary DCs are most commonly based on commodity Ethernet switches that may impose constraints such as high power consumption and slow (low bit rate) switching ability. Optical networking technologies, on the other hand, offer features like low power consumption by switching many bits per switching operation, high bandwidth and reliability [7], though limited to simple functionalities [23].

This PhD thesis has presented power-efficient serial optical communication based high-capacity short-range networking scenarios as serial communication uses few components with ultra-short pulses and very high bit rates. The optical networking scenarios have concerned high-capacity data packets generation and reception (Chapter 3), optical packet labeling (Chapter 4), optical label detection (Chapter 5) and optical packet switching (Chapter 6). The key results of each chapter are summarized.

7.1 Summary

High-capacity serial packet generation and reception

A high-capacity optical networking scenario has been introduced for ultra-high bit rate serial data packets. 640 Gbit/s and 1.28 Tbit/s serial data packets have been generated and it has been shown that their duration can be very flexibility. However, the way the data streams have been packetized is only applicable for amplitude modulations formats. Hence, techniques such as packet carving [115] should be employed for phase modulations

formats. Furthermore, the 640 Gbit/s and 1.28 Tbit/s packets have been successfully demultiplexed in to 10 Gbit/s tributary channels using the nonlinear optical loop mirror (NOLM) and time lens based serial-to-parallel converter, receptively. It has been found that the fiber based NOLM is bulky and it can only demultiplex one channel while the serial-to-parallel converter has the ability to demultiplexed many (up to nineteen) tributary channels at once. The 1.28 Tbit/s tributaries have achieved bit-error ratio (BER) performance well below the forward error correction (FEC) of 3×10^{-3} but the FEC uses digital signal processing (DSP) modules which can increase power consumption of the Tbit system in short-range networks. However, it remains ultimately difficult task, up-to-date, to receive all tributaries successfully without the help of the DSP.

Optical packet labeling

A novel optical labeling technique has been proposed and demonstrated to embed optical information within the spectrum of a high-capacity serial data packet using an in-band notch-filtering scheme. After the scheme has been numerically characterized using 0.3-nm wide and 30-dB deep 4^{th} order super-Gaussian optical notch-filters (ONFs), up to eight ONFs have been employed within the 3 dB and 20 dB signal bandwidth of high-capacity data packets. It has been found that a maximum of a 256 label words (LWs) can be generated based on permutation of the eight spectral positions of the ONFs. The notch-filtering effects on the data has been investigated using eye-opening penalty (EOP) and it has been shown that 60, 72, and 92 LWs for 640 Gbit/s serial data packets can be generated, by employing up to four ONFs simultaneously, at the expense of <1-dB, <1.1-dB and <1.12-dB EOPs, respectively.

The scalable optical labeling scheme has been experimentally demonstrated for 640 Gbit/s and and 1.28 Tbit/s serial data packets and the notch-filtering impact has been investigated using BER measurements. Scalability of the labeling scheme for 640 Gbit/s data packets has been verified by employing a maximum of eight ONFs. The impact of the eight ONFs on the data quality has led to <1-dB of penalty in receiver sensitivity, paving the way for up to 1×256 optical packet switching (OPS) operation. Furthermore, the optical labeling technique has been employed for record-high 1.28 Tbit/s serial data packets. It has been shown that the optical labeling can be made very scalable by employing sixteen ONFs simultaneously and up to 65.536 unique LWs have been generated. Impact of the notch-filtering on the Tbit data quality has been investigated using BER measurements and

all tributaries of the Tbit/s data packet has achieved BER below the FEC limit of 3×10^{-3}.

The main attractive features of the proposed optical labeling scheme are simplicity, scalability, and modulation format and packet length independence. But, it lacks flexibility as the narrow-band ONFs were applied using a wavelength selective switch (WSS) that has a slow reconfiguration time. In the future, the drawback can be solved using tunable filters, for instance, based on programmable ring resonators [141, 142].

Optical label detection

Successful extraction of optical labels of the high-capacity data packets has been achieved using a simple opto-electronic module consisting of a narrow-band optical band-pass filter (OBPF), a slow speed photodiode (PD) and 1-bit comparator circuits. The module has been employed to extract electrical control signals for 640 Gbit/s and 1.28 Tbit/s data packets. It has been found that the extracted optical power, containing the label information, varies with spectral position of the optical label due to bit-pattern dependence of the on-off keying (OOK) modulated spectra of the high-capacity data packets. Resilience of the opto-electronic module to such optical power fluctuations has been verified by extracting stable electrical control signals from sixteen different spectral positions.

The optical label has been embedded within the signal bandwidth using ONFs and quality of the extracted label information has been investigated in label contrast (LC) for different parameters of the ONF. It has been found that the 3 dB bandwidth doesn't affect the quality whereas the LC increases with the suppression ratio (SR) of the ONF. Furthermore, every ±1 GHz mismatch between center frequencies of the ONF and OBPF has led to around 1-dB reduction in LC. Packet length independence of the optical labeling and label detection schemes has been verified by extracting four stable electrical control signals from variable length 640 Gbit/s data packets. Finally, scalability of the opto-electronic module to extract electrical control signals from large number of optical labels has been discussed using two approaches.

From a practical perspective, each regenerated control signal should be at two stable voltage levels with very fast falling/rising transitions. Moreover, the duration of the control signal at each level should match with the length of its respective packet and the high voltage level should be set to the optimum value to drive the switching operation properly. The 1-bit comparator circuit has been used to regenerate the two voltage level con-

trol signal with rising/falling time of 10 ns (on average) and to adjust the duration of the high/voltage levels using delay line. Whereas, a field-effect transistor has been employed to regulated to the high voltage level to the required value with minimal effect on the sharpness of the rising/falling time and smoothness of the control signal.

Optical packet switching

Three high-capacity OPS scenarios have been experimentally demonstrated in electro-optic based $LiNbO_3$ switches. System performance of the optical networking scenarios have been thoroughly analyzed using BER measurements. In the first experiment, a 1×2 OPS of 640 Gbit/s serial data packets has been demonstrated. After the two data packets have been optically labeled with/without notch in their spectra carved by using the notch-filter labeling scheme, the label detection module has generated a stable electrical signal that controls operation of the optical switch. The NOLM has been employed to demultiplex each switched 640 Gbit/s packet into its 10 Gbit/s tributaries. Error free operation, i.e., BER $\leq 10^{-9}$, has achieved at the expense of 4.1-dB penalty caused by packet generation, labeling, switching and demultiplexing. A non-uniform BER curves have been observed mainly due to the limited SR of the '0'-bits used to reserve free time slots for packet multiplexing.

Furthermore, a 1×4 OPS of 640 Gbit/s variable length serial data packets has been demonstrated. After in-band optical labeling of four data packets by employing up to eight ONF, four electrical control signals haven been generated from two (out of the eight) spectral positions and derived the 1×4 OPS operation. Each switched packet has been demultiplexed using the NOLM and all tributaries have achieved error free performance at the expenses of only 2.7-dB system penalty, thus scalability of the optical labeling for 1×256 OPS has been verified.

Finally, a record-high 1×2 OPS of 1.28 Tbit/s data packets has been demonstrated. The data packets have been packetised, optically labeled, transmitted over 3 km of standard fiber and subsequently optically switched in the $LiNbO_3$ switch. Scalability of the notch-filter labeling scheme for 1×65.536 OPS operation has been verified by employing sixteen ONFs. Each switched Tbit/s data packets, including the 16×notched, has been demultiplexed in to 10 Gbit/s tributaries using the time lens based serial-to-parallel converter. All tributaries have achieved BER performance below the FEC limit of 3×10^{-3}, suggesting OPS of 1.2 Tbit/s packets using only 1.2 pJ/bit switching energy.

It has been found that the total power consumption of both the label detection module and the 1×2 optical switch is 1.5 W, and this leads, at a data rate of 1.2 Tbit/s, to 1.25 pJ/bit switching energy [23]. Comparing it with commercialized Cisco Nexus 7000 and 9000 series, and Juniper EX8200 and EX9200 series Ethernet switches in case where the added functionality of a full Ethernet switch is not required, it has been found that energy per bit of the Ethernet switches varies from 0.6 nJ/bit [139] or 4.6 nJ/bit [140] up to 10 nJ/bit for data rates ranging from 640 Gbit/s up to 10.24 Tbit/s. Thus, introducing high-capacity optical switching in parts of a network, where simple switching functionality is sufficient, can deliver significant energy and cost savings at reduced complexity.

7.2 Outlook

In this section, we present a brief outlook and suggest for possible future work on OTDM and OPS.

OTDM

Even though OTDM has been actively researched for more than thirty years [34], future innovative works are still required for low loss multiplexing and easy demultiplexing of the high-capacity data packets using stable and resilience techniques. Recently, a coherent receiver based demultiplexing technique has been proposed for Nyquist optical time-division multiplexing (N-OTDM) data [143, 144] though such technique can be expensive and power inefficient for short range networks. Moreover, only preliminary research has been carried out, for instance in [145], to identify one tributary channel from other tributaries during the demultiplexing and it still remains a challenge that needs further investigations. Finally, the high-capacity serial data packets can be vulnerable to small polarization mode dispersion (PMD). For instance, a 1.28 Tbit/s data packet has a bit period of 0.78 ps which means the tolerance to PMD is as small as 78 fs (10% of a bit period). Therefore, the performance of the high-capacity networking scenarios can be enhanced using a polarization diversity [145] and PMD compensation [146] techniques.

Optical packet switching

The proposed optical network scenarios can be further improved by introducing optical buffering schemes, for example using programmable delay

lines [147,148] or a compact optical memory [149], to solve possible packet contention at each OPS node. Furthermore, both the optical labeling and the label detection schemes can be reconfigured using external controllers, for example using software defined network (SDN) [6,101], and implementing such controllers can add further flexibility to the proposed network scenarios. Finally, features such as error detection using parity bits can be added to the 8-bit and 16-bit LWs so that the label detection module can have a means to identify erroneous optical labels of a given high-capacity data packet.

Acronyms

ASE	amplified spontaneous emission
AWG	arrayed waveguide-grating
BER	bit-error ratio
BPG	bit pattern generator
BW	bandwidth
CAGR	compound annual growth rate
CW	continuous wave
DC	datacenter
DCF	dispersion compensating fiber
DCN	datacenter network
DF-HNLF	dispersion-flatten highly nonlinear fiber
DSP	digital signal processing
EAM	electroabsorption modulator
EDFA	erbium-doped fiber amplifier
ELPF	electrical low-pass filter
EO	eye-opening
EOP	eye-opening penalty
ERGO-PGL	erbium glass oscillator pulse generating laser

ETDM electrical time-division multiplexing

FBG fiber Brag grating

FEC forward error correction

FWHM full-width at half-maximum

FWM four-wave mixing

GMPLS generalized multiprotocol label switching

HNLF highly nonlinear fiber

HPC high-performance computing

LC label contrast

LW label word

MEMS micro-electro-mechanical system

MMF multi-mode fiber

MPLS multiprotocol label switching

MZM Mach-Zehnder modulator

MZS Mach-Zehnder switch

NOLM non-linear optical loop mirror

N-OTDM Nyquist optical time-division multiplexing

OBPF optical band-pass filter

OBS optical burst switching

OCS optical circuit switching

OEO optical-to-electrical-to-optical

OFDM orthogonal frequency-division multiplexing

OLS optical label switching

ONF optical notch-filter

OOK on-off keying

OPS optical packet switching

OSNR optical signal-to-noise ratio

OTDM optical time-division multiplexing

PD photodiode

PDM polarization-division multiplexing

PMD polarization mode dispersion

PRBS pseudo-random binary sequence

PTER pulse-to-tail extinction ratio

RZ return-to-zero

SDM space-division multiplexing

SDN software defined network

SHG second-harmonic generation

SMF single mode fiber

SOA semiconductor optical amplifier

SOCRATES Serial Optical Communications for Advanced Terabit Ethernet Systems

SPM self-phase modulation

SR suppression ratio

TDM time division multiplexing

TOR top-of-rack

VOA variable optical attenuator

WDM wavelength-division multiplexing

WSS wavelength selective switch

XPM cross-phase modulation

Bibliography

[1] The Zettabyte Era: Trends and Analysis, [online] (Available: www.cisco.com/c/en/us/solutions/collateral/service-provider/visual-networking-index-vni/VNI_Hyperconnectivity_WP.pdf).

[2] G. P. Agrawal, *Fiber-Optic Communication Systems*, 4^{th} Edition, A John Wiley & Sons, Inc., 2010.

[3] K. Sato, H. Hasegawa, T. Niwa, and T. Watanabe, "A Large-Scale Wavelength Routing Optical Switch for Data Center Networks," *IEEE Communications Magazine*, **51**, 46–52 (2013).

[4] W. Miao, J. Luo, S. D Lucente, H. Dorren, and N. Calabretta, "Novel flat datacenter network architecture based on scalable and flow-controlled optical switch system," in *European Conference on Optical Communication*, ECOC (2013), postdeadline.

[5] P. N. Ji, D. Qian, K. Kanonakis, C. Kachris, and I. Tomkos, "Design and Evaluation of a Flexible-Bandwidth OFDM-Based Intra-Data Center Interconnect," *IEEE Journal of Selected Topics in Quantum Electron*, **19**, 2013.

[6] N. Amaya, S. Yan, M. Channegowda, B. R. Rofoee, Y. Shu, M. Rashidi, Y. Ou, G. Zervas, R. Nejabati, D. Simeonidou, B. J. Puttnam, W. Klaus, J. Sakaguchi, T. Miyazawa, Y. Awaji, H. Harai, and N. Wada, "First Demonstration of Software Defined Networking (SDN) over Space Division Multiplexing (SDM) Optical Networks," in *European Conference on Optical Communication*, ECOC (2013), postdeadline.

[7] F. Gomez-Agis, H. Hu, J. Luo, H. C. H. Mulvad, M. Galili, N. Calabretta, L. K. Oxenløwe, H. J. S. Dorren, and P. Jeppesen, "Optical

switching and detection of 640 Gbits/s optical time-division multiplexed data packets transmitted over 50 km of fiber," *Optics Letters*, **36**, 3473–3475 (2011).

[8] 2015 Ethernet roadmap, [online] (Available: http://www.ethernetalliance.org/roadmap/).

[9] R. Ramaswami, K. N. Sivarajan, and G. H. Sasoki, *Optical Networks: A practical Perspective*, 3^{rd} Edition, ELSEVIER Inc., 2010.

[10] C. F. Lam, H. Liu, B. Koley, X. Zhao, V. Kamalov, and V. Gil, "Fiber Optic Communication Technologies - what's needed for datacenter network operations," *IEEE Optical Communications*, 32–39 (2010).

[11] T. D. Nadeau, and K. Gray, *SDN: Software Defined Networks*, O'Reilly Media, 2013.

[12] Cisco Global Cloud Index: Forecast and Methodology, 2013–2018, [online] (Available: http://www.cisco.com/c/en/us/solutions/collateral/service-provider/global-cloud-index-gci/Cloud_Index_White_Paper.pdf).

[13] K. Kant, "Data center evolution A tutorial on state of the art, issues, and challenges," *Computer Networks*, **53**, 2939–2965 (2009).

[14] J. Kim, W. J. Dally, B. Towles, and A. K. Gupta, "Microarchitecture of a High-Radix Router," in *the International Symposium on Computer Architecture*, ISCA (2005), 420–431.

[15] T. Benson, A. Akella, and D. A. Maltz, "Network Traffic Characteristics of Data Centers in the Wild," in *conference on Internet measurement*, IMC (2010).

[16] https://code.facebook.com/posts/360346274145943/introducing-data-center-fabric-the-next-generation-facebook-data-center-network.

[17] M. Al-Fares, A. Loukissas, and A. Vahdat, "A scalable, commodity data center network architecture," in *ACM SIGCOMM*, 63–74 (2008).

[18] http://www.nrdc.org/energy/data-center-efficiency-assessment.asp.

[19] *SMART 2020: Enabling the low carbon economy in the information age.* A report by The Climate Group on behalf of the Global eSustainability Initiative (GeSI), 2008.

[20] GreenDataProject (2008), *Where does power go?*, [online] (Available: http://www.greendataproject.org).

[21] L. Huff, "Berk-Tek: The Choice for Data Center Cabling," *Berk-Tek Technology Summit*, 2008 (http://www.nexans.us/US/2008/DC_Cabling%20Best%20Practices_092808.pdf).

[22] http://www.ieee802.org/3/hssg/public/nov07/tatah_01_1107.pdf.

[23] R. S. Tucker, "Scalability and Energy Consumption of Optical and Electronic Packet Switching," *Journal of Lighwave Technology*, **29**, 2410–2421 (2011).

[24] E. Ip, P. Ji, E. Mateo, Y.-K. Huang, L. Xu, D. Qian, N. Bai, and T. Wang, "100G and Beyond Transmission Technologies for Evolving Optical Networks and Relevant Physical-Layer Issues," *Proceedings of the IEEE*, **100**, 1065–1078 (2012).

[25] C. Kachris, and I. Tomkos, "A Survey on Optical Interconnects for Data Centers," *IEEE Communications Surveys & Tutorials*, **14**, 1021–1036 (2012).

[26] G. Wang, D. G. Andersen, M. Kaminsky, K. Papagiannaki, T. E. Ng, M. Kozuch, and M. Ryan, "c-Through: Part-time Optics in Data Centers," in *ACM SIGCOMM*, 327–338 (2010).

[27] N. Farrington, G. Porter, S. Radhakrishnan, H. H. Bazzaz, V. Subramanya, Y. Fainman, G. Papen, and A. Vahdat, "Helios: a hybrid electrical/optical switch architecture for modular data centers," in *ACM SIGCOMM*, 339–350 (2010).

[28] X. Ye, Y. Yin, S. J. B. Yoo, P. Mejia, R. Proietti, and V. Akella, "DOS: A scalable optical switch for datacenters," in *ACM/IEEE Symposium on Architectures for Networking and Communications Systems*, ANCS(2010), 1–12.

[29] R. Proietti, X. Ye, Y. Yin, A. Potter, R. Yu, J. Kurumida, V. Akella, and S. J. B. Yoo, "40 Gb/s 8x8 Low-latency Optical Switch for Data Centers," in *Optical Fiber Communication Conference*, OFC (2011), paper OMV4.

[30] K. Xia, Y.-H. Kaob, M. Yangb, and H. J. Chao, "Petabit Optical Switch for Data Center Networks," in *Technical report*, Polytechnic Institute of NYU, 2010.

[31] L. Schares, B. G. Lee, F. Checconi, P. Fuentes, O. Mattes, R. Budd, A. Rylyakov, N. Dupuis, C. Minkenberg, F. Petrini, and C. L. Schow, "A Throughput-Optimized Optical Network for Data-Intensive Computing," *IEEE Micro*, **34**, 52–63 (2014).

[32] A. M. Fagertun, M. S. Berger, S. R. Ruepp, V. Kamchevska, M. Galili, L. K. Oxenløwe, and L. Dittmann, "Ring-based All-Optical Datacenter Networks," in *European Conference on Optical Communications*, ECOC (2015), paper P.6.9.

[33] L. Schares, R. Budd, D. Kuchta, C. Schow, F. Doany, M. Moehrle, A. Sigmund, and W. Rehbein, "Etched-Facet Semiconductor Optical Amplifiers for Gain-Integrated Photonic Switch Fabrics," *European Conference on Optical Communications*, ECOC (2015), paper Mo.3.2.1.

[34] K. Suzuki, K. Iwatsuki, S. Nishi, and M. Saruwatari, "Error-free demultiplexing of 160 Gbit/s pulse signal using optical loop mirror including semiconductor laser amplifier," *Electronics letters*, **30**, 1501–1503 (1994).

[35] S. Kawanishi, H. Takara, T. Morioka, O. Kamatani, and M. Saruwatari, "200 Gbit/s, 100 km time-division-multiplexed optical transmission using supercontinuum pulses with prescaled PLL timing extraction and all-optical demultiplexing," *Electronics letters*, **31**, 816–817 (1995).

[36] S. Kawanishi, H. Takara, T. Morioka, O. Kamatani, K. Takiguchi, T. Kitoh, and M. Saruwatari, "400 Gbit/s TDM Transmission of 0.98 ps Pulses over 40 km Employing Dispersion Slope Compensation," in *Optical Fiber Communication Conference*, OFC (1996), paper PD24.

[37] R. A. Barry, V. W. S. Chan, K. L. Hall, E. S. Kintzer, J. D. Moores, A. Rauschenbach, E. A. Swanson, L. E. Adams, C. R. Doerr, S. G. Finn, H. A. Haus, E. P. Ippen, W. S. Wong, and M. Haner, "All-Optical Network Consortium-Ultrafast TDM Networks," *IEEE Journal on selected areas in communications*, **14**, 999–1013 (1996).

[38] R. S. Tucker, G. Eisensein, and S. K. Korotky, "Optical Time-Division Multiplexing For Very High Bit-Rate Transmission," *Journal of Lightwave Technology*, **6**, 1737–1749 (1998).

[39] M. Nakazawa, E. Yoshida, T. Yamamoto, E. Yamada, and A. Sahara, "TDM single channel 640 Gbit/s transmission experiment over 60 km using 400 fs pulse train and walk-off free, dispersion flattened nonlinear optical loop mirror," *Electronics Letters*, **34**, 907–908 (1998).

[40] H. C. H. Mulvad, L. K. Oxenløwe, M. Galili, A. T. Clausen, L. Grüner-Nielsen, and P. Jeppesen, "1.28 Tbit/s single-polarisation serial OOK optical data generation and demultiplexing," *Electronics Letters*, **45**, 280–281 (2009).

[41] H. G. Weber, S. Ferber, M. Kroh, C. Schmidt-Langhorst, R. Ludwig, V. Marembert, C. Boerner, F. Futami, S. Watanabe, and C. Schubert, "Single Channel 1.28 Tbitls and 2.56 Tbitls DQPSK Transmission," in *European Conference on Optical Communications*, ECOC (2005), paper Th 4.1.2.

[42] H. C. H. Mulvad, M. Galili, L. K. Oxenløwe, H. Hu, A. T. Clausen, J. B. Jensen, C. Peucheret, and P. Jeppesen "Demonstration of 5.1 Tbit/s data capacity on a single-wavelength channe," *Optics Express*, **18**, 1438–1443 (2010).

[43] T. Richter, E. Palushani, C. Schmidt-Langhorst, M. Nölle, R. Ludwig, J. K. Fischer, and C. Schubert, "Single wavelength channel 10.2 Tb/s TDM-data capacity using 16-QAM and coherent detectio," in *Optical Fiber Communication Conference*, OFC (2011), paper PDPA9.

[44] H. Hu, D. Kong, E. Palushani, J. D. Andersen, A. Rasmussen, B. M. Sørensen, M. Galili, H. C. H. Mulvad, K. J. Larsen, S. Forchhammer, P. Jeppesen, and L. K. Oxenløwe, "1.28 Tbaud Nyquist Signal Transmission using Time-Domain Optical Fourier Transformation based Receiver," in *Conference on Lasers & Electro-Optics*, CLEO (2013), paper CTh5D.5.

[45] R. Ludwig, S. Diez, A. Ehrhardt, L. Küller, W. Pieper, H. G. Weber, "A Tunable Femtosecond Modelocked Semiconductor Laser for Applications in OTDM-Systems," *IEICE Transactions on Electronics*, **E81-C**, 140–145 (1998).

[46] K. R. Tamura, and M. Nakazawa, "Spectral-Smoothing and Pedestal Reduction of Wavelength Tunable Quasi-Adiabatically Compressed Femtosecond Solitons Using a Dispersion-Flattened Dispersion-Imbalanced Loop Mirror," *IEEE Photonics Technology Letters*, **11**, 230–232 (1999).

[47] A. Shen, S. Bouchoule, P. Crozat, D. Mathoorasing, J.-M. Lourtioz, and C. Kazmierski, "Low timing jitter of gain- and Q-switched laser diodes for high bit rate OTDM applications," *Electronics Letters*, **33**, 1875–1877 (1997).

[48] L. Krainer, R. Paschotta, G. J. Spühler, I. Klimov, C. Y. Teisset, K. J. Weingarten, and U. Keller, "Tunable picosecond pulse-generating laser with a repetition rate exceeding 10 GHz," *Electronics Letters*, **38**, 225–227 (2002).

[49] V. Kaman, Y.-J. Chiu, T. Liljeberg S. Z. Zhang, and J. E. Bowers, "Integrated Tandem Traveling-Wave Electroabsorption Modulators for $>$ 100 Gbit/s OTDM Applications," *IEEE Photonics Technology Letters*, **12**, 1471–1573 (2000).

[50] Govind P. Agrawal, *Nonlinear Fiber Optics*, 4^{th} Edition, Elesevier Inc., 2006.

[51] K. Yoshino, T. Takeshita, I. Kotaka, S. Kondo, Y. Noguchi, R. Igaband, and K. Wakita, "Compact and Stable Electroabsorption Optical Modulator Modules," *Journal of Lighwave Technology*, **17**, 1700–1707 (1997).

[52] P. J. Winzer, and R.-J. Essiambre, "Advanced Optical Modulation Formats," *Proceedings of the IEEE*, **94**, 952–985 (2006).

[53] B. Howley, X. Wang, M. Chen, and R. T. Chen, "Reconfigurable Delay Time Polymer Planar Lightwave Circuit for an X-band Phased-Array Antenna Demonstration," *Journal of Lighwave Technology*, **25**, 883–890 (2007).

[54] R. Trebino, "Measuring Ultrashort Laser Pulses," *School of Physics, Georgia Institute of Technology*, [online] (Available: http://citeseerx.ist.psu.edu/viewdoc/download?doi=10.1.1.458.3886&rep=rep1&type=pdf).

[55] http://standards.ieee.org/getieee802/download/802.3-2012_section1.pdf.

[56] A. Beling, J. C. Campbell, H.-G Bach, G. Mekonnen, and D. Schmidt, "Parallel-Fed Traveling Wave Photodetector for $>$ 100-GHz Applications," *Journal of Lighwave Technology*, **26**, 16–20 (2008).

[57] A. I. Siahlo, A. T. Clausen, L. K. Oxenløwe, J. Seoane, and P. Jeppesen, "640 Gb/s OTDM transmission and demultiplexing using a NOLM with commercially available highly non-linear fiber," in *Conference on Lasers & Electro-Optics*, CLEO (2005), paper CTuO1.

[58] S. Watanabe, R. Okabe, F. Futami, R. Hainberger, C. Schmidt-Langhorst, C. Schubert, and H. Weber, " Novel fiber Kerr-switch with parametric gain: Demonstration of optical demultiplexing and sampling up to 640 Gb/s," in *European Conference on Optical Communication*, ECOC (2004), paper Th4.1.6.

[59] E. Tangdiongga, Y. Liu, H. de Waardt, G. Khoe, A. Koonen, H. Dorren, X. Shu, and I. Bennion, "All-optical demultiplexing of 640 to 40 Gbit/s using filtered chirp of a semiconductor optical amplifier," *Optics Letters*, **32**, 835–837 (2007).

[60] M. Eiselt, "Optimum Pump Pulse Selection for Demultiplexer Application of Four-Wave Mixing in Semiconductor Laser Amplifiers," *Photonics Technology Leters*, **7**, 1312–1314 (1995).

[61] J. Xu, M. Galili, H. C. H. Mulvad, L. K. Oxenløwe, A. T. Clausen, P. Jeppesen, B. Luther-Davis, S. Madden, A. Rode, D.-Y. Choi, M. Pelusi, F. Luan, and B. J. Eggleton, "Error-free 640 Gbit/s demultiplexing using a chalcogenide planar waveguide chip," in *Opto Electronics and Communications Conference*, OECC (2008), paper PDP-3.

[62] R. Salem, M. A. Foster, A. C. Turner, D. F. Geraghty, M. Lipson, and A. L. Gaeta, "Optical time lens based on four-wave mixing on a silicon chip," *Optics Letters*, **33**, 1047–1049 (2008).

[63] M. Jinno, and T. Matsumoto, "Nonlinear Sagnac Interferometer Switch and Its Applications," *IEEE Journal of Quantum electronics*, **28**, 875–882 (1992).

[64] A. Bogoni, M. Scaffardi, P. Ghelfi, and L. Potì, "Nonlinear Optical Loop Mirrors: Investigation Solution and Experimental Validation for Undesirable Counterpropagating Effects in All-Optical Signal Processing," *IEEE Journal of Selected Topics in Quantum Electronics*, **10**, 1115–1123 (2004).

[65] *ITU-T G.694.1: Spectral grids for WDM applications: DWDM frequency grid*, ITU-T (2012).

[66] H. C. H. Mulvad, E. Palushani, H. Hu, H. Ji, M. Lillieholm, M. Galili, A. T. Clausen, M. Pu, K. Yvind, J. M. Hvam, P. Jeppesen, and L. K. Oxenløwe, "Ultra-high-speed optical serial-to-parallel data conversion by time-domain optical Fourier transformation in a silicon nanowire," *Optics Express*, **19**, B825–B835 (2011).

[67] E. Palushani, H. C. H. Mulvad, M. Galili, H. Hu, L. K. Oxenløwe, A. T. Clausen, and P. Jeppesen, "OTDM-to-WDM Conversion Based on Time-to-Frequency Mapping by Time-Domain Optical Fourier Transformation," *IEEE Journal of Selected Topics in Quantum Electronics*, **18**, 681–688 (2012).

[68] B. H. Kolner, "Space-time duality and the theory of temporal imaging," *IEEE Journal of Quantum Electronics*, **30**, 1951–1963 (1994).

[69] P. J. Almeida, P. Petropoulos, B. C. Thomsen, M. Ibsen, and D. J. Richardson, "All-Optical Packet Compression Based on Time-to-Wavelength Conversion," *IEEE Photonics Technology Letters*, **16**, 1688–1690 (2004).

[70] C. V. Bennett, R. P. Scott, and B. H. Kolne, "Temporal magnification and reversal of 100 Gb/s optical data with an up-conversion time microscope," *Applied Physics Letters*, **65**, 2513–2515 (1994).

[71] S. Wabnitz, and B. J. Eggleton, *All-Optical Signal Processing: Data Communication and Storage Applications*, illustrated Edition, Springer International Publishing, 2015.

[72] C. A. Brackett, "Dense wavelength division multiplexing networks: Principles, and applications," *IEEE Journal of Selected Areas in Communications*, **8**, 948–964 (1990).

[73] S. Aleksić, "Energy Efficiency of Electronic and Optical Network Elements," *IEEE Journal of Selected Topics in Quantum Electronics*, **17**, 296–308 (2012).

[74] D. J. Blumenthal, P. R. Prucnal, and J. R. Sauer, "Photonic Packet Switches: Architectures and Experimental Implementations," *Proceedings of the IEEE*, **82**, 1650–1667 (1994).

[75] S. L. Danielsen, C. Joergensen, B. Mikkelsen, and K. E. Stubkjaer, "Optical Packet Switched Network Layer Without Optical Buffers," *IEEE Photonics Technology Letters*, **10**, 896–898 (1998).

[76] C. Qiao, and M. Yoo, "Optical Burst Switching (OBS)-A New Paradigm for an Optical Internet," *Journal of High Speed Networks*, **8**, 69–84 (1999).

[77] S. J. B. Yoo, "Optical Packet, and Burst Switching Technologies for the Future Photonic Internet," *Journal of Lightwave Technology*, **24**, 4468–4490 (2006).

[78] B. Saleh, and M. Teich, *Fundamentals of Photonics*, 2^{nd} Edition, John Wiley & Sons, Inc., 2007.

[79] C. Guillemot, M. Renaud, P. Gambini, C. Janz, I. Andonovic, R. Bauknecht, B. Bostica, M. Burzio, F. Callegati, M. Casoni, D. Chiaroni, F. Clerot, L. Danielsen, F. Dorgeuille, A. Dupas, A. Franzen, P. B. Hansen, K. Hunter, A. Kloch, R. Krahenbuhl, B. Lavigne, A. Le Corre, C. Raffaelli, M. Schilling, J. C. Simon, and L. Zucchelli, "Transparent optical packet switching: The European ACTS KEOPS project approach," *Journal of Lightwave Technology*, **16**, 2117–2134 (1998).

[80] D. Chiaroni, B. Lavigne, A. Jourdan, M. Sotom, L. Hamon, C. Chauzat, J. C. Jacquinot, A. Barroso, T. Zami, F. Dorgeuille, C. Janz, J. Y. Emery, E. Grard, and M. Renaud, "Physical and logical validation of a network based on all-optical packet switching systems," *Journal of Lightwave Technology*, **16**, 2255–2264 (1998).

[81] C. Bintjas, N. Pleros, K. Yiannopoulos, G. Theophilopoulos, M. Kalyvas, H. Avramopoulos, and G. Guekos, "All-optical packet address and payload separation," *IEEE Photonics Technology Letters*, **14**, 1728–1730 (2002).

[82] E. Park, and A. E. Willner, "Self-routing of wavelength packets using an all-optical wavelength shifter and QPSK subcarrier routing control headers," *IEEE Photonics Technology Letters*, **8**, 938—940 (1996).

[83] Y. M. Lin, W. I. Way, and G. K. Chang, "A novel optical label swapping technique using erasable optical single-sideband subcarrier label," *IEEE Photonics Technology Letters*, **12**, 1088–1090 (2000).

[84] H. J. Lee, S. J. B. Yoo, V. K. Tsui, and S. K. H. Fong, "A simple all-optical label detection and swapping technique incorporating a fiber Bragg grating filter," *IEEE Photonics Technology Letters*, **13**, 635–637 (2001).

[85] J. J. Yu, and G. K. Chang, "A novel technique for optical label and payload generation and multiplexing using optical carrier suppression and separation," *IEEE Photonics Technology Letters*, **16**, 320–322 (2004).

[86] H. Tsushima, M. Shabeer, P. Barnsley, and D. Pitcher, "Demonstration of an optical packet add drop with wavelength-coded header," *IEEE Photonics Technology Letters*, **7**, 320–322 (1995).

[87] A. Okada, "All-optical packet routing in AWG-based wavelength routing networks using an out-of-band optical label," in *Optical Fiber Communication Conference*, OFC (2002), paper ThG5-1.

[88] N. Chi, L. Xu, L. Christiansen, K. Yvind, J. Zhang, P. Holm-Nielsen, C. Peucheret, C. Zhang, and P. Jeppesen, "Optical label swapping and packet transmission based on ASK/DPSK orthogonal modulation format in IP-over-WDM networks," in *Optical Fiber Communication Conference*, OFC (2003), paper FS2.

[89] V. Olmos, J. Zhang, P. V. Holm-Nielsen, I. T. Monroy, V. Polo, A. M. J. Koonen, C. Peucheret, and J. Prat, "Simultaneous optical label erasure and insertion in a single wavelength conversion stage of combined FSK/IM modulated signals," *IEEE Photonics Technology Letters*, **16**, 2144–2146 (2004).

[90] N. Chi, C. Mikkelsen, L. Xu, J. F. Zhang, P. V. Holm-Nielsen, H. Y. Ou, J. Seoane, C. Peucheret, and P. Jeppesen, "Transmission and label encoding/erasure of orthogonally labelled signal using 40 Gb/s RZ-DPSK payload and 2.5 Gb/s IM label," *Electronics Letters*, **39**, 1335–1337 (2003).

[91] N. C. L. Xu, J. Zbang, P. V. Holm-Nielsen, C. Peucheret, C. Mikkelsen, H. On, J. Seoane, and P. Jeppesen, "Orthogonal optical labeling based on a 40 Gbit/s DPSK payload and a 2.5 Gbit/s IM label," in *Optical Fiber Communication Conference*, OFC (2004), paper FO6.

[92] C. W. Chow, C. S. Wong, and H. K. Tsang, "Optical packet labeling based on simultaneous polarization shift keying and amplitude shift keying," *Optical Letters*, **29**, 1861–1863 (2004).

[93] K. Kitayama, N. Wada, and H. Sotobayashi, "Architectural Considerations for Photonic IP Router Based upon Optical Code Correlation," *Journal of Lightwave of Technology*, **18**, 1834–1844 (2000).

[94] N. Wada, G. Cincotti, S. Yoshima, N. Kataoka, and K. I. Kitayama, "Characterization of a full encoder/decoder in the AWG configuration for code-based photonic routers—Part II: Experiments and applications," *Journal of Lightwave Technologies*, **24**, 113–121 (2006).

[95] T. E. Darcie, "Subcarrier multiplexing for lightwave networks and video distribution system," *IEEE Journal on Selected Areas in Communications*, **8**, 1240–1248 (2006).

[96] S. J. B. Yoo, and G. K. Chang, "High-throughput, low-latency next generation internet using optical tag switching," *U.S. Patent 6 111 673*, 1997.

[97] S. Yao, S. J. B. Yoo, B. Mukherjee, and S. Dixit, "All-optical packet switching for metropolitan area networks: Opportunities and challenges," *IEEE Communications Magazine*, **39**, 142–148 (2001).

[98] F. Xue, Z. Pan, Y. Bansal, J. Cao, Y. Jeon, K. Okamoto, S. Kamei, V. Akella, and S. J. B. Yoo, "End-to-end contention resolution schemes for an optical packet switching network with enhanced edge routers," *Journal of Lightwave Technology*, **21**, 2595–2604 (2003).

[99] *RFC 3031 Multiprotocol Label Switching Architecture*, RFC (2001).

[100] K. Sato, N. Yamanaka, Y. Takigawa, M. Koga, S. Okamoto, K. Shiomoto, E. Oki, and W. Imajuku, "GMPLS-based photonic multilayer router (Hikari router) architecture: An overview of traffic engineering and signaling technology," *IEEE Communications Magazine*, **40**, 96–101 (2002).

[101] S. Das, G. Parulkar, and N. McKeown, "Why OpenFlow/SDN Can Succeed Where GMPLS Failed," in *European Conference on Optical Communication*, ECOC (2012), paper Tu.1.D.1.

[102] N. Calabretta, O. Raz, W. Wang, T. Ditewig, F. Gomez Agis, S. Zhang, H. de Waardt, E. Tangdiongga, and H. J. S. Dorren, "Scalable Optical Packet Switch for Optical Packets with Multiple Modulation Formats and Data Rates," in *European Conference on Optical Communications*, ECOC (2009), Paper 6.3.4.

[103] N. Calabretta, H. Jung, E. Tangdiongga, and H. Dorren, "All-Optical Packet Switching and Label Rewriting for Data Packets Beyond 160 Gb/s," *IEEE Photonics Journal*, **2**, 113–129 (2010).

[104] *RFC 2460 - Internet Protocol, Version 6 (IPv6) Specification*, RFC (1998).

[105] K. Hirano, S. Nishimura, and S. K. Mitra, "Design of Digital Notch Filters," *IEEE Transactions on Communications*, **com-22**, 964–970 (1974).

[106] T. A. Strasser, and J. L. Wagener, "Wavelength-Selective Switches for ROADM Applications," *IEEE Journal of Selected Topics in Quantum Electronics*, **16**, 1150–1157 (2010).

[107] G. Breed, "Analyzing signal using the eye diagram," *High Frequency Electronics*, Summit Technical Media, 50–53 (2005).

[108] G. Baxter, S. Frisken, D. Abakoumov, H. Zhou, I. Clarke, A. Bartos, and S. Poole, "Highly programmable Wavelength Selective Switch based on Liquid Crystal on Silicon switching elements," in *Optical Fiber Communication Conference*, OFC (2006), paper OTuF2.

[109] https://www.finisar.com/sites/default/files/downloads/waveshaper_4000s_product_brief_11_14.pdf.

[110] D. J. Blumenthal, B.-E. Olsson, G. Rossi, T. E. Dimmick, L. Rau, M. Másanović, O. Lavrova, R. Doshi, O. Jerphagnon, J. E. Bowers, V. Kaman, L. A. Coldren, and J. Barton, "All-Optical Label Swapping Networks and Technologies," *Journal of Lightwave Technology*, **18**, 2000–2074 (2000).

[111] M. C. Cardakli, S. Lee, A. E. Willner, V. Grubsky, D. Starodubov, and J. Feinberg, "Reconfigurable Optical Packet Header Recognition and Routing Using Time-To-Wavelength Mapping and Tunable Fiber Bragg Gratings for Correlation Decoding," *IEEE Photonics Technology Letters*, **12**, 552–554 (2000).

[112] H. J. S. Dorren, M. T. Hill, Y. Liu, N. Calabretta, A. Srivatsa, F. M. Huijskens, H. de Waardt, and G. D. Khoe, "Optical packet switching and buffering by using all-optical signal processing methods," *Journal of Lightwave Technology*, **21**, 2–12 (2003).

[113] J. P. Wang, B. S. Robinson, S. A. Hamilton, and E. P. Ippen, "40-Gb/s all-optical header processing for packet routing," in *Optical Fiber Communication Conference*, OFC (2006), Paper OThS1.

[114] N. Calabretta, G. Contestabile, A. D'Errico, and E. Ciaramella, "All-optical label processing techniques for pure DPSK optical packets," *Journal of Selected Topics in Quantum Electronics*, **12**, 686–696 (2006).

[115] H. Hu, H. Ji, M. Galili, M. Pu, K. Yvind, P. Jeppesen, and L. K. Oxenløwe, "160 Gbit/s optical packet switching using a silicon chip," in *IEEE Photonics Conference*, IPC (2012), 915–916.

[116] T. S. El-Bawab, *Optical Switching*, Springer Science & Business Media, 2008.

[117] J. Kim, C. Nuzman, B. Kumar, D. Lieuwen, J. Kraus, A. Weiss, C. Lichtenwalner, A. Papazian, R. Frahm, N. Basavanhally, D. Ramsey, V. Aksyuk, F. Pardo, M. Simon, V. Lifton, H. Chan, M. Haueis, A. Gasparyan, H. Shea, S. Arney, C. Bolle, P. Kolodner, R. Ryf, D. Neilson, and J. Gates, "1100x1100 port MEMS-based optical crossconnect with 4-dB maximum loss," *Photonics Technology Letters*, **15**, 1537–1539 (2003).

[118] S. Han, T. J. Seok, N. Quack, B.-W. Yoo, and M. C. Wu, "Monolithic 50x50 MEMS silicon photonic switches with microsecond response time," in *Optical Fiber Communication Conference*, OFC (2014), paper M2K.2.

[119] N. Farrington, A. Forencich, P.-C. Sun, S. Fainma, "A 10 μs Hybrid Optical-Circuit/Electrical-Packet Network for Datacenters," in *Optical Fiber Communication Conference*, OFC (2013).

[120] Y.-K. Yeo, "Large Port-Count Optical Cross-connects for Data Centers," in *Photonics in Switching*, PS (2012).

[121] R. S. Tucker, "Optical Packet-Switched WDM Networks: A Cost and Energy Perspective," in *Optical Fiber Communication Conference*, OFC (2008).

[122] V. Jayaraman, D. A. Cohen, and L. A. Coldren, "Demonstration of broad-band tunability in a semiconductor-laser using sampled gratings," *Applied Physics Letters*, *60*, 2321–2323 (1992).

[123] S. J. B. Yoo, H. J. Lee, Z. Pan, J. Cao, Y. Zhang, K. Okamoto, and S. Kamei, "Rapidly switching all-optical packet routing system with optical-label swapping incorporating tunable wavelength conversion and a uniform-loss cyclic frequency AWGR," *Photonics Technology Letters*, **14**, 1211–1213 (2002).

[124] D. Klonidis, C. T. Politi, R. Nejabati, M. J. O'Mahony, and D. Simeonidou, "OPSnet: Design and demonstration of an asynchronous high-speed optical packet switch," *Journal of Lightwave Technology*, **10**, 2914–2925 (2005).

[125] H. Jiang, and C. Dovrolis, "Why Is the Internet Traffic Bursty in Short Time Scales?," in *ACM SIGMETRICS* 2005.

[126] D. Cotter, J. K. Lucek, M. Shabeer, K. Smith, D. C. Rogers, D. Nesset, and P. Gunning, "Self-routing of 100 Gbit/s packets using 6-bit keyword address recognition," *Electronics Letters*, **31**, 2201–2202 (1995).

[127] I. Glesk, K. I. Kang, and P. R. Prucnal, "Demonstration of ultrafast all- optical packet routing," *Electronics Letters*, **33**, 794–795 (1997).

[128] A. Carena, M. D. Vaughn, R.Gaudino, M. Shell, and D. J. Blumenthal, "OPERA: An optical packet experimental routing architecture with label swapping capability," *Journal of Lightwave Technology*, **16**, 2135–2145 (1998).

[129] J. S. Turner, "Terabit burst switching," *Journal of HighSpeed Networks*, **8**, 3–16 (1999).

[130] D. Blumenthal, P. R. Prucnal, and L. Thylen, "Performance of an 8x8 $LiNbO_3$ switch matrix as a gigahertz self-routing switching node," *Electronics Letters*, **23**, 1359–1360 (1987).

[131] J. V Campenhout, W. M. J. Green, S. Assefa, and Y. A. Vlasov, "Low-power, 2×2 silicon electro-optic switch with 110-nm bandwidth for broadband reconfigurable optical networks," *Optics Express*, **17**, 24020–24020 (2009).

[132] N. Dupuis, B. G. Lee, A. V. Rylyakov, D. M. Kuchta, C. W. Baks, J. S. Orcutt, D. M. Gill, W. M. J. Green, and C. L. Schow, "Modeling and Characterization of a Nonblocking 4×4 Mach–Zehnder Silicon

Photonic Switch Fabric," *Journal of Lightwave Technology*, **33**, 4329–4337 (2015).

[133] A. Wonfor, H. Wang, R. V. Penty, and I. H. White, "Large Port Count High-Speed Optical Switch Fabric for Use Within Datacenters," *Journal of Optical Communication Networks*, **3**, A32–A39 (2011).

[134] Q. Cheng, A. Wonfor, R. V. Penty, and I. H. White, "Scalable, Low-Energy Hybrid Photonic Space Switch," *Journal of Lightwave Technology*, **31**, 3077–3084 (2013).

[135] I. M. Soganci, T. Tanemura, K. A. Williams, N. Calabretta, T. de Vries, E. Smalbrugge, M. K. Smit, H. Dorren, and Y. Nakano, "High-speed 1x16 optical switch monolithically integrated on InP," in *European Conference on Optcal Communication*, ECOC (2009), paper 1.2.1.

[136] E. J. Murphy, T. O. Murphy, A. F. Ambrose, R. W. Irvin, B. H. Lee, P. Peng, G. W. Richards, and A. Yorinks, "16x16 strictly nonblocking guided-wave optical switching system," *Journal of Lightwave Technology*, **14**, 352–358 (1996).

[137] R. S. Tucker, "Green Optical Communications—Part II: Energy Limitations in Networks," *Journal of Selected Topics in Quantum Electronics*, **17**, 261–274 (2011).

[138] J. Herrera, O. Raz, E. Tangdiongga, Y. Liu, H. C. H. Mulvad, F. Ramos, J. Marti, G. Maxwell, A. Poustie, M. T. Hill, H. de Waardt, G. D. Khoe, A. M. J. Koonen, and H. J. S. Dorren, "160-Gb/s All-Optical Packet Switching Over a 110-km Field Installed Optical Fiber Link," *Journal of Lightwave Technology*, **26**, 176–183 (2008).

[139] Cisco Nexus 9500 Platform Switches: http://www.cisco.com/c/en/us/products/collateral/switches/nexus-9000-series-switches/datasheet-c78-729404.pdf, 2014.

[140] Juniper, EX8216 Ethernet switch: http://www.juniper.net/us/en/local/pdf/datasheets/1000283-en.pdf, 2014.

[141] E. J. Norberg, R. S. Guzzon, J. S. Parker, L. A. Johansson, and L. A. Coldren, "Programmable Photonic Microwave Filters Monolithically Integrated in InP–InGaAsP," *Journal of Lightwave Technology*, **29**, 1611–1619 (2011).

[142] B. E. Little, S. T. Chu, H. A. Haus, J. Foresi, and J.-P. Laine, "Microring Resonator Channel Dropping Filters," *Journal of Lightwave Technology*, **15**, 998–1005 (1997).

[143] D. Seya, K. Harako, T. Hirooka, and M. Nakazawa, "All-Optical High-Performance Demultiplexing Using Optical Nyquist Pulse Sampling," in *Optical Fiber Communication conference*, OFC (2014), papaer W4F.2.

[144] D. Kong, J. Zang, M. Yu, Y. Li, S. Zhou, H. Guo, and J. Wu, "A Novel Detection Scheme for Nyquist Optical Time-division Multiplexed Signal with Coherent Matched Sampling," in *Optical Fiber Communication conference*, OFC (2015), paper W3C.4.

[145] M. Galili, H. C. H. Mulvad, H. Hu, L.K. Oxenløwe, F. Gomez Agis†, C. Ware, D. Erasme, A. T. Clausen, P. Jeppesen, "650 Gbit/s OTDM transmission over 80 km SSMF incorporating clock recovery, channel identification and demultiplexing in a polarisation insensitive receiver," in *Optical Fiber Communication conference*, OFC (2010), paper OWO3.

[146] M. H. Eiselt, "PMD compensation: A system perspective," in *Optical Fiber Communication conference*, OFC (2004), paper ThF4.

[147] H. Yang, and S. J. B. Yoo,"All-Optical Variable Buffering Strategies and Switch Fabric Architectures for Future All-Optical Data Routers," *Journal of Lightwave Technology*, **23**, 3321–3330 (2005).

[148] R. Langenhorst, M. Eiselt, W. Pieper, G. GroBkopf, R. Ludwig, L. Kuller, E. Dietrich, and H. G. Weber, "Fiber Loop Optical Buffer," *Journal of Lightwave Technology*, **14**, 324–335 (1996).

[149] K. Nozaki, A. Shinya, S. Matsuo, Y. Suzaki, T. Segawa, T. Sato, Y. Kawaguchi, R. Takahashi, and M. Notomi, "Ultralow-power all-optical RAM based on nanocavities," *Nature Photonics*, **6**, 248–252 (2012).